FERMILAB-PUB-07-034-T

Stable Massive Particles at Colliders

M. Fairbairn [a] A.C. Kraan [b] D.A. Milstead [a] T. Sjöstrand [c]
P. Skands [d] T. Sloan [e]

[a] *Fysikum, Stockholm University, Sweden*

[b] *Department of Physics and Astronomy, University of Pennsylvania, USA; Presently at: Istituto Nazionale di Fisica Nucleare, Pisa, Italy*

[c] *Department of Theoretical Physics, Lund University, Sweden; also at CERN, Switzerland*

[d] *Theoretical Physics Department, Fermi National Accelerator Laboratory, USA.*

[e] *Department of Physics, Lancaster University, UK*

Abstract

We review the theoretical motivations and experimental status of searches for stable massive particles (SMPs) which could be sufficiently long-lived as to be directly detected at collider experiments. The discovery of such particles would address a number of important questions in modern physics including the origin and composition of dark matter in the universe and the unification of the fundamental forces. This review describes the techniques used in SMP-searches at collider experiments and the limits so far obtained on the production of SMPs which possess various colour, electric and magnetic charge quantum numbers. We also describe theoretical scenarios which predict SMPs, the phenomenology needed to model their production at colliders and interactions with matter. In addition, the interplay between collider searches and open questions in cosmology such as dark matter composition are addressed.

Key words: review, experimental results, colliders, SMP, monopole, SUSY, extra dimensions
PACS: 14.80, Hv
PACS: 14.80, Ly
PACS: 29.40, Gx

1 Introduction

An open question in modern physics is the possible existence of heavy, exotic particles, which can be directly detected at collider experiments through their interactions with matter. This paper describes collider searches for these so-called Stable

Massive Particles (SMPs), together with a review of theoretical models in which such states appear. We also discuss the astrophysical consequences that an SMP discovery would imply. In this work, we define an SMP as a particle which does not decay during its passage through a detector, and which would undergo electromagnetic and/or strong interactions with matter. Normally we would expect such particles to be heavier than a proton.

Historically, the strange, long-lived kaons heralded a revolution in particle physics, in terms of new fundamental matter, and also in the shape of a new (approximately) conserved quantum number. Today, states classifiable as SMPs recur in many theoretical extensions of the Standard Model (SM). One crucial aspect in this context is naturally the question of dark matter in the universe, but also charge quantisation (magnetic monopoles? millicharges? grand unification?), the flavour question (more generations?), parity violation (vector-like fermions? mirror fermions?), the hierarchy problem (supersymmetric SMPs?), and more (SMPs from extra dimensions? your favourite particle?) are relevant. We devote Section 2 to a review of theoretical scenarios with SMP states.

Due to the symbiosis between accelerator particle physics and astrophysics for long-lived particles, we focus on the cosmological and astrophysical implications of SMPs in Section 3. This discussion includes the implications of an SMP discovery at an accelerator on topics such as dark matter and nucleosynthesis.

In most non-generic searches for SMPs, theoretical models are needed to calculate their production cross sections and final-state topologies. In the case of massive coloured objects, their fragmentation into jets must be described. Section 4 contains an overview of the techniques used to model the production of SMPs.

The detection of SMPs is only possible once the interactions in matter are understood. In Section 5 we summarise the phenomenology used to model the interactions of SMPs with detector material, including a description of their electromagnetic and hadronic interactions.

In Section 6, a range of possible search techniques which can be used to identify SMPs are described. These include techniques based on ionisation energy losses, Cherenkov techniques and time-of-flight methods. Additionally, specific techniques used in magnetic monopole searches are summarised.

A wide variety of SMP searches have been performed in lepton-hadron, electron-positron and hadron-hadron reactions [1], yielding important constraints on the parameter spaces of a number of theories. The searches vary from the very general types, which make minimal assumptions regarding the quantum numbers of the SMP, to those performed within a specific theoretical scenario. Section 7 presents a summary of the most important model-independent searches, as well as a selection of searches made within commonly studied exotic physics scenarios.

Approaching the exciting time when the Large Hadron Collider (LHC) will produce its first collisions, it is appropiate to discuss prospects for the discovery of SMPs with this machine. Searches for SMPs with masses up to several TeV will be possible, representing an order of magnitude increase in mass sensitivity compared with earlier colliders. Section 8 discusses the the discovery potential of a range of types of SMPs at the LHC. Finally, Section 9 contains a summary of this report.

Our report is complementary to, and differs from, previous reviews of SMPs [2–5] in a number of ways. The principal difference is that we focus on collider searches, although non-accelerator results such as those obtained using mass spectroscopy and cosmic ray detection are discussed, when appropriate. In view of the circa 50 accelerator searches, which have taken place over the past two decades, an up-to-date and detailed description of the techniques and results of these searches, and of their theoretical motivation, is overdue. By specialising in collider studies we are able to cover searches for many different proposed species of SMPs and the experimental challenges specific to each of them. For example, we provide a detailed treatment of hadronic SMPs, which is lacking in earlier reviews. Furthermore, although magnetic monopoles are usually treated separately to electrically charged SMPs in this type of article, they are included here since both types of particles are expected to share many common experimental signatures. Magnetic monopole searches can provide sensitivity to SMPs with values of electric charge beyond those covered by dedicated searches for electrically charged SMPs, and vice versa. Thus, by considering a broader range of collider searches, it is possible to more fully describe the types of SMPs, and their possible masses, which have been excluded, and those which could have been produced at colliders but which potentially remain unobserved.

2 Theoretical scenarios for SMPs

In this section, we first give a brief introduction to theoretical possibilities for SMP states, followed by in-depth discussions on some of the more commonly considered scenarios. In particular we discuss supersymmetric models in Section 2.1 and models with universal extra dimensions in Section 2.2. Sections 2.3 and 2.4 concern alternative possibilities that do not fit smoothly into either of the above categories, such as Z'-induced millicharges and magnetic monopoles.

To gain an impression of the wide range of possible SMP states, it is instructive first to take a look at the Standard Model itself. Protons, neutrons, electrons, and muons are all examples of stable particles which undergo interactions in a detector. So are π^+, K^+, and K^0_L. These well-studied states also illustrate very well the spectrum of possibilities *beyond* the Standard Model. Consider the following well-known properties, and apply them implicitly to hypothetical new states. The electron is a fundamental particle. It does not decay, e.g. to neutrinos due to the conservation of a

gauged quantum number, electric charge in this case. It is the lightest state carrying that quantum number. The proton is a complicated bound state composed of a set of more fundamental particles which are held together by a high-strength short-range gauge force. The kinematically allowed decay of the proton to, e.g. $e^+\pi^0$ does not occur due to conservation of certain global (i.e. non-gauged) quantum numbers, in this case baryon and lepton number. The conservation of these numbers are accidental symmetries of the model. The long lifetime of the neutron owes to a combination of the weak force being involved and the very small decay phase space. Though unstable in free space, there are still many of them around, due to the existence of stable "composites of composites", the nuclei of baryonic matter. The muon has a comparatively long lifetime due to the hierarchy between the muon mass and the weak scale ($\Gamma_\mu \propto m_\mu^5/m_W^4$). At low energies, the decay appears to proceed via a non-renormalisable dimension-6 operator which, in the fundamental theory, arises due to a virtual massive gauge boson, the W. Finally, also the atom furnishes an example. Its stability could not be understood in terms of Maxwell's theory. Only after a drastic revision, quantum mechanics, could it be accounted for. The corresponding case today would be the discovery of a state whose stability could not be accounted for within the framework of quantum field theory.

Thus, already the SM contains quite a varied history of stable interacting states. Turning now to physics beyond the SM, there are several generic possibilities for SMP's, essentially all recurrences of the states mentioned above, with the addition of topological defects, like cosmic strings or magnetic monopoles.

The most obvious possibility for an SMP is that one or more new states exist which carry a new conserved, or almost conserved, global quantum number [1] . SUSY with R-parity, extra dimensions with KK-parity, and several other models fall into this category. The lightest of the new states will be stable, due to the conservation of this new "parity", and depending on quantum numbers, mass spectra, and interaction strengths, one or more higher-lying states may also be stable or meta-stable. In general, electrically charged stable states are excluded by cosmology, and also coloured particles are strongly constrained, as will be discussed in Section 3. For this reason, and to obtain a solution to the dark-matter problem, models are usually constructed to provide *un*-charged stable dark-matter candidates, most often in the guise of weakly interacting massive particles (WIMPs). From a motivational point of view, SMP models thus come in two categories:

(1) Models which solve the dark-matter problem with a WIMP-type dark-matter particle, but which also have one or more higher-lying meta-stable SMP states.
(2) Models which have long-lived SMP states, but which either do not address

[1] As an aside, at the most fundamental level any such global symmetry probably has to be the remnant of a broken gauge or space–time symmetry (e.g. KK parity is the remnant of broken higher-dimensional Poincaré invariance), to avoid stability problems [6–8], but we shall here treat them simply as discrete global symmetries, whatever their origin.

dark matter or address it with a non-WIMP dark-matter particle.

As a quick reference, Tabs. 1 and 2 give a condensed overview of the SMP states discussed in the text, along with a description of which scenario(s) give rise to each of them.

2.1 SMP states in Supersymmetry

Among the most interesting and comprehensively studied possibilities for observable new physics is supersymmetry (SUSY) — for excellent reviews see, e.g. [9, 10]. Interesting in its own right by being the largest possible space–time symmetry, it was chiefly with a number of additional theoretical successes during the eighties that supersymmetry gained widespread acceptance, among these successful gauge coupling unification, a natural candidate for dark matter, and an elegant solution to the so-called hierarchy problem associated with the smallness of $M_Z^2/M_{\rm Planck}^2$.

Stated briefly, supersymmetry promotes all the fields of the SM to superfields. Each ($N = 1$) superfield contains one boson and one fermion as dynamical degrees of freedom. Hence not only should all the SM particles (including at least one more Higgs doublet) have 'sparticle' superpartners, with spins differing by 1/2, but also the interactions of these superpartners should to a large extent be fixed by supersymmetry. However, due to the absence of observed sparticles so far, there must exist a mass gap between the SM particles and their superpartners, implying that supersymmetry must be broken at the weak scale. This mass gap cannot be much larger than $\sim$ 1 TeV without invalidating the solution to the hierarchy problem. Independently, both SUSY dark matter and SUSY grand unification also point to roughly the TeV scale, hence there is good reason to believe that SUSY, if it exists, should manifest itself at the next generation of colliders, and a long list of sophisticated theory tools for SUSY phenomenology are available, see, e.g. [11–15].

In the most general SUSY models, both lepton and baryon number are violated. If the SUSY-breaking mass scale [16] is $\mathcal{O}(1\ \text{TeV})$, then bounds on proton decay [1, 17] require the product of the B and L violating couplings to be less than 10^{-25} [18]. Hence, either one or both of the accidental symmetries that protect B and L in the Standard Model are usually promoted to explicit ones in SUSY models. The most common way to accomplish this is through postulating the conservation of the quantum number $R = (-1)^{3B+L+2S}$ [19], where $B(L)$ is baryon (lepton) number and S is spin. Since SM particles carry $R = +1$ and their SUSY partners $R = -1$, the lightest supersymmetric particle (LSP) is stable, providing a possible solution to the dark-matter problem. If R-parity is violated, either lepton or baryon number must still be conserved, to avoid rapid proton decay. In this case, the LSP is not stable (though it may still be long-lived) and the dark-matter problem is not addressed. For a charged LSP, R-parity violation can be invoked to obtain a lifetime

SMP	LSP	Scenario	Conditions
$\tilde{\tau}_1$	$\tilde{\chi}_1^0$	MSSM	$\tilde{\tau}_1$ mass (determined by $m^2_{\tilde{\tau}_{L,R}}$, μ, $\tan\beta$, and A_τ) close to $\tilde{\chi}_1^0$ mass.
	$\tilde{G}$	GMSB	Large N, small M, and/or large $\tan\beta$.
		$\tilde{g}$MSB	No detailed phenomenology studies, see [20].
		SUGRA	Supergravity with a gravitino LSP, see [21].
	$\tilde{\tau}_1$	MSSM	Small $m_{\tilde{\tau}_{L,R}}$ and/or large $\tan\beta$ and/or very large A_τ.
		AMSB	Small m_0, large $\tan\beta$.
		$\tilde{g}$MSB	Generic in minimal models.
$\tilde{\ell}_{i1}$	$\tilde{G}$	GMSB	$\tilde{\tau}_1$ NLSP (see above). $\tilde{e}_1$ and $\tilde{\mu}_1$ co-NLSP and also SMP for small $\tan\beta$ and μ.
	$\tilde{\tau}_1$	$\tilde{g}$MSB	$\tilde{e}_1$ and $\tilde{\mu}_1$ co-LSP and also SMP when stau mixing small.
$\tilde{\chi}_1^+$	$\tilde{\chi}_1^0$	MSSM	$m_{\tilde{\chi}_1^+} - m_{\tilde{\chi}_1^0} \lesssim m_{\pi^+}$. Very large $M_{1,2} \gtrsim 2$ TeV $\gg \lvert\mu\rvert$ (Higgsino region) or non-universal gaugino masses $M_1 \gtrsim 4M_2$, with the latter condition relaxed to $M_1 \gtrsim M_2$ for $M_2 \ll \lvert\mu\rvert$. Natural in O-II models, where simultaneously also the $\tilde{g}$ can be long-lived near $\delta_{\rm GS} = -3$.
		AMSB	$M_1 > M_2$ natural. m_0 not too small. See MSSM above.
$\tilde{g}$	$\tilde{\chi}_1^0$	MSSM	Very large $m^2_{\tilde{q}} \gg M_3$, e.g. split SUSY.
	$\tilde{G}$	GMSB	SUSY GUT extensions [22–24].
	$\tilde{g}$	MSSM	Very small $M_3 \ll M_{1,2}$, O-II models near $\delta_{\rm GS} = -3$.
		GMSB	SUSY GUT extensions [22–26].
$\tilde{t}_1$	$\tilde{\chi}_1^0$	MSSM	Non-universal squark and gaugino masses. Small $m^2_{\tilde{q}}$ and M_3, small $\tan\beta$, large A_t.
$\tilde{b}_1$			Small $m^2_{\tilde{q}}$ and M_3, large $\tan\beta$ and/or large $A_b \gg A_t$.

Table 1
Brief overview of possible SUSY SMP states considered in the literature. Classified by SMP, LSP, scenario, and typical conditions for this case to materialise in the given scenario. See text for details.

in the allowed range 10^{-8} s$< \tau_{\rm LSP} < 1$ s [18].

2.1.1 The MSSM and CMSSM

At present, little is known for certain about the nature of the SUSY-breaking mechanism. Some special cases will be discussed below, but at the most general level we define the minimal supersymmetric Standard Model (MSSM) to contain all pos-

sible SUSY-breaking interactions, which are consistent with gauge and Poincaré invariance, and which do not cause the hierarchy problem to reappear (so-called soft SUSY-breaking). This implies an additional mass term for each of the gauginos $M_{1,2,3}$, extra mass terms squared m_{ij}^2 for each pair of scalars i and j, and also trilinear couplings A_{ijk} between combinations of three scalars i, j, and k. Due to significant constraints on CP and flavour violation, these parameters are normally taken to be real and flavour diagonal. To further limit the number of parameters, the additional assumption of GUT scale unification of the scalar masses m_0, gaugino masses $m_{1/2}$, and trilinear parameters A_0 is often made, a choice sometimes referred to as the constrained MSSM or CMSSM. In addition, there are also the SUSY-conserving Yukawa couplings Y_{ijk}, gauge couplings g_i, vacuum expectation values (vev's) for each of the Higgs doublets $v_{1,2}$, the μ parameter (a SUSY-conserving mixing term between the two Higgs doublets), and, if R-parity is violated, Yukawa-like interactions between lepton and quark superfields as well as L-violating mixing terms between one of the Higgs superfields and the lepton superfields. The sum of the Higgs vev's is fixed by the Z mass, and their relative size is usually cast in terms of the parameter $\tan\beta = v_2/v_1$, with $\tan\beta \lesssim 50$ required for perturbativity up to the GUT scale. See [9, 10] for further details.

As Tab. 1 suggests, the general MSSM allows for essentially any sparticle to be an SMP. In models with neutralino dark matter, the NLSP can be long-lived if its decay phase space is small or zero, mimicking the case of the neutron in the SM. An interesting scenario here is that of a light stop NLSP, as motivated by electroweak baryogenesis [27, 28]. In this scenario non-universal squark mass terms are used to arrange a small mass difference between the $\tilde{t}_1$ and the LSP $\tilde{\chi}_1^0$, while the lightest chargino is kept too heavy for the decay $\tilde{t}_1 \to b\tilde{\chi}_1^+$ to occur. In this case, only the radiative process $\tilde{t}_1 \to \tilde{c}_1\tilde{\chi}_1^0$ is open, and the $\tilde{t}_1$ can be quite long-lived. See [27–30] for detailed studies.

Though not equally well motivated at present, a light NLSP $\tilde{\tau}_1$ (small slepton masses and/or large $\tan\beta$ and/or large A_τ) or less likely $\tilde{b}_1$ (small squark masses and large $\tan\beta$ and/or very large $A_b \gg A_t$) could also be possible. For a $\tilde{\tau}_1$ NLSP with small mixing (small $\tan\beta$ and A_τ), the $\tilde{e}_1$ and $\tilde{\mu}_1$ could simultaneously also be long-lived. A small mass difference $m_{\tilde{\chi}_1^+} - m_{\tilde{\chi}_1^0} \lesssim m_{\pi^+}$ can occur for very large $M_{1,2} \gtrsim 2$ TeV $\gg |\mu|$ (Higgsino region) or non-universal gaugino masses [31–33] $M_1 \gtrsim 4M_2$, with the latter condition relaxed to $M_1 \gtrsim M_2$ for $M_2 \ll |\mu|$. To obtain a long-lived gluino NLSP, the requirement is small M_3, possibly in combination with very large $m_{\tilde{q}}^2$, since the gluino decay proceeds via intermediate squarks (see, e.g. the discussion of split supersymmetry below).

If the LSP is not required to be a neutralino, essentially all of the cases just mentioned have obvious extensions where the NLSP becomes the LSP. In this case, dark matter is much more problematic, and R-parity violation may be necessary to render the LSP unstable.

When gravity is included, as in supergravity models, also the gravitino can in principle be the LSP, depending on its mass. If the gravitino is light, the NLSP will then often be long-lived due to the smallness of the gravitational coupling. For supergravity models with a long-lived $\tilde{\tau}$ NLSP see [21]; other models with a gravitino LSP will be discussed below.

2.1.2 Gauge Mediated Supersymmetry Breaking

In models with gauge mediation [34, 35] (GMSB, see [36–38] for mass spectra and [39] for a review), the gravitino is very light ($m_{\tilde{G}} \lesssim 1\,\text{keV}$) and hence the LSP for any relevant choice of parameters. Minimal models are cast in terms of six parameters, typically N, Λ, M, $\tan\beta$, $\text{sgn}(\mu)$, and c_{grav}. Briefly stated, the meaning of these parameters is that N chiral $SU(5)$ multiplets are added to the theory at the scale $M \lesssim 10^{15}$ GeV [39]. If not only $SU(5)$ multiplets are added, the counting gets more complicated, but there is still an effective N. These "messengers" couple directly both to the MSSM fields (via the ordinary SM gauge interactions) and also to an unspecified source of SUSY-breaking. $\Lambda \sim 10 - 100$ TeV is the effective SUSY-breaking scale, related to the fundamental SUSY-breaking scale $\sqrt{F}$ by a relation $\Lambda = F/M$. The next-to-lightest sparticle (NLSP) decays only via the gravitational coupling and can be very long-lived. For a slepton NLSP [39]:

$$c\tau_{\text{NLSP}} = 0.1 \left(\frac{100\text{ GeV}}{m_{\text{NLSP}}}\right)^5 \left(\frac{m_{\tilde{G}}}{2.4\text{ eV}}\right) \text{ mm} \quad , \tag{1}$$

with the gravitino mass $m_{\tilde{G}}$ controlled by $c_{\text{grav}} < 1$ and F:

$$m_{\tilde{G}} = 2.4 c_{\text{grav}} \left(\frac{\sqrt{F}}{100\text{ TeV}}\right)^2 \text{ eV} \quad . \tag{2}$$

Since the SUSY-breaking terms are induced by gauge interactions, they are flavour universal and their sizes are proportional to the amount of gauge charge carried by each field. In minimal models, the next-to-lightest supersymmetric particle is therefore always the "least charged" of either the gauginos or the scalars. The latter occurs in particular for large values of the messenger index N. In a tiny and near-excluded parameter region at small values of the model parameters Λ and M, the NLSP is then a sneutrino, otherwise it is the $\tilde{\tau}_1$ (for a benchmark and model line, see Snowmass point 7 [40]). Note, however, that N cannot be chosen arbitrarily large, perturbativity of the theory up to the GUT scale requiring, e.g. $N \lesssim 5$ for small $M \lesssim 10^6$ GeV and $N \lesssim 10$ for $M \sim 10^{10}$ GeV. To illustrate the parameter space, Fig. 1 shows the smallest messenger index N required to have a $\tilde{\tau}_1$ NLSP for $\mu > 0$ and *a)* relatively light messengers $M = 2\Lambda$ and *b)* heavy messengers $M = 10^{10}$ GeV, as a function of $\tan\beta$ and Λ (since c_{grav} only affects the decay we leave it unspecified). The numbers were obtained with ISAJET v.7.71 [41] using $m_t = 175$ GeV. The light grey areas at small Λ are theoretically excluded due to un-

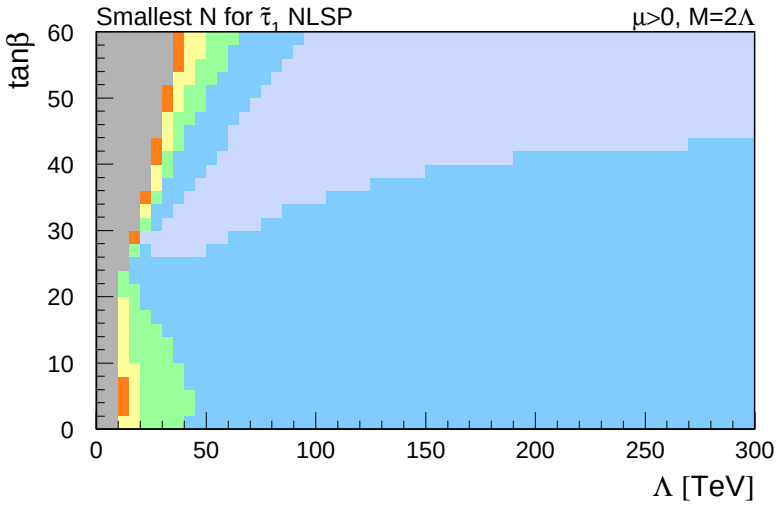

a)

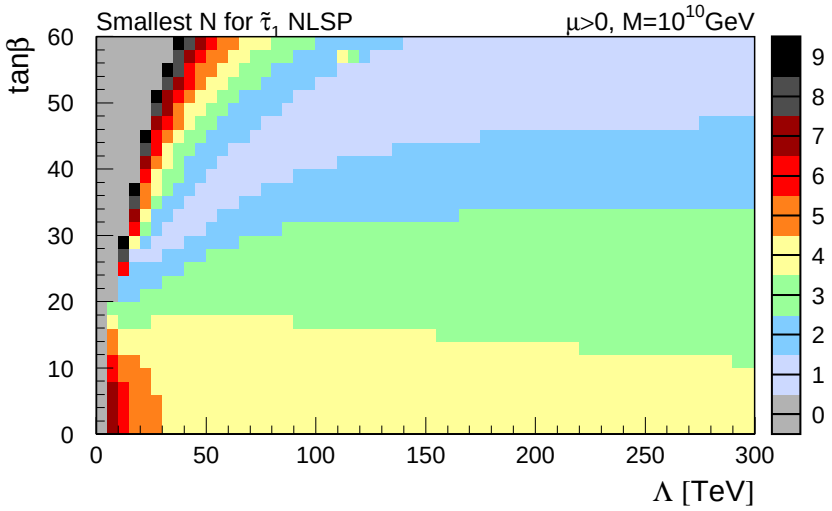

b)

Fig. 1. GMSB: the smallest index number N required to obtain a $\tilde{\tau}_1$ NLSP as a function of Λ and $\tan\beta$ for *a)* light messengers ($M = 2\Lambda$) and *b)* heavy messengers ($M = 10^{10}$ GeV). The colour coding is the same for both plots and corresponds to the legend shown with *b)*.

stable vacua and/or non-perturbative couplings at the GUT scale; no experimental or indirect constraints were included here.

With regard to dark matter, it is interesting to note that even in the presence of B-violation, the gravitino would still be stable and a dark-matter candidate, since no kinematically allowed decays would be available. For other possibilities for GMSB dark matter, see [39].

Finally, a long-lived $\tilde{\tau}_1$ is not the only SMP possibility in GMSB. If the mixing and consequently the mass splitting in the stau sector is not too large (small

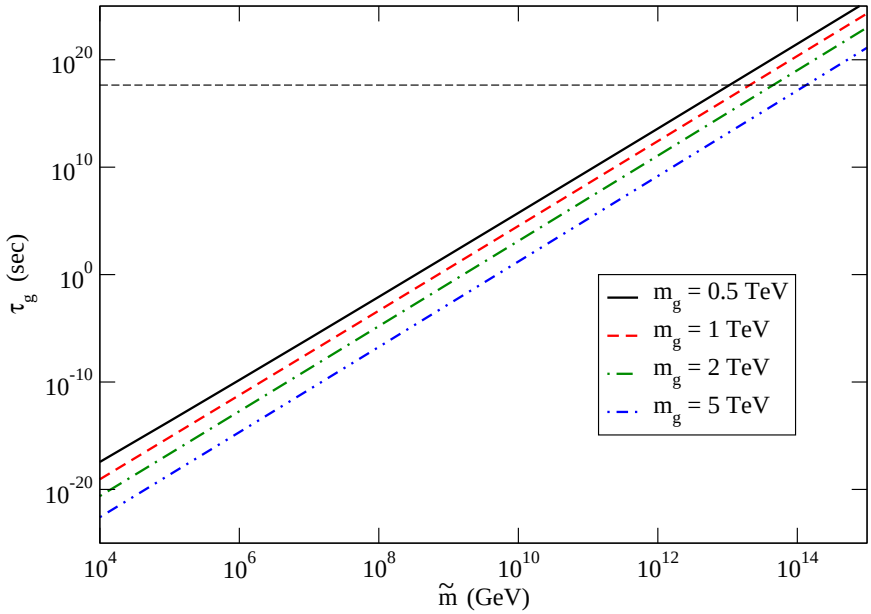

Fig. 2. The gluino lifetime in split SUSY as a function of the scalar mass parameter $\tilde{m}$ for $\tan\beta = 2$, $\mu > 0$, and various choices of the gluino mass, as calculated by [45]. The dashed horizontal line indicates the age of the Universe, $\tau_U = 14$ Gyr.

$\tan\beta \lesssim 8$ [42]), then the $\tilde{e}_1$ and $\tilde{\mu}_1$ may be nearly mass-degenerate (co-NLSP) with the $\tilde{\tau}_1$ and hence can simultaneously be SMPs. As with all supersymmetric scenarios, there is also a very large space of possible non-minimal models, cf. [39]. Of particular interest here are SUSY GUT extensions of GMSB in which the coloured messengers are naturally much heavier than their weak counterparts, resulting in a gluino NLSP [22–24] or even LSP [22–26], depending on the gravitino mass.

2.1.3 Split Supersymmetry

Meta-stable coloured sparticles also arise in the so-called split SUSY scenario [43,44], in which all the scalars (except the ordinary Higgs) have very large masses, while the gaugino and higgsino masses remain at or around the weak scale. Though the hierarchy problem is not addressed (except anthropically), this naturally suppresses both proton decay and CP and flavour violation. Since gluinos can only decay via squarks (independently of whether R-parity is conserved or not), the gluino lifetime can be very large in this scenario, somewhat similar to the case of the muon in the SM. The competing channels are tree-level 3-body decays to two quarks plus a chargino or neutralino and radiative 2-body decays into a gluon plus a neutralino, see [45] for explicit calculations or [46] for a simplified treatment. For illustration, in Fig. 2 we include a plot from [45] showing the gluino lifetime as a function of the scalar mass parameter $\tilde{m}$ for $\tan\beta = 2$, $\mu > 0$, and various choices of the gluino mass.

Another interesting possibility in split SUSY, which is not ordinarily viable, is that

SUSY-breaking could be communicated directly at tree-level [47, 48]. In this case, the scalar masses $\tilde{m}$ could be very close to the fundamental SUSY-breaking scale $\sqrt{F}$. Since the gluino decays via virtual squarks discussed above are suppressed by $\tilde{m}^{-2}$ and the coupling to the gravitino goes like $1/F$, this would open the possibility for a large branching fraction for gluinos to gravitinos, $\tilde{g} \to g\tilde{G}$ [45].

2.1.4 Other SUSY-breaking scenarios: AMSB, O-II, and $\tilde{g}$MSB

Anomaly mediated SUSY-breaking (AMSB, see [49–51]) is a variant of supergravity, where the explicit SUSY-breaking terms are 'switched off' (or at least heavily suppressed), leaving a scaling (conformal) anomaly in the supergravity Lagrangian as the sole source of supersymmetry breaking. This "anomaly-mediated" contribution is always present, but is usually much smaller than other supergravity terms. Akin to GMSB, its virtue is that it is flavour universal by construction. In its pure form, however, AMSB gives rise to tachyonic sleptons (negative $m^2_{\tilde{\ell}}$), hence, to obtain a viable phenomenology, additional positive lepton mass squared terms have to be included. The parameters of a minimal model are thus the gravitino mass $m_{3/2}$, the usual $\tan\beta$ and $\mathrm{sgn}(\mu)$, as well as additional soft SUSY-breaking masses for all sfermions m_0. The ratio of gaugino masses at the weak scale is approximately $|M_1| : |M_2| : |M_3| \sim 2.8 : 1 : 8$ [51], making the lightest chargino and neutralino nearly mass-degenerate and wino-like. For large m_0, the neutralino is the LSP, and hence the chargino can be long-lived. For small m_0 the LSP can be the $\tilde{\tau}_1$, except at small $\tan\beta$ and $m_{3/2}$ where it is the $\nu_{\tilde{\tau}1}$ [51]. For an LHC phenomenology study, see [52].

Another interesting explicit realisation of non-universal gaugino masses is furnished by the so-called O-II orbifold model, a string-inspired scenario in which supersymmetry breaking is dominated by the overall 'size' modulus field arising from the orbifold compactification [53, 54]. Gaugino masses arise at one loop, and a large degree of non-universality is generated naturally. The free parameters of a minimal model are m_0, $\tan\beta$, $\mathrm{sgn}(\mu)$, and δ_{GS}. The latter is called the Green-Schwarz mixing parameter and preferentially lies in the range $-5 \lesssim \delta_{\mathrm{GS}} < 0$, with the negative integers -4 and -5 preferred for the model studied in [54]. The mass spectrum depends sensitively on δ_{GS} but a typical feature, unless $|\delta_{\mathrm{GS}}|$ is very large, is $|M_1| \gg |M_2|$, resulting in a near-degeneracy between the lightest neutralino and chargino, both of which will be wino-like as in AMSB. Consequently, the chargino can be very long-lived. For $\delta_{\mathrm{GS}} = -3$, the gluino mass is zero at the high scale, $M_3^0 = 0$, and hence close to this value the gluino is typically the LSP [23, 54] or, slightly farther away from the minimum, nearly mass-degenerate with both the $\tilde{\chi}_1^+$ and the $\tilde{\chi}_1^0$. Note, however, that the other gauginos also have minima around $\delta_{\mathrm{GS}} = -3$, so the entire gaugino spectrum can become very light in this region.

In gaugino-mediated SUSY-breaking [55,56] ($\tilde{g}$MSB), the MSSM is embedded in a 5-dimensional compactified braneworld setup. The only non-vanishing soft SUSY-

breaking terms at the compactification scale, M_c, are the gaugino masses. In the original models, $M_c = M_{\rm GUT}$, which gives a $\tilde{\tau}_1$ LSP. The $\tilde{\mu}_1$ and $\tilde{e}_1$ are typically slightly heavier, due to the smaller mixing in the first two generations, but they can also be SMP candidates. Due to the obvious constraints from cosmology, most subsequent attempts have focussed on finding models beyond the minimal where a WIMP-like LSP could be recovered. In particular, if $M_c > M_{\rm GUT}$, then the extra GUT running from M_c (where the boundary conditions are true) to $M_{\rm GUT}$ (below which the SM running takes over) can generate non-zero scalar masses at the GUT scale [57–59], which may push the $\tilde{\tau}_1$ mass above the $\tilde{\chi}_1^0$ one. Another way of modifying the spectrum is by introducing non-universal gaugino masses, e.g. as in higher-dimensional GUT models where the extra dimension is larger than the inverse GUT scale, $M_c < M_{\rm GUT}$ [60], but except for small parameter regions the $\tilde{\tau}_1$ LSP still dominates. A Tevatron study of gaugino mediation can be found in [61]. The interesting case of a GMSB-like phenomenology could also be possible, with a gravitino LSP and the $\tilde{\tau}_1$ the NLSP [20], but detailed phenomenology studies have so far not been carried out.

2.2 SMP States in Universal Extra Dimensions

In models of Universal Extra Dimensions (UED) all the fields of the SM, including both matter and forces, are allowed to propagate in some number of extra dimensions, usually taken to be one or two. These models [62–64] provide an interesting scenario for TeV scale physics and are consistent with low-energy constraints [65]. The compactification is constructed such that momentum conservation in the extra dimensions is preserved at tree level, leading to a discrete Kaluza-Klein (KK) quantum number in the effective 4D theory. This quantum number is then broken to a KK parity at the loop level [64]. At least the lightest of the KK excitations of SM particles will thus be stable and can be a dark-matter candidate [66–68].

In the simplest analysis, all the KK modes of the light SM particles (the photon, gluon, and first generation fermions) may be sufficiently long-lived to be SMP candidates as well (they are stable at tree level and are almost mass-degenerate level by level), but note that the presence of non-zero boundary terms in the extra dimension(s) can change this picture drastically [69]. If small, these boundary terms can be treated perturbatively [70], but they are not calculable from fundamental principles and should be considered free parameters of the theory.

The Minimal UED (MUED) model with one extra dimension can be specified in terms of three parameters, R, Λ, and m_H, where R is the size of the extra dimension (an S^1/Z_2 orbifold stretched from 0 to πR), $\Lambda > R^{-1}$ is a scale at which the boundary terms mentioned above are assumed to vanish, and m_H is the mass of the (ground state) Higgs boson. The viable range of R found in [62] is $300\,\text{GeV} < R^{-1} < 10\,\text{TeV}$. For two extra dimensions [71] the lower bound becomes more

dependent on the compactification and ranges between 300 and 700 GeV, while for more extra dimensions a bound cannot be reliably estimated. See [72] for a Monte Carlo implementation of this model.

Finally, we note that a GMSB-like phenomenology with a stable KK graviton and a meta-stable next-to-lightest KK particle, e.g. τ_1, has also been considered, see [68, 73].

2.3 SMP States in other scenarios beyond the Standard Model (BSM)

We now turn to a brief overview of more exotic possibilities for SMP states in BSM physics. In particular, it is interesting to investigate the extent to which other models which have been proposed to address the dark-matter problem can also give rise to SMP states. We do not claim to be complete — model space is in principle infinite — nor do we give a detailed discussion of each scenario, but we hope to illustrate the spectrum of ideas, and where possible point the reader to relevant literature where further information can be found. Also keep in mind that for essentially all these scenarios, with the exception of leptoquarks and to a lesser extent Little Higgs models, no convenient package of collider phenomenology tools yet exists.

2.3.1 Models with parity-like symmetries

A class of models which have recently attracted attention is Little Higgs with T-parity (for recent reviews, see, e.g. [74, 75]). As with several of the other proposals discussed here, T-parity (not to be confused with time reversal) serves the dual purpose of simultaneously suppressing contributions to electroweak precision observables [76] and providing a WIMP–like dark-matter candidate [77], the "Lightest T-odd particle" (LTP). In the context of SMPs, however, minimal models do not have much to offer. The only corner of parameter space where the LTP can be charged and/or coloured [77], at large values of the symmetry-breaking scale f and small T-odd fermion masses $\tilde{m}$, roughly $f \gtrsim 1\,\text{TeV}$ and $\tilde{m} \lesssim 300\,\text{GeV}$, is excluded from Tevatron squark searches. It should be possible to construct more viable models with SMPs using non-universal $\tilde{m}_{\text{coloured}} > \tilde{m}_{\text{leptons}}$, but so far no explicit models in this direction have been constructed.

More exotic possibilities for supersymmetric SMP candidates also exist, in particular in models where the MSSM gauge groups and particle content are extended to include more superfields. A recent example is a variant of the so-called Fat Higgs model, based on the MSSM with an extra confining $SU(3)$ symmetry [78], the "Fat Higgs with a Fat Top" [79]. In this model, quasi-stable exotic chiral superfields (i.e. a complex scalar and a fermion) appear, which are charged under a global Z_2 symmetry, which makes them approximately stable. The strongly interacting ones

are probably outside the range of colliders, but there is a weak-scale electrically charged multiplet whose members have SMP properties [79].

In warped extra dimensions with "GUT parity" [80–83], the combination of extra dimensions and an effective TeV scale supersymmetric grand unification results in KK towers not only of the SM gauge and Higgs fields but also of their SUSY-GUT partners, including XY bosons and coloured Higgs multiplets. In models where the SM fermions also propagate in the bulk, add KK-towers for these and their SUSY-GUT partners as well. A parity can be chosen such that the MSSM particles are even and their GUT partners odd, hence the lightest "GUT-odd" particle (LGP) is stable or long-lived if this quantum number is conserved or approximately conserved, respectively. In the earliest scenario of [80], the LGP is typically a light isospin-up (-down) colour triplet XY gaugino, with electric charge -1/3 (-4/3), but in the more recent models [81–83] a wide range of possibilities are open.

In a recent 5D model [84] of dynamical SUSY-breaking (DSB), TeV scale exotic scalars with the quantum numbers of GUT XY bosons appear, so-called xyons. If a condition similar to R-parity holds in the DSB sector, these states are long-lived. Their precise quantum numbers depend on the details of the DSB — in general they are both coloured and charged. In the simplest $SU(5)$ case they lie in a colour triplet isospin doublet with electric charges $Q = -1/3, -4/3$, but also $SO(10)$ assignments are possible, for example an additional doublet with $Q = 1/3, -2/3$, could easily be possible. See [84] for mass spectra and phenomenology.

Finally, there also exist a few more general ideas for possible (quasi-)stable BSM particles, including long-lived leptoquarks (see, e.g. [85]) and additional (generations of) fermions [86, 87]. The latter can either be straightforward additions to the SM generations, e.g. a 4th generation with 4th flavour approximately conserved [88], or they can have a non-SM like structure. Mirror fermions (see, e.g. [89, 90]) are extra fermions whose right-chiral members lie in $SU(2)$ doublets while the left-handed ones are singlets, i.e. opposite to the SM. A 'vector-like' generation is comprised of an extra SM generation together with its mirror, as e.g. in $N = 2$ supersymmetric models [89, 91].

2.4 Models with gauged symmetries

When moving from global symmetries to local ones, several new possibilities open up. Even though explicit models are scarce, we shall still try to provide a reasonable overview and discussion.

Consider first the case of a new $U(1)_X$ gauge group. If X is conserved then a corresponding new massless exotic photon exists, γ' (or "paraphoton" [92]), which mediates a new long-range gauge force between particles charged under X. If any SM field is charged under X, then X must be $B - L$ [93], and the coupling is con-

$Q_{\rm em}$	$C_{\rm QCD}$	S	Model(s)
0	**8**	1	Universal Extra Dimensions (KK gluon)
± 1	**1**	$\frac{1}{2}$	Universal Extra Dimensions (KK lepton)
			Fat Higgs with a fat top (ψ fermions)
			4th generation (chiral) fermions
			Mirror and/or vector-like fermions
		0	Fat Higgs with a fat top (ψ scalars)
$\pm\frac{4}{3}$	**3**	$\frac{1}{2}$	Warped Extra Dimensions with GUT parity (XY gaugino)
		0	5D Dynamical SUSY-breaking (xyon)
$-\frac{1}{3}$,$\frac{2}{3}$	**3**	$\frac{1}{2}$	Universal Extra Dimensions (KK down, KK up)
			4th generation (chiral) fermions
			Mirror and/or vector-like fermions
			Warped Extra Dimensions with GUT parity (XY gaugino)
$\epsilon < 1$	**1**	$\frac{1}{2}$	GUT with $U(1) - U(1)'$ mixing
			Extra singlets with hypercharge $Y = 2\epsilon$
			Millicharged neutrinos
?	?	0/$\frac{1}{2}$/1	"Technibaryons"

Table 2
Examples of possible SMP states in a variety of models beyond the MSSM (for MSSM SMPs, see Tab. 1). Classified by electric charge Q, colour representation CQCD, spin S, and scenario.

strained to be extremely tiny $g_{B-L} \lesssim 10^{-19}$ [94]. Furthermore, only a state carrying a non-SM-like combination of quantum numbers could be stable, since it would otherwise decay to SM particles via prompt photon (or W/Z) emission. The stability would hence not rely directly on the smallness of g_{B-L} but rather on the conservation of other quantum numbers. We shall therefore not dwell on this possibility further.

The simplest is thus to postulate a genuinely new $U(1)_X$, with all SM particles having $X = 0$. The lightest $U(1)_X$ charged state would be absolutely stable (any instability would violate X), similarly to the electron, and if also charged under $U(1)_Q$ and/or $SU(3)_C$, an SMP. As above, even if a lighter electrical- and/or colour-neutral state with $X \neq 0$ also exists, the lightest charged one may still be long-lived, depending on what decay mechanisms are available.

A second possibility arises from kinetic mixing between the photon and paraphoton which implies that a particle charged only under $U(1)_X$ will appear to also have a

(small) coupling to the photon [92]. Experimental constraints on millicharged particles [3, 95, 96] leave a significant parameter space open, including a region of interest to accelerator searches, with relatively large charges $\epsilon \gtrsim 10^{-4}$ in units of the electron charge and masses $m \sim 0.1 - 1000\,\text{GeV}$, with the lower mass bound increasing rapidly above $\epsilon \sim 10^{-2}$. Recently, a 5-dimensional variant of this model has been proposed [97] in which the kinetic mixing, and hence the observable millicharge, is enhanced as compared to the 4D case.

In the Standard Model without an additional $U(1)_X$, two additional possibilities for millicharged states in principle exist. Firstly, additional $SU(3) \times SU(2)$ singlets with hypercharge $Y = 2\epsilon$ are not forbidden, but would be difficult to reconcile with grand unified theories [98] and suffer from much tighter experimental constraints than in the $U(1)_X$ case [96]. A small region of interest to accelerator searches still exists at large $\epsilon = 10^{-3} - 10^{-1}$ and moderate masses $m = 0.1 - 10\,\text{GeV}$. Secondly, though massless millicharged neutrinos could be generated by a redefinition of the SM hypercharge coupling, this is significantly more difficult in the massive case and also implies an unobserved proton-electron charge difference unless $\epsilon < 10^{-21}$ [99].

For a conserved non-Abelian gauge symmetry the phenomenon of millicharge is excluded and the only possibility is that the lightest state itself carries charge and/or colour, in addition to its exotic charge, X. The running coupling constant with N_{fX} exoflavours in $SU(N)_X$ is given by the β function (see, e.g. [100]):

$$\beta_0 = \frac{1}{(4\pi)^2} \frac{11N - 2N_{fX}}{3} \quad , \tag{3}$$

with $\beta < 0$ corresponding to a non-confining theory and $\beta > 0$ to an asymptotically free one. For example, QCD is asymptotically free for $N_f \leq 16$. Thus there are two distinct cases, one $U(1)$-like in which the exotic particles are not confined, and the second technicolour-like, in which the exotic particles first "hadronise" among themselves into composite states of zero total X. Mesonic X-hadrons would normally decay rapidly, but the lightest totally antisymmetric $SU(N)$ state (the X-proton) could be stable if an analogue of Baryon Number conservation holds in the new sector (see, e.g. [101, 102]). A QCD hadronisation would then follow, neutralizing any leftover colour. Some similarity to this picture is found in the hidden-valley models of [103], though mainly neutral exotics are considered there.

Finally, we note that if the new gauge symmetry is broken, then it is hard to see how the new states charged under it could be stable, since there should be interactions which violate the conservation of the corresponding charge. For the state to be long-lived *and* light, it would have to be an analogue of the muon, which has a small mass due to a small coupling with the relevant symmetry-breaking sector (the Higgs), but simultaneously a long lifetime due to the gauge boson (the W) having a much larger mass.

2.4.1 Magnetic Monopoles

All particles so far observed possess values of magnetic charge consistent with zero. The magnetic charge of the electron is constrained by experiment to be $q_e^m < 10^{-24} g_D$ [104], where g_D is the elementary (Dirac) magnetic charge. However, in spite of a plethora of experimental evidence to the contrary, strong theoretical arguments continue to motivate searches for magnetic monopoles.

A potent motivation for searching for monopoles was given by Dirac in 1931 [105, 106]. Dirac demonstrated that the existence of only one monopole is necessary to accommodate electric charge quantisation within quantum electrodynamics (QED). In a modern form of Dirac's argument [107], the quantisation of the total angular momentum in the field of a system of an electric charge q and a monopole with magnetic charge g leads to the quantisation condition $qg = \frac{nhc}{4\pi}$. Here h is Planck's constant, c is the speed of light in vacuum, and n is a quantum number. Taking $q = e$ as the elementary electric charge, $n = 1$ sets the theoretical minimum magnetic charge which can be possessed by a particle, $g_D = n\frac{137}{2}e$. A particle with magnetic charge g_D is known as a Dirac monopole. The value of the minimum magnetic charge has profound implications for the construction of a theory of high-energy monopole scattering. The magnetic fine structure constant for a Dirac monopole is $\alpha_m \approx \frac{137}{4}$, rendering perturbative field theory inapplicable. This has implications for the reliability of models of monopole production at colliders and for the exclusion limits, as described in Sections 4.6 and 7.2, respectively. A further consequence is that a Dirac monopole will be largely equivalent to an electrically charged particle with charge $\sim \frac{137e}{2}$ in terms of the electromagnetic force it exercises and experiences. This implies that a Dirac monopole will suffer a huge electromagnetic energy loss in matter compared with a minimum ionising particle (MIP). This is discussed further in Section 5.1.2.

Although experiments typically search for Dirac monopoles there are a number of reasons why alternative values of the minimum charge may be favoured. If the elementary electric charge is considered to be held by the down quark then the Dirac condition implies that the minimum magnetic charge could be $3g_D$. However, it has been argued that the Dirac condition is not appropriate for a confined quark [2, 108, 109] and an observed minimum charge of $3g_D$ may suggest the existence of isolated particles with charge $\frac{1}{3}e$ (free quarks). The existence of isolated millicharged particles could imply a minimum charge which is higher still. The value of the fundamental charge is also affected if the Dirac argument is applied to a particle possessing both electric and magnetic charge. Such a particle is known as a dyon [110–115] [2]. It has been speculated that a dyon could exist either as a fundamental particle or as a composite of two particles, one of which possesses electric and the other magnetic charge. Schwinger argued that generalising the Dirac condi-

[2] Unless made clear by the context, the term monopole is used to refer to both magnetic monopoles and dyons in this paper.

tion for a dyon restricts values of n to be even [110–112]. It is therefore important that searches are sensitive to as wide a range of magnetic charge as is experimentally possible.

While the Dirac argument provides strong motivation for the existence of monopoles it gives no prediction of the likely monopole mass. Naive arguments based on the classical radius of a Dirac monopole would suggest a mass of the order of a few GeV [116]. However, as long as the production cross section is not vanishingly small, such a low-mass monopole would long ago have been discovered at colliders. The available window in mass for Dirac monopoles is largely determined not by theoretical arguments but the results of the searches which are described later in Section 7.2.

A further motivation for monopole hunting is provided by their presence in grand unified theories (GUTs). 't Hooft and Polyakov showed that monopoles possessing the Dirac charge, or multiples of it, arise as topological defects of space–time. They occur when a simple gauge group is spontaneously broken into an exact $U(1)$ subgroup [117, 118]. This would occur, for example, in the phase transition

$$SU(5) \rightarrow SU(3) \otimes SU(2) \otimes U(1) \rightarrow SU(3) \otimes U(1) \tag{4}$$

The spontaneous symmetry-breaking mechanism generates vector bosons X with masses, m_X. The monopole size R_m can be related to the boson mass via $R_m \sim m_X^{-1}$ and the monopole mass is $m_m \sim \frac{g_m^2}{R_m} \sim \frac{m_w}{\alpha}$, where α is the common gauge coupling at unification energy. Here, m_X is typically of the order of 10^{15} GeV, implying a super-heavy monopole of around $10^{15} - 10^{16}$ GeV.

In addition to massive GUT monopoles, it has also been postulated that lighter monopoles can be produced through other symmetry-breaking schemes. So-called intermediate-mass monopoles (IMMs) with masses between 10^7 and 10^{14} GeV have been proposed [119, 120]. These could occur in models containing a more complicated gauge group than $SU(5)$, such as $SO(10)$. Both GUT monopoles and IMMs are beyond the reach of accelerator searches. Such monopoles are sought as primordial relics, which could be be bound in matter or found in cosmic rays [121–124].

To obtain lower-mass gauge monopoles, to which accelerators could be sensitive, requires their production via the electroweak symmetry-breaking mechanism. Contrary to earlier work, which asserted that the Weinberg-Salam model could not admit monopoles [125, 126], it has been established that monopole solutions are possible [127–129]. Furthermore, it has been proposed that monopoles may possess masses as low as ~ 1 TeV if the coupling strength of the quartic self-coupling of W-bosons was modified, or the group $SU(2) \otimes U(1)$ is embedded into a larger gauge group [130]. However, as the authors of this work point out, there are theoretical difficulties with this approach. For example, the modification of the Lagrangian may spoil the renormalisability of the Weinberg-Salam model.

In higher-dimensional theories such as string theory, space–time is often compactified on a topologically non-trivial manifold. This naturally leads to a vacuum structure suitable for many different kinds of defects, including monopoles. For example, in Ref. [131] a magnetic monopole solution is presented in the context of heterotic string theory. The mass of this monopole is related to the size of the compact space, the string length and coupling. Since these parameters combine to determine the low-energy Planck mass and gauge coupling, the mass is constrained to be rather large, within a few orders of magnitude of the Planck scale.

Given the large amount of freedom in higher-dimensional theories with regard to the size, dimension and topology of the compact space it is not unrealistic to believe that there may be monopole solutions with correspondingly low masses, so that they may be discovered at the LHC.

It should be noted that Dirac monopoles differ from monopoles expected from gauge-symmetry breaking. Whilst Dirac monopoles are considered point-like, gauge monopoles are expected to have a size $R_m \sim \frac{1}{m_X} \sim 10^{-31}$m (for GUTs) and to possess a complicated structure of vacuum particles surrounding it. It has been argued that, compared to point-like monopoles, the production of gauge monopoles from particle collisions will be suppressed by a factor of $\geq 10^{30}$ due to form factors [132].

2.4.2 Q-balls

Q-balls represent a further possibility of producing topological SMPs. The fastest way to understand what they are is to consider a theory of charged scalars with SO(2) internal symmetry, in other words a two dimensional internal space of scalar fields ϕ_1 and ϕ_2 with a potential which is only a function of $\phi = \sqrt{\phi_1^2 + \phi_2^2}$. We assume that ϕ is constant within a (real space) sphere of radius R and zero outside that sphere. If ϕ_i is rotating around the internal SO(2) symmetry with a specific angular frequency ω, then the conserved charge Q is given by

$$Q = \int d^3x \left[\phi_1 \partial_0 \phi_2 - \phi_2 \partial_0 \phi_1\right] = \frac{4\pi}{3}, R^3 \omega \phi^2 \tag{5}$$

whereas the energy E is given by

$$E = \frac{4\pi}{3} R^3 \left(\frac{1}{2}\omega^2 \phi^2 + V\right), \tag{6}$$

where V is the potential of ϕ. Using Eq. 5 to replace ω in Eq. 6, it is clear that there is a certain radius R at which the energy is minimised, and at this minimum $E = Q\sqrt{2V/\phi^2}$. This field configuration or "Q-ball", could decay by emitting the basic scalar particle associated with the equations which has unit charge and mass $m^2 = \partial^2 V/\partial\phi^2|_{\phi=0}$. However the energy per unit charge of the configuration will

be $E/Q = \sqrt{2V/\phi^2}$, so that if the mass of the scalar $m > \sqrt{2V/\phi^2}$, the Q-ball will not be able to decay into these scalar particles [133–137]. Many potentials have characteristic logarithmic one-loop corrections which allow $m > \sqrt{2V/\phi^2}$, not least in SUSY. There are examples of Q-balls in both gravity mediated [138] and gauge mediated [139] SUSY-breaking models. For generic values of the parameters in these models, Q-balls must have rather large masses, much higher than the electroweak scale, in order to be stable [140, 141].Although they may be created at the end of inflation, it is less likely that they would appear at the LHC. However, if present, they could manifest themselves as very highly ionising particles. Coupling the scalar field to fermions can make the Q-ball unstable, since decay into those fermions would be possible [142].

3 Cosmological implications of SMPs at colliders

If stable or quasi-stable particles are produced at the LHC, they will also have been produced in the early universe. If they are unstable, the lifetime of those particles then determines at which cosmological epoch they will decay. Such decays generically involve the creation of energetic SM particles, which cause a variety of problems that we outline below. In this way one can put constraints upon the regions of parameter space where quasi-stable objects might be created.

If there are relic stable or quasi-stable particles which are produced in the early universe then they fall into three broad categories:

- particles which serve as dark-matter candidates.
- particles which are ruled out since their presence or decay is in one way or another incompatible with what is observed (see below).
- particles which exist in such small quantities that they do not serve as dark matter candidates and have not yet been detected.

Of particles which appear in extensions of the SM, very few fulfill the criteria necessary to fall into the first category whereas very many fall into the second or third.

“Incompatible with what is observed” can have several meanings, the first being due to general relativity. The Friedman-Robertson-Walker solutions of Einstein’s equations tell us that the rate at which the universe expands depends upon the energy density of the contents of the universe. One way a relic particle could be incompatible with what is seen is that the presence of that particle would change, via gravity, the expansion history of the universe in a way which would be contrary to the expansion history derived from observations. The second possible meaning is that the particle would decay and its decay products would destroy the observed light elements (which are formed in the first few minutes after the Big Bang) or

be visible today, for example in the form of gamma rays. A third possible meaning is that the particle should have already been detected experimentally by magnetic monopole detectors, searches for anomalous isotopes or other experiments of that nature. Finally the particle might exist in such an abundance that it gives the correct expansion history gravitationally, but its interaction with itself or SM particles is such as to rule it out as a dark-matter candidate.

We will introduce the current state of cosmology before outlining the known properties of dark matter. We will then discuss the constraints upon two supersymmetric candidates for quasi-stable objects, which could be produced at the LHC, namely gluinos and sleptons. Then we will summarise the constraints from cosmology and astrophysics upon magnetic monopoles. Finally we will discuss the implications for cosmology if a charged massive stable object is produced at the LHC.

3.1 Cosmology Overview

Here we will describe briefly how the energy of the universe is divided between normal matter, dark matter, and dark energy in a way relevant for the subsequent discussion of SMPs at colliders. For more in depth reviews of cosmology see e.g. [143].

The ratios between the abundances of light elements such as hydrogen, helium, and lithium in the universe depend upon the baryon to photon ratio roughly one minute after the Big Bang [144]. By comparing their observed abundances with the number of photons we observe in the cosmic microwave background (CMB) today, we can obtain the number of baryons in the universe. One can also measure the abundance of baryons using the CMB alone [145].

General relativity provides us with the relationship between the expansion of the universe and the density of matter inside it [143]. The density in the form of baryons is not enough to explain the observed expansion measured by, for example, the Hubble Space Telescope [146]. Furthermore, there appears to be invisible matter in galaxies and clusters of galaxies, the presence of which is deduced from the motion of gas and stars in those objects [147, 148]. Studies of the clustering of galaxies predict that there is 6-8 times as much dark matter as there is baryonic matter [149, 150]. Observations of type 1a supernovae tell us that the universe recently started to accelerate [151, 152].

The conclusions drawn from these different observations are the following - around 95% of the energy density in the universe is non-baryonic and it couples at most weakly to SM particles so that it cannot be seen. Roughly one third of it is dark matter while the other two thirds does not dilute quickly as the universe expands, i.e. it is dark energy rather than dark matter. At the time of writing, dark energy does not appear to be related to particles produced at the LHC in any direct way and we

shall not discuss it further. The identity of the dark matter however is obviously closely related to the rest of this review. Dark-matter particles may be produced at the LHC, so the more we can learn about their behaviour and properties from cosmology, the easier it will be to find them.

If stable massive particles are discovered at the LHC, their couplings and masses should not be such that they are over-produced in the early universe. If there is too much matter in the universe, then the radiation-dominated regime would finish earlier and the universe would be younger by the time the CMB had been redshifted to the temperature that we see today. The universe needs to be at least around 12×10^9 years old since observed objects such as globular clusters are at least that old. Together with structure formation, this limit provides strong constraints upon the over-production of new forms of matter (see e.g. [153]).

3.2 Constraints on the basic properties and interactions of dark matter.

Before we look at possible particle candidates for the dark matter in the universe, it is interesting to summarise the information we have about its properties.

3.2.1 Cold dark matter

By definition, dark matter is at most weakly coupled to Standard Model fields so it can only have been produced in the early universe. The simplest mechanism for dark-matter production is to have the relics be in thermal equilibrium with the rest of the (standard model) plasma at early times. We can use crossing symmetry to relate the annihilation rate to the production rate. The criterion for thermal equilibrium is that this annihilation rate, which depends upon the coupling and mass of the dark-matter candidate, is comparable to the inverse timescale of the expansion of the universe, which depends only, via gravity, upon the energy density of the universe. This means that the universe will not change its size or temperature much over the timescale of the particle interaction or decay rate. The dark matter observed in the universe today is probably cold, meaning that it was non-relativistic at the temperature at which it came out of thermal equilibrium or 'froze' out of the plasma. In contrast, the upper bound on the neutrino mass [154] tells us that neutrinos were relativistic until rather late times, at most just starting to slow down at matter-radiation equality. Indeed, depending upon the mass hierarchy, some of the neutrino species may still be relativistic today. Such fast-moving or hot dark-matter candidates will be able to escape all but the largest collapsing structure in the universe, so structure formation in a universe with hot dark matter would start with the largest structures forming first.

Observations suggest that the opposite is true, and that the smallest structures form first [150] indicating that the dark matter was non-relativistic in the early universe.

This provides us with information about the coupling of the particle to the Standard Model (annihilation rate) and the mass of the particle: the annihilation rate should still be large at temperatures when the particle is not extremely relativistic.

Strictly speaking however, the fact that dark matter is cold does not mean that it had to be non-relativistic at freeze-out; its kinetic energy may have been red-shifted away by the expansion of the universe between freeze-out and the epoch at which structure formation begins when the universe becomes matter-dominated, a few thousand years after the Big Bang. Because of this, one can obtain cold dark matter candidates with masses at least as low as the MeV range [155] and probably even lower. Most models of cold dark matter under consideration today involve particles with masses in the GeV to TeV range, and the combination of this mass range with the coupling that will give good relic abundance means that it is possible that they could be created at the LHC [156] (one notable exception is the axion [157]). Cold dark-matter candidates which interact weakly with Standard Model particles are called weakly interacting massive particles or WIMPS.

3.2.2 Warm dark matter

Dark-matter haloes in computer simulations have steeply varying density profiles in the core, so that typically one would expect that the density of dark matter $\rho \propto r^{-\gamma}$ where r is the radius from the centre of the halo, and γ typically has values between 1 and 1.5 [158, 159]. However, reconstructions of the distribution of dark matter based upon observations of low surface brightness galaxies suggest a much less steep density profile. Such galaxies seem to possess an approximately constant density core of dark matter [160]. Another discrepancy is that there are many more satellite galaxies (smaller galaxies like the Magellanic clouds) produced in N-body simulations of cold dark-matter universes than are observed in nature (for instance, in the vicinity of the Milky Way) [161]. There are a number of people who have suggested that these discrepancies can be explained if the dark-matter candidate is 'warm', in other words half way between cold and hot dark matter [162]. This latent thermal energy would smooth out the central density cusps.

A warm dark-matter candidate produced thermally would usually have a much smaller mass than a GeV, so the prospects for dark-matter physics at the LHC would change considerably. There is the possibility that weakly interacting neutralinos are produced non-thermally just before nucleosynthesis [163] so that they could be fast moving during structure formation, but producing a relic density of neutralinos in this way ignores the fact that one can obtain the correct relic density thermally without too much fine-tuning. There are equally a number of people who think that these discrepancies between observations and computer simulations may be explained using astrophysics rather than changing the properties of cold dark matter [164].

3.2.3 Dark-matter self-interaction

Constraints upon the self-interaction of dark matter can be obtained by looking at colliding galaxy clusters. The bullet cluster is an example of two galaxy clusters colliding, the hot gas forming shock waves at the interface [165]. Gravitational lensing shows that the two dark-matter populations have moved through each other without forming shocks as far as can be observed. This allows one to place (mass dependent) constraints upon the self-interaction cross section of dark matter of $\sigma/M < 2$ barn/GeV. This is actually rather a large cross section in terms of what we are familiar with in the Standard Model, for comparison $\sigma_{QCD} \sim$ barn (at MeV energies). Some authors have in fact suggested that the dark matter does interact with itself, and that this feature solves some of the same problems which people try to solve using warm dark matter [166] (see the previous subsection). One might therefore think that a colour-singlet particle with a typical QCD cross section $\sigma \sim \Lambda_{QCD}^{-2}$ (for example, perhaps some kind of glueball) might be a viable cold dark-matter candidate. However, the constraints on the interaction between dark matter and baryonic matter are much stronger (as we shall see in the next section).

3.2.4 Dark-matter coupling to Standard Model particles

The coupling of the dark matter to SM particles is constrained experimentally in two basic ways. The first is by direct experiments, which are looking for momentum exchange between the dark matter and sensitive detectors such as CDMS, CRESST, DAMA and ZEPLIN [167–170]. Observations of rotation curves of the Milky Way suggest that the density of dark matter near the earth is approximately 0.3 GeV cm^{-3} and the velocity corresponding to the gravitational potential of the Milky Way is around 200 km s^{-1}. These numbers are based upon the assumption of a smooth dark-matter halo and could turn out to be (locally) wrong by more than an order of magnitude. Using these numbers, the experimental status is outlined in Fig. 3 and the low-energy cross section between a 100 GeV dark-matter particle and a nucleon is constrained to be less than $\sim 10^{-43}$ cm^2. A heavy particle produced at the LHC undergoing Standard Model strong or electromagnetic interactions cannot therefore be a dark-matter candidate.

The annihilation of dark-matter particles into Standard Model particles determines the rate of interaction of dark matter with the rest of the plasma and hence determines if the dark matter is in thermal equilibrium with the rest of the universe or not [143]. When the dark matter goes out of thermal equilibrium, it essentially stops interacting and its number density becomes constant (more precisely the number density per co-moving volume - the universe is expanding, so the actual number density will decrease due to dilution).

The analysis of the three-year WMAP data tells us that the density of dark matter is

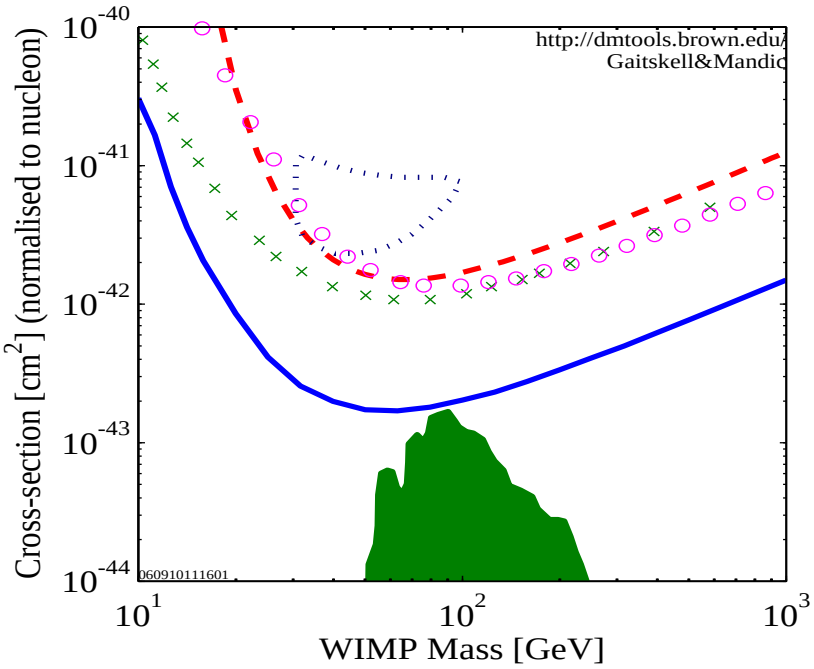

Fig. 3. Constraints upon direct detection of dark matter [167–171]. The red dashed curve is from CRESST, purple circles are from Edelweiss 1, green crosses are from ZEPLIN 1 and the solid blue curve is from CDMS. The region enclosed by dashes is the claimed detection from the DAMA collaboration which does not seem to be confirmed by the other experiments. The dark green filled region are a set of example SUSY models from Ref. [172].

$\Omega_{DM}h^2 = 0.102 \pm 0.009$ where Ω_{DM} is ρ_{DM}/ρ_{crit}, ρ_{crit} is the density corresponding to a flat universe [143] and h is the Hubble constant in units of 100 km s^{-1} Mpc^{-1}. In order to obtain this relic density, the thermally averaged cross section for dark-matter self-annihilation into Standard Model particles should be [173]

$$\Omega_{DM}h^2 \sim \frac{3 \times 10^{-27}\mathrm{cm}^3\mathrm{s}^{-1}}{\langle\sigma v\rangle} \tag{7}$$

so that $\langle\sigma v\rangle \sim 3\times10^{-26}\mathrm{cm}^3\mathrm{s}^{-1}$ is favoured. A cold dark-matter candidate produced at the LHC should therefore have this annihilation cross section. This quantity leads us to the second method of measuring the coupling of dark matter to Standard Model particles, namely through the search for the annihilation or decay products of dark matter coming from high-density regions such as the centre of galaxies [174]. Since the WMAP results give us rather good information about $\langle\sigma v\rangle$, the uncertainties in this approach lie in the lack of knowledge of the exact density of dark matter in dense regions such as the centre of galaxies and in separating the signal from dark-matter annihilation from possible background signals.

3.2.5 Dark matter at the LHC

In Section 2 we have learnt about a number of dark-matter candidates. The most common SUSY candidates in the literature are neutralinos. These are WIMPS, which are deemed attractive candidates for dark matter since there is considerable parameter space in SUSY models where these particles have annihilation cross sections rather similar to what is required to obtain the abundance suggested by WMAP, as described in Eq. 7 [173, 175].

Universal extra dimensions also provide a natural dark-matter candidate if radiative corrections make the lowest excitation of the hypercharge gauge boson B the lightest KK mode [176]. KK modes of other species will decay into the lightest mode by emitting zero mode excitations, in other words normal SM particles. The lightest mode is stable and if it is aslso weakly interacting it can be a good WIMP candidate. There are tight constraints upon the radius and the number of compact dimensions if this kind of UED KK dark matter is to provide us with the correct abundance, in particular a KK mass around a TeV is favoured, which is encouraging for LHC studies. If the lightest KK mode turned out to be a particle with EM or colour charge rather than the photon then it would be difficult to see how UED could remain a good candidate for dark matter.

There is a large amount of literature on WIMPS (see e.g. [173–175, 177] and references therein) and since they are only weakly charged we will not concentrate on them here. They do however form candidates for the LSP in SUSY models when the NLSP is a charged particle, which then decays into neutralinos.

3.3 Cosmological constraints on quasi-stable sleptons

As described in Section 2 if the LSP is the gravitino and the NLSP is the stau, i.e. the scalar super-partner of the tau lepton, then the lifetime for the stau decay into tau lepton plus gravitino will be relatively large due to the Planck-suppressed couplings to the gravitino [178].

The gravitino itself is a perfectly good cold dark-matter candidate, although it would be impossible to observe through its coupling to the Standard Model fields. There is however a potential problem with gravitino dark matter related to nucleosynthesis.

The epoch of nucleosynthesis in the early universe occurred when the temperature was low enough for photodisintegration of nuclei to have ceased but high enough for nuclear fusion reactions to occur. Protons and neutrons interchange regularly due to beta and inverse beta decay driven by the background thermal bath of neutrinos and electrons. Eventually the plasma becomes cool enough for various light elements and isotopes such as deuterium, helium-3 and 4, and lithium-6 and 7, to

form.

Nucleosynthesis gives very specific predictions for the ratio between the light elements H, He, D, Li etc. that one should observe when one makes observations of the abundance of these elements in regions of the universe where they have not been processed in stars.

The strongest constraint upon the quasi-stable stau comes from this observed light element abundance. If the decay of the slepton into lepton plus gravitino takes place during or after nucleosynthesis then energetic particles will be injected into the plasma, leading to various effects such as the dissociation of these light elements.

In particular, the injection of energetic protons into the plasma due to the decay of unstable relic particles will lead to the reaction $\mathrm{p} + {}^4\mathrm{He} \rightarrow {}^3\mathrm{He} + \mathrm{D}$ which increases the abundance of deuterium [179, 180]. This deuterium can also subsequently interact with helium to increase the abundance of ${}^6\mathrm{Li}$.

The ${}^3\mathrm{He}/\mathrm{D}$ ratio is a strong function of the decay of the slepton into gravitino [181] and the observed value of ${}^3\mathrm{He}/\mathrm{D}$ restricts the stau mass $m_{\tilde{\tau}}$ to be greater than about $5m_{\tilde{G}}$ for $m_{\tilde{\tau}} \sim 500$ GeV or $20m_{\tilde{G}}$ for $m_{\tilde{\tau}} \sim 100$ GeV. This cuts into the interesting region for collider searches. For instance, one can in principle reconstruct the gravitino mass by simply measuring the mass of the stau and the energy of the emitted tau [178]

$$m_{\tilde{G}}^2 = m_{\tilde{\tau}}^2 + m_{\tau}^2 - 2m_{\tilde{\tau}}E_{\tau} \tag{8}$$

but $m_{\tilde{G}}$ can only be measured in this way if it is not too small. Since the constraints from light element abundance restrict the gravitino mass for a given stau mass, much of the interesting parameter space is ruled out. One way of avoiding this is for there to be entropy production at some temperature below the freeze-out of staus from the plasma and the era of nucleosynthesis. Such entropy production will increase the number of relativistic particles in the plasma and effectively dilute the sleptons, so that when they do decay, their effect upon the light element abundances is diminished. We will mention this more in Section 3.5.

3.4 Stable and quasi-stable gluino

In this section we present the cosmological constraints upon the stable and quasi-stable gluino.

3.4.1 Stable gluino

The case of the stable gluino is presented in detail in Ref. [23]. If the gluino is the LSP then the relic abundance is calculated by obtaining the thermally averaged annihilation rate and comparing it to the expansion of the universe, giving the

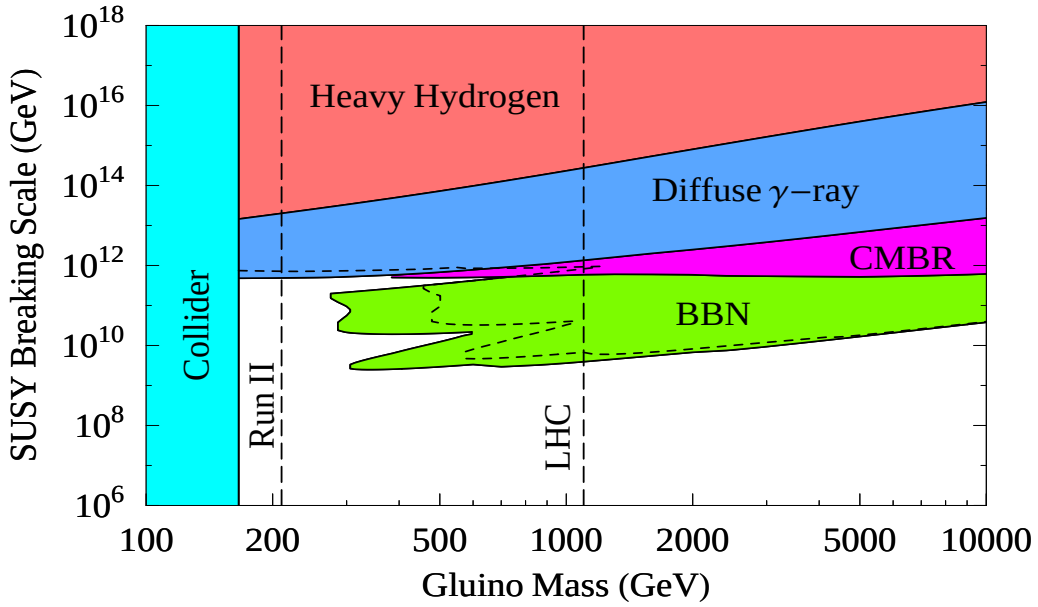

Fig. 4. Constraints upon the gluino mass and SUSY breaking scale parameters in models of split supersymmetry. Shaded regions are ruled out by different cosmological observations. The tightest constraints come from the diffuse gamma ray background for $m_{\tilde{g}} < 300$ GeV and from Big Bang nucleosynthesis (BBN) for $m_{\tilde{g}} > 300$ GeV. The plot is taken from Ref. [180].

approximate result

$$\Omega_{\tilde{g}} h^2 \sim \left(\frac{m_{\tilde{g}}}{10\mathrm{TeV}}\right)^2 . \tag{9}$$

The stable gluino could not be the dark matter as its coupling with Standard Model fields is greatly in excess of cross sections that are already ruled out (see fig. 3). We therefore require $\Omega_{\tilde{g}} h^2 \ll 0.1$, giving a maximum mass for the gluino of a few TeV. These gluinos will be captured by nuclei, leading to the possible detection of (highly) unusual isotopes of nuclei [182]. Non-observance of these isotopes restrict values of $m_{\tilde{g}} \geq 100$ GeV although non-perturbative effects could change the values predicted by equation (9).

3.4.2 Quasi-stable gluino

The constraints upon the quasi-stable gluino come from the same places as the constraints upon the slepton described in the previous section. We have seen in some versions of split supersymmetry [183] that gluinos can be produced which then decay outside the detector. The lifetime of these gluinos is given by

$$\tau = 3 \times 10^{-2}\mathrm{s} \left(\frac{\mathrm{m_S}}{10^9\mathrm{GeV}}\right)^4 \left(\frac{1\mathrm{TeV}}{\mathrm{m_{\tilde{g}}}}\right)^5 \tag{10}$$

where m_S is the scale of supersymmetry breaking, which is typically very large in these models, $\gg 10^{10}$ GeV. The gluino lifetime as function of m_S is displayed in

Fig. 2. As for the stable gluino, constraints from the non-observance of anomalous isotopes become stronger as one raises the energy of m_S, since the anomalous isotopes will be increasingly stable for cosmological time-scales. Fig. 4 shows how different cosmological constraints rule out values of m_S which depend upon $m_{\tilde{g}}$, for example, m_S must be less than 10^{13} GeV for a gluino mass $m_{\tilde{g}} \sim 200$ GeV or less than 10^{16} GeV for $m_{\tilde{g}} \sim 10$ TeV [180].

As one lowers the value of m_S, the lifetime of the gluino falls, and the annihilation products become progressively more troublesome for cosmology. As one would expect, as the lifetime drops, the time at which the strongest constraints emerge relates to progressively earlier epochs in cosmology. For example, at values of m_S, lower than those ruled out by searches for heavy isotopes, the parameter space is ruled out through constraints upon the diffuse gamma-ray background today made by the EGRET gamma ray observatory [184, 185].

Values of m_S greater than about 10^{12} GeV are ruled out since the decay of such gluinos would lead to distortions in the thermalisation of the CMB before recombination. The CMB is the radiation remaining from the time when the temperature of the universe decreased such that the mean free path for photons approaches infinity. At this epoch, a few hundred thousand years after the Big Bang, the universe becomes transparent. The CMB is the most perfect blackbody ever observed, so distortion of the spectrum by the injection of high-energy photons into the plasma leads to strong constraints [186].

Finally gluinos with very short lifetimes will, like the unstable stau, cause problems for light-element abundance. The decaying gluinos will photo-dissociate the light elements left over after nucleosynthesis although for $m_{\tilde{g}} < 300$ GeV the gluino lifetime is long enough to avoid the nucleosynthesis constraint [180].

Very roughly, the combined constraints upon the gluino are as follows - if the gluino mass $m_{\tilde{g}} < 300$ GeV then the SUSY scale $m_S < 10^{12}$ GeV whereas if $m_{\tilde{g}} > 300$ GeV then $m_S < 10^{10}$ GeV.

3.5 Consequences of the observation of a charged stable object at the LHC

3.5.1 Electrically charged particles

If a charged massive stable object is discovered at the LHC then it may be very interesting for cosmology. If the object were truly stable, then it would be difficult to understand why it is not observed today. We have already discussed that such a charged object could not be the dark matter. On the other hand, if the object were found to possess a lifetime such that one would expect its decay to be problematic for nucleosynthesis or the CMB, or that it would overproduce gamma rays, again it would be difficult to understand.

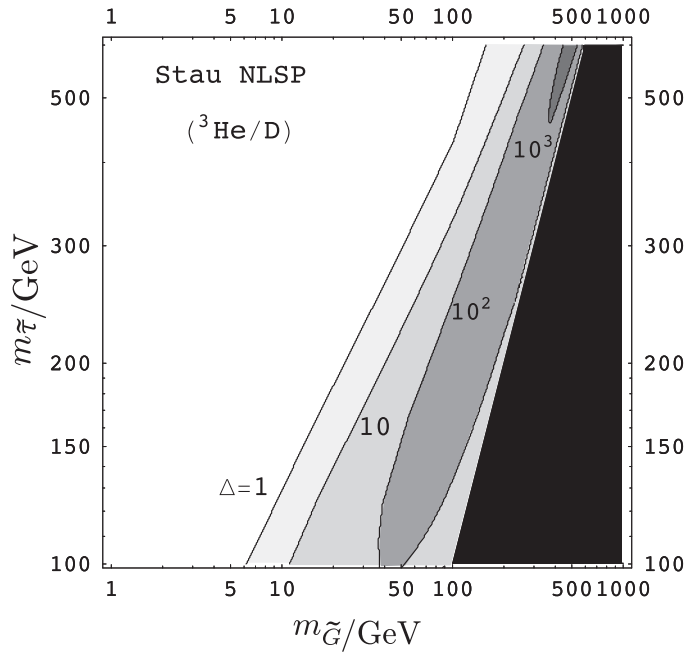

Fig. 5. Amount of entropy which needs to be produced in order for the unstable stau to be consistent with nucleosynthesis constraints, see Eq. 11. Plot taken from [181].

If such a situation were to arise, it would be necessary to invoke a mechanism, which would dilute the density of the relic. Let us call our problematic charged stable particle X. If there were another species of particle Y, which decayed in between the time at which the stable relic X froze out of the plasma and the time at which it (X) causes problems (by decaying or by not being observed), then it might be possible to dilute the particle. The decay of the particle Y may produce more light particles such as photons, thereby reducing the number density per photon of the dangerous relic X. Another way of looking at this is to say that the decay of particle Y into light particles temporarily stops the temperature in the radiation bath from dropping as the universe expands. At the same time, the number density of particle X *would* drop as it is no longer in equilibrium with the radiation bath but has already frozen out. In each particular scenario, the dangerous relic particles would have to be diluted by a factor Δ in order for their decay not to be dangerous for light element abundance. The dilution of the dangerous X particle (in this case the stau) is written

$$\frac{n_{Xbefore}}{s} = \frac{1}{\Delta}\frac{n_{Xafter}}{s} \tag{11}$$

where n_X is the number density of the X particle and s is the entropy density, which is roughly equal to the number of relativistic particles in the plasma per unit volume. As an example, Fig. 5 shows the amount of entropy, written as the required value of Δ, which should be produced after freeze-out in order for the unstable stau described in Section 3.3 to be compatible with constraints from light element abundance [181].

Another effectively equivalent way of diluting the density of a stable relic is via inflation and reheating. In principle there could be a period of inflation at an energy scale lower than that of the LHC. However, if this period of inflation were driven by an inflaton it would have to be rather strongly coupled to the Standard Model particles in order to achieve thermalisation before the beginning of nucleosynthesis (see however [187–189]).

3.5.2 Magnetic monopoles

Theories which contain the possibility of spontaneous breaking of some gauge symmetry to a true vacuum with a non-trivial topology contain solitonic objects, which are topologically stable. These objects are simply classical field configurations of the equations of motion. The simplest example of this is when there are two discrete degenerate vacua; this is the familiar case of a massive real scalar field with self-interaction and a negative mass-squared term. In separate, causally disconnected regions in the early universe, the field will take a random decision as to which vacuum it will inhabit when the temperature drops below the critical temperature corresponding to the phase transition. Later, as the horizon grows and different parts of the universe come into causal contact with each other, regions are found where the field is forced to interpolate (smoothly due to the equations of motion) between one vacuum and another vacuum. This region corresponds to a domain wall, a wall trapped in the symmetric state of the early universe. For different vacuum structures, different classes of objects can be produced such as strings for a U(1) vacuum. It is in this way that monopoles are formed cosmologically, when the vacuum state is a continuum of degenerate vacua with a spherical topology in field space. For more details on different topological objects, see [190, 191].

The idea that there should be on average one monopole created per causally disconnected region in the early universe was first intoduced by Kibble [190]. Any theory of particle physics where there is too much non-relativistic matter created in the early universe gives problems for cosmology since no monopoles have been detected. One of the initial motivations for the theory of inflation was to provide a dilution of the density of monopoles created in the early universe [192].

A very tight constraint upon the density of monopoles comes from the observation by Parker that the presence of magnetic monopoles would limit the ability of astronomical objects to build up magnetic fields [193]. The constraint for interstellar space is that there should be less than one monopole per 10^{28} nucleons today. This means any symmetry-breaking scale larger than 10^{10} GeV would lead to an unacceptably large number of magnetic monopoles if inflation does not occur.

4 Modelling the production of SMPs at colliders

In this section the techniques used to model the production of heavy particles at colliders are discussed. The aim of this section is not to provide an overdetailed description of the phenomenology of proposed, undiscovered particles, but instead to show how techniques and models developed for SM particles can profitably be used to predict the gross features of SMP production at colliders. We focus mainly on SMPs which do not possess magnetic charge in view of the inapplicability of perturbative field theory to monopole processes. A description of monopole production mechanisms which have been considered in collider searches, and the approximations which have been used to calculate their rates is given at the end in Section 4.6.

4.1 Production rates

Exotic stable or long-lived new particles are usually thought to be pair-produced at a collider:

$$ab \to X_c X_d, \tag{12}$$

where a and b are normal constituents of the incoming beams, and X_c and X_d belong to the same new theory. While pair production may occur at a large rate, the decay of particles X_c and X_d may be suppressed by the existence of a new (almost) preserved quantum number, possibly resulting in long-lived particles which could interact in the detector as an SMP. Besides direct production, SMPs could be produced via the decay of a heavier particle, for example if a state X_i would decay rapidly into a lighter state, which in turn cannot (rapidly) decay any further.

If the production of a particle X is allowed singly

$$ab \to X, \tag{13}$$

then the decay $X \to ab$ may also occur. The production cross section is directly proportional to the decay width, $\sigma(ab \to X) \propto \Gamma(X \to ab)$, where the constant of proportionality involves mass, spin and colour factors, as well as the ab partonic flux, but no model-specific details. A singly-produced particle which is sufficiently long-lived so as to penetrate through a detector, has, therefore, a production rate which will be negligible, as can be seen from the following example. Consider a colour-singlet scalar state with mass 200 GeV, coupling only to gluons. A lifetime of $c\tau = 1$ mm will translate into a small production rate of 0.0002 events per year, assuming full LHC luminosity, 100 fb^{-1}. The larger the lifetime, the smaller is the production rate. If the state is a colour octet, there is a factor eight enhancement, or if the particle has spin one, another factor three must be added. However the production rates will still be negligible. A potential exception could be off-shell decays, such as $X \to W^+W^-$ for $m_X \ll 2m_W$, where Γ may be strongly kinematically

suppressed, while σ would be less affected since the incoming W's, emitted off the beam constituent quarks, are spacelike. In practice, taking into account current experimental limits discussed in Section 7 as well as the impact of loop-induced decays, such prospects are excluded.

Given the Lagrangian of the theory, and the values of relevant couplings and masses, the parton-level differential cross section for $\mathrm{d}\hat{\sigma}(ab \to X_c X_d)$ is readily obtained. Convolution with the a and b parton densities gives all relevant differential distributions, and integration over phase space provides the total cross section. The pair production cross section of coloured particles is of $O(\alpha_s^2)$, while that of colour-singlet ones is of $O(\alpha_{ew}^2)$, where α_{ew} represents electroweak couplings. Thus the production rate for colour-singlet particles would be a factor $(\alpha_{ew}/\alpha_s)^2$ times smaller. Additionally, the latter cannot couple directly to the gluonic content of the beams, so typical production rates for colour-singlet particles are about 2 to 4 orders of magnitude lower in rate. To illustrate this, Fig. 6 shows PYTHIA predictions for the pair-production cross section at the LHC of exotic fourth-generation quarks with charge $\pm\frac{2}{3}e$ and fourth-generation leptons with charge $\pm e$, as a function of the mass of exotic particles. The lepton cross section is clearly dwarfed by that of the quarks. However, this argument only concerns the direct production mechanisms. Weakly interacting particles can be produced at a large rate in the cascade decays of heavier, strongly interacting particles.

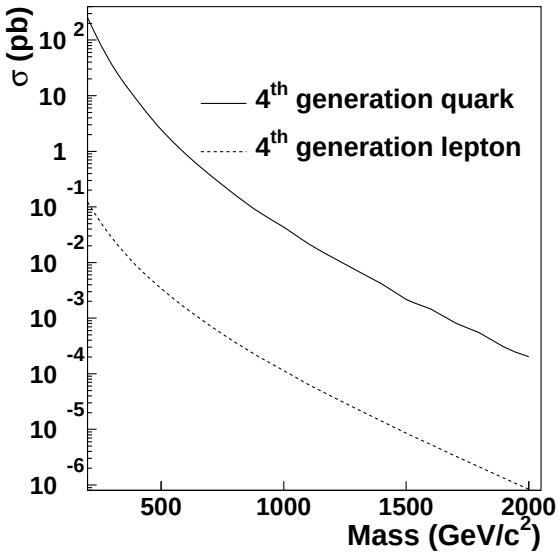

Fig. 6. PYTHIA predictions of the pair-production cross section for fourth-generation quarks of charge $\pm\frac{2}{3}e$, and leptons of charge $\pm e$ at the LHC.

Next-to-leading-order (NLO) calculations of event rates have been performed for many exotic scenarios, such as SUSY [194–196], but not for all. Experience shows that $K = \sigma_{\mathrm{NLO}}/\sigma_{\mathrm{LO}}$ typically range between 1 and 2 [197]. In this article $K = 1$ will be assumed throughout, which will provide conservative estimates of the

experimental feasibility of discovery.

4.2 Event topologies

Higher-order perturbative calculations involve emissions of further partons. This can be understood as $ab \to X_c X_d$ generalising to $ab \to X_c X_d\, e$ and $ab \to X_c X_d\, ef$, etc., where e and f will mainly be gluons for incoming hadron beams, but also could be quarks, leptons or photons, Fig. 7. Such emissions modify event shapes and thereby the experimental signatures.

These processes can be described either by higher-order matrix elements or by parton showers applied to lower-order matrix elements. There are relative advantages and limitations for both approaches. The former are more accurate for a few well-separated emissions, and of course contain all the model-specific details, but they diverge in the soft/collinear limits and are not meaningful there. The latter are based on model-independent approximations that work especially well in the soft/collinear regions, in which dampening by Sudakov factors and resummation of multiple emissions ensures a physically meaningful behaviour. In practice, showers have turned out to be reasonable approximations up to the scale of the lowest-order process, i.e. typically for the additional-jet transverse momenta below the mass scale of the produced X particles [198]. For exploratory studies the shower picture alone is therefore sufficient, while, for precision studies, matrix-element information also has to be supplied. Various methods to combine the two approaches, so that the matrix-element behaviour is reproduced at large separation scales and the parton-shower one at small scales, are under active study [199–203]. Following a discovery, both higher-order matrix-element calculations and corresponding matchings would have to be carried out.

In the shower approach, one distinguishes between initial-state radiation (ISR) from the incoming a and b partons and final-state radiation (FSR) from the outgoing X_c and X_d, with interference effects neglected. In the current case, since the X_i particles are heavy, radiation from them is strongly suppressed [204] in comparison to light particles. Thus ISR dominates. The main experimental consequences of ISR is that the $X_c X_d$ pair is produced in association with a number of further jets, and that X_c and X_d do not have opposite and compensating transverse momenta, as they do in the LO picture. This $p_\perp$ imbalance is in itself a revealing observable, especially when the X_i are not directly detectable. On the other hand, the activity of the additional jets, and of the underlying event, may be a nuisance for some studies. Jets from FSR could be important, as will be discussed in the following section.

The kinematics of heavy particles produced in collisions can be studied with the help of several programs. The two general-purpose generators PYTHIA [205] and

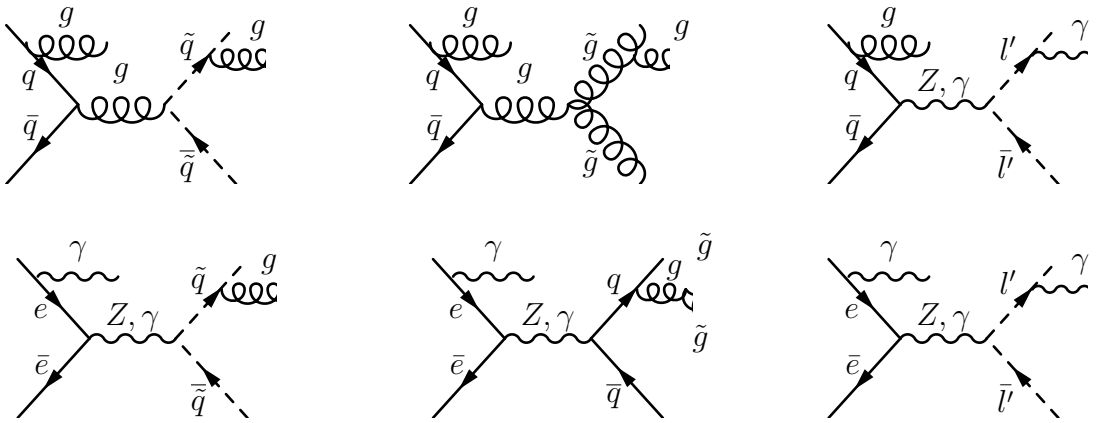

Fig. 7. Top: examples of production of squarks (top left), gluinos (top center) and heavy leptons (top right) in hadron-hadron colliders. Bottom: examples of production of squarks (bottom left), gluinos (bottom center) and heavy leptons (bottom right) in e^+e^--colliders. Examples of ISR and FSR are displayed.

HERWIG [206, 207] are traditionally used to study physics within and beyond the Standard Model. They are mainly based on leading-order matrix elements, but in a few cases also NLO matching is available. Their strength is that they provide complete event topologies, such as they could be observed in a detector, including descriptions of parton showers, underlying events, and hadronisation. Many of these aspects are handled in different fashions in the two programs, e.g. with respect to the choice of shower evolution variables or hadronisation schemes, but they tend to give similar results. They have both been supplemented with routines to handle hadronisation into SMPs, as will be described in the next subsection. Other general-purpose generators, but currently without hadronisation into SMPs, are ISAJET [41] and SHERPA [208].

Many other programs provide matrix elements to LO or NLO. A comprehensive survey is given in the "Les Houches Guidebook" [209], while dedicated BSM tools descriptions and an online repository can be found in [12, 13]. Examples of programs that can calculate arbitrary LO processes, once the Feynman rules have been encoded, are MADGRAPH/SMADGRAPH [210–212] and COMPHEP/CALCHEP [213,214]. Examples of programs that contain NLO matrix elements are PROSPINO [215] for SUSY particle production and SDECAY [216] for SUSY decays. In UED, production cross sections for gluon and quark KK excitations at hadron colliders have been calculated [63] and are available as an extension [72] of the PYTHIA generator. These programs do *not* provide complete events, however, and therefore have to be interfaced with general-purpose generators to be fully useful. This process is rather well automated: the original Les Houches Accord (LHA) [217, 218] provides a standard format to transfer simple parton-level configurations, including information on flavours, colours and momenta, while the SUSY Les Houches Accord (SLHA) [14] allows standard exchange of SUSY parameters, couplings, masses, and branching ratios.

For colourless new particles the story ends here. Once produced, the X_i's will sail out towards the detector. A coloured particle, however, cannot escape the confinement forces. Therefore it will pass through a hadronisation stage, during which it picks up light-quark or gluon degrees of freedom to form a colour-singlet "hadron". For a colour-triplet, denoted C_3 to highlight its coloured nature, this may either be a "meson" $C_3\overline{q}$ or a "baryon" $C_3q_1q_2$. For a colour-octet, denoted C_8, the alternatives are a "meson" $C_8q_1\overline{q}_2$, a "baryon" $C_8q_1q_2q_3$ (or corresponding antibaryon), or a "glueball" C_8g. Collectively, such states will be referred to as R-hadrons, irrespective of the physics scenario which gives rise to them. The name is borrowed from SUSY, where it refers to the nontrivial R-parity possessed by such hadrons. Specific states will be denoted by an R with the flavour content as lower indices and the charge as upper one [3], e.g. $R^+_{\tilde{g}u\overline{d}}$ for a $\tilde{g}u\overline{d}$ state. In order to avoid too unwieldy a notation, spin information is suppressed.

The hadronisation process does not appreciably slow down the R-hadron relative to the original $C_{3,8}$, as can be seen from the following. Consider a colour triplet C_3 with energy E_{C_3} and longitudinal momentum $p_{\parallel C_3}$ (here longitudinal is defined in the direction of the C_3), which hadronises into an R-hadron with energy E_R and longitudinal momentum $p_{\parallel R}$, plus a set of "normal" hadrons that (approximately) take the remaining energy–momentum. These hadrons are produced in the colour field pulled out behind the C_3, and therefore ought to be limited to have smaller velocities than that of the endpoint C_3 itself or, more precisely, to have smaller rapidities y defined with respect to the C_3 direction. Now recall that $E+p_\parallel = m_\perp e^y$, where $m_\perp$ is the transverse mass of a particle. So if a normal hadron h, with a $\langle m_{\perp h}\rangle \approx 1$ GeV, could at most reach the same rapidity as the C_3, then it follows from the above that the ratio between the $E + p_\parallel$ value of the normal hadron and that of the C_3 could at most be $\langle m_{\perp h}\rangle / m_{C_3} \approx 1$ GeV$/m_{C_3}$. Finally, assume that the normal hadrons are produced behind the C_3, located at some rapidity y_0, with a typical rapidity separation of $\langle \Delta y\rangle \approx 0.7 \approx \ln 2$, as in ordinary jets, i.e. at $y_0 - \ln 2$, $y_0 - 2\ln 2$, $y_0 - 3\ln 2$, ... The above upper bound for $E+p_\parallel$ of a single hadron then is replaced by an average for the summed effect of the normal hadrons produced in association with the C_3: $m_\perp \exp(y_0)(\exp(-\ln 2) + \exp(-2\ln 2) + \exp(-3\ln 2) + \cdots) = m_\perp \exp(y_0)$, where each term expresses the $E+p_\parallel$ value of the next hadron. The R-hadron will retain all the C_3 energy not taken away by these normal hadrons. One therefore arrives at the expectation [219] that the fragmentation parameter z typically is

$$\langle z\rangle = \langle \frac{E_R + p_{\parallel R}}{E_{C_3} + p_{\parallel C_3}}\rangle \approx \langle \frac{E_R}{E_{C_3}}\rangle \approx 1 - \frac{\langle m_{\perp h}\rangle}{m_{C_3}} \approx 1 - \frac{1 \text{ GeV}}{m_{C_3}} \,. \tag{14}$$

[3] This is the convention adopted in the 2006 *Review of Particle Physics* [1].

That is, if C_3 has a large mass, $\langle z \rangle$ is close to unity, and all other normal hadrons in the jet take a very small amount of energy, ~ 1 GeV $\cdot \gamma_{C_3}$, where $\gamma_{C_3} = E_{C_3}/m_{C_3}$ is not large for a massive state C_3. For a colour octet the energy loss from the R-hadron to the rest of the jet would be about twice as big as for a colour triplet ($C_A/C_F = 9/4$), but otherwise the argument for colour triplets applies in the same way.

The above z value is not accessible experimentally since, in a busy hadronic environment, it is not possible to know which particles come directly from the $C_{3,8}$ hadronisation. Instead, with an R-hadron being part of a jet, the natural observable is the fraction z^* of the jet energy, $E_{\rm jet}$, which is carried by the R-hadron: $z^* = E_R/E_{\rm jet}$. Fig. 8 shows the expected distribution of z^* for gluino R-hadrons of mass 300 GeV produced at the LHC. The jets were reconstructed with the CDF Run I cone algorithm with $R = 0.7$ [220]. Predictions are shown using the string and cluster models of PYTHIA and HERWIG, respectively. The details of these models are given later in this section. Also shown are PYTHIA predictions for the distribution of z^* of the leading particles contained in jets produced in Standard Model 2-to-2 QCD processes (labelled SM-jets).

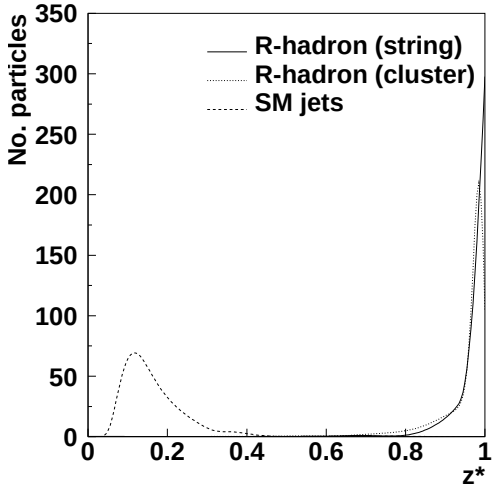

Fig. 8. The predicted distribution of the fragmentation variable $z^* = E_R/E_{\rm jet}$ for gluino R-hadrons of mass 300 GeV produced at the LHC. The expectations of the string and cluster hadronisation schemes, implemented in PYTHIA and HERWIG, respectively, are shown. Also shown is the prediction from PYTHIA of the z^* distribution of leading particles within SM jets.

Note that the R-hadron $\langle z^* \rangle$ is significantly smaller than the prediction of Eq. 14, $\langle z \rangle \approx 1 - 2/300 \approx 0.993$, including a factor of two for the colour-octet nature of gluinos, but not taking into account the possible loss of particles outside the cone. Instead several other physics components contribute to the final curve, by depositing further particles inside the jet cone.

• Final-state radiation from the gluino, although small, is still larger than the non-perturbative effect discussed above. Since collinear FSR is strongly suppressed

[204], the additional FSR jets will not be correlated with the gluino direction, and so may or may not end up inside the R-jet cone. At hadron colliders the FSR jets tend to drown among the more numerous ISR jets. They could stand out at a lepton collider, at which there is no QCD ISR.
• Initial-state radiation from the incoming quarks and gluons is not suppressed by any mass effects. The ISR jets may appear anywhere in phase space, by chance also inside the R-jet cone, and may then deposit a significant amount of extra energy.
• The underlying events ("beam remnants" and "multiple interactions") tend to deposit particles inside any jet cone, in proportion to the size of the cone. Normally these particles would be rather soft, but upwards fluctuations can occur.

For the actual hadronisation of the coloured heavy object there are two main models available. In PYTHIA the Lund string fragmentation model [221] is used, wherein an assumed linear confinement potential is approximated by a string with a constant tension of $\kappa \approx 1$ GeV/fm. A *colour triplet* C_3 (or $C_{\overline{3}}$) is at the endpoint of such a string. When the C_3 moves away from its production vertex it pulls out the string behind itself, to which it loses energy. This string may then break by the production of a light quark-antiquark or diquark-antidiquark pair, where the $\overline{q}$ or $q_1 q_2$ is in a colour-antitriplet state which can combine with the C_3 to form a singlet. Further breaks of the string may occur, which causes the formation of a jet of hadrons. The composition of the different light flavours is assumed universal and thus constrained e.g. by LEP data [222, 223] ($u : d : s \approx 1 : 1 : 0.3$, with diquarks further suppressed). A mixture of different charge states is finally produced. The energy-momentum fraction z retained by the R-hadron is described by an appropriate fragmentation function, with parameters that fit e.g. B meson spectra [224, 225]. These functions have a mass dependence consistent with Eq. 14 for the extrapolation from b to C_3 hadronisation.

A *colour octet* C_8 in the Lund string model is viewed as the incoherent sum of a colour and an anticolour charge (the planar or $N_C \to \infty$ approximation [226]), such that an octet C_8 is attached to two string pieces instead of one only. Each of these pieces is allowed to break as above. One gives a quark or an antidiquark, the other an antiquark or diquark, and these combine to form an R-meson or R-baryon. Diquark-antidiquark "hadrons" are rejected. In addition, a new mechanism is introduced: a gg pair may be produced, such that an R-glueball is formed and the leftover gluon attaches to the two string pieces. Its relative importance is not known. The equivalent mechanism for normal gluons would lead to the production of glueballs. There are a few indications that this may occur, [227, 228], but it cannot be at a significant rate. Based on the absence of real evidence for normal glueballs [229], the default value for the R-glueball fraction in PYTHIA is 10%, and can be changed. Clearly a scenario in which glueballs are predominantly formed in the hadronisation step will have a large impact on experimental searches which rely on the reconstruction of tracks. However, as is outlined in Section 4.4, the behaviour of an R-glueball when it interacts in material is expected to be similar to that of a neutral R-meson and it may therefore convert into a charged R-hadron

which would leave behind a track.

Predictions from PYTHIA of the fractions of different R-hadron species formed in the hadronisation of a gluino and a stop are shown in Tab. 3. The predicted species of an R-hadron arising from an antistop are almost exactly the charge conjugates of a stop R-hadron. The key observation is that, when neglecting the *a priori* fraction of R-glueballs of 10%, roughly 50% of the produced states are charged. The gluino R-baryon numbers are somewhat lower than expected. This is an artifact of approximations used in hadronisation model. However, these should anyway contribute less than 10% of the R-hadrons produced. It is also interesting to note that, as discussed in Section 5.2, although R-hadrons will largely start out as mesons, nuclear scattering in calorimeters will ensure that they mostly end up as baryons as they leave the detector.

HERWIG is based on cluster fragmentation. In this picture all gluons are nonperturbatively split into quark-antiquark pairs at the end of the perturbative cascade. Partons from adjacent such breaks, and from original (anti)triplets, are then grouped into colour-singlet clusters. Large-mass clusters are broken into smaller ones, along the "string" direction. These clusters then decay to two hadrons, using phase-space weights to pick between allowed flavours. A colour octet C_8 is combined with a q_1 and a $\overline{q}_2$ from two adjacent nonperturbative splittings to form a cluster [230]. The cluster decay can be either of $C_8 q_1 \overline{q}_2 \to C_8 q_3 \overline{q}_2 + q_1 \overline{q}_3$, $\to C_8 q_1 \overline{q}_3 + q_3 \overline{q}_2$, or $\to C_8 g + q_1 \overline{q}_2$. The two former possibilities are handled as usual based on phase space weights, while the latter R-glueball possibility is added with a free normalisation. By default it is set to zero. The resulting gluino R-hadron composition is shown in Tab. 3.

Thus, although the technical details in PYTHIA and HERWIG are quite different the basic principles are similar. In both models, R-hadron production occurs predominantly by the $C_{3,8}$ picking up u and d quarks, while s is more rare, and c or b can only be produced in the shower, at an even lower rate. Apart from the unknown fraction of R-glueballs, the u-d charge difference ensures that approximately half of the produced R-hadrons will be charged. The two generators should therefore provide similar phenomenology for the flavours and momenta of produced R-hadron events. Any differences would reflect true uncertainties in our current understanding.

4.4 R-hadron properties

The mass splittings of R-hadrons are of critical importance when designing a search strategy. If one state would be significantly lighter than another, one would expect this state to be dominantly present in the detector. If the lightest state would be neutral, a completely different (and far more experimentally challenging) signature

R-hadron	PYTHIA Fraction (%)	HERWIG Fraction (%)
$R^+_{\tilde{g}u\bar{d}}$, $R^-_{\tilde{g}d\bar{u}}$	34.2	28.2
$R^0_{\tilde{g}u\bar{u}}$, $R^0_{\tilde{g}d\bar{d}}$	34.2	28.2
$R^+_{\tilde{g}u\bar{s}}$, $R^-_{\tilde{g}s\bar{u}}$	9.7	17.5
$R^0_{\tilde{g}d\bar{s}}$, $R^0_{\tilde{g}s\bar{d}}$, $R^0_{\tilde{g}s\bar{s}}$	10.4	26.1
$R^0_{\tilde{g}g}$	9.9	—
$R^{++}_{\tilde{g}}$, $R^{--}_{\tilde{g}}$ (anti)baryons	0.1	—
$R^+_{\tilde{g}}$, $R^-_{\tilde{g}}$ (anti)baryons	0.8	—
$R^0_{\tilde{g}}$ (anti)baryons	0.7	—

R-hadron	Fraction (%)
$R^+_{\tilde{t}\bar{d}}$	39.6
$R^0_{\tilde{t}\bar{u}}$	39.6
$R^+_{\tilde{t}\bar{s}}$	11.8
$R^{++}_{\tilde{t}}$ baryons	0.8
$R^+_{\tilde{t}}$ baryons	6.7
$R^0_{\tilde{t}}$ baryons	1.5

Table 3
Predictions from PYTHIA of the fractions of different species of R-hadrons following the hadronisation of a gluino (left) and a stop (right) of mass 500 GeV produced at the LHC. The HERWIG gluino predictions [230] are for a 2000 GeV mass, but almost identical for 50 GeV.

is expected than if the lightest state would be charged.

The masses of the produced R-hadrons are best understood from the mass formula for the lowest-level (i.e. no radial or orbital excitation) hadrons [231, 232]

$$m_{\text{hadron}} \approx \sum_i m_i - k \sum_{i \neq j} \frac{(\mathbf{F}_i \cdot \mathbf{F}_j)\,(\mathbf{S}_i \cdot \mathbf{S}_j)}{m_i\, m_j} \tag{15}$$

where m_i are the constituent masses, $\mathbf{F}_i$ are the colour **SU(3)** matrices, $\mathbf{S}_i$ the spin **SU(2)** ones, and k a parameter related to the wave function at the origin. The $C_{3,8}$ is so heavy that it provides an almost static colour field in the rest frame of the R-hadron, and therefore its spin, if any, is decoupled (cf. "Heavy Quark Effective Theory" [233]). The heavy $C_{3,8}$ has thus a strongly localised wave function, while the light degrees of freedom are spread over normal hadronic distance scales. The relative localisation of the wave functions largely accounts for the expected energy loss and scattering behaviour of R-hadrons in matter, as discussed in detail in Section 5.2. It also ensures that the mass splittings, given by the second term in Eq. 15, are determined by the light degrees of freedom. It must be noted that the "experimentally observable" constituent masses used below are different from the renormalisation-scheme-dependent running masses found in the Lagrangian of a theory although it is possible to provide an approximate translation for any specific case. The mass splittings discussed below agree with those obtained earlier with a similar bag model approach [234, 235], and with lattice calculations [236].

For a colour-triplet C_3 the hadron mass is easily obtained from standard quark and diquark constituent masses. For C_3 mesons ($C_{\bar{3}}q$, $C_3\bar{q}$), no significant mass splitting is expected to occur [232], in analogy with the absence of mass splittings of B-hadrons. For C_3 baryons such as C_3qq states (and, by symmetry for the $C_{\bar{3}}\bar{q}\bar{q}$ baryons) the mass spectrum would be (all units in GeV)

$$\begin{aligned} M_{C_3qq} &\approx M_{C_3} + 0.3 + 0.3 - 0.026 \times \frac{(-\frac{2}{3} \times -\frac{3}{4})}{0.3 \times 0.3} && s_{qq} = 0 \\ &\approx M_{C_3} + 0.46 \\ M_{C_3qq} &\approx M_{C_3} + 0.3 + 0.3 - 0.026 \times \frac{(-\frac{2}{3} \times +\frac{1}{4})}{0.3 \times 0.3} && s_{qq} = 1 \\ &\approx M_{C_3} + 0.65 \end{aligned}$$

where s_{qq} denotes the total spin of the qq system.

In the case of a C_8 state, R-mesons, R-baryons and R-glueballs could arise from hadronisation. The R-mesons $C_8q_1\bar{q}_2$ give a colour factor $\mathbf{F}_1 \cdot \mathbf{F}_2 = 1/6$ for the light quarks, to be compared with $-4/3$ in a normal $q_1\bar{q}_2$ meson. For a $C_8q\bar{q}$ state, the mass spectrum is thus given by:

$$\begin{aligned} M_{C_8q\bar{q}} &\approx M_{C_8} + 0.3 + 0.3 - 0.043 \times \frac{(\frac{1}{6} \times -\frac{3}{4})}{0.3 \times 0.3} && s_{q\bar{q}} = 0 \\ &\approx M_{C_8} + 0.66 \\ M_{C_8q\bar{q}} &\approx M_{C_8} + 0.3 + 0.3 - 0.043 \times \frac{(\frac{1}{6} \times +\frac{1}{4})}{0.3 \times 0.3} && s_{q\bar{q}} = 1 \\ &\approx M_{C_8} + 0.58 \end{aligned}$$

The ρ-π mass difference therefore flips sign and is considerably reduced in size for the corresponding R-mesons. Further, a gluon constituent mass is about twice a light-quark [237,238], so the C_8g state is almost mass degenerate with the $C_8u\overline{u}$ and $C_8d\overline{d}$ ones, and will have similar properties. Assuming that the constituent mass of a gluon is approximately 700 MeV [237, 238], the mass of a C_8g state is then

$$M_{C_8g} \approx M_{C_8} + 0.7. \tag{16}$$

The expressions for the masses of the R-baryons (C_8qqq) are somewhat more cumbersome, since there are more colour and spin combinations possible, but do not offer any peculiar features. Splittings are expected to be less than the order of a 100 MeV [232], and the mass of the C_8qqq states is thus approximately

$$M_{C_8qqq} = M_{C_8} + 0.9. \tag{17}$$

Furthermore, the orbital and radial excited states would follow patterns not too dissimilar from normal hadronic spectra. However, before a discovery of R-hadrons

it is not useful to attempt to calculate the full hadron spectrum including excited states. In case such an excited state is produced it would probably decay electromagnetically or strongly at such a short time scales that no secondary vertex is resolved. Owing to the small mass splittings and the small boost factor of a massive R-hadron, the additional photon or pion produced will also be of low momentum, and so drown in the general hadronic environment. For the current studies it is sufficient to simulate the production of the lowest-lying state of each allowed flavour combination.

Although this paper is only concerned with stable R-hadrons, it is worthwhile to briefly consider the possibility of R-hadron decays. If unstable over nanosecond time scales, R-hadrons could decay inside the detector. This would take place as an almost free decay of the $C_{3,8}$, with the rest of the hadron acting as spectators, and could therefore be described by the standard perturbative picture. Showering and hadronisation can be added, the latter also involving the spectators. These decays may well violate baryon or lepton number, via such processes as $\tilde{g} \to uds$, and give rise to unusual hadronisation scenarios [239, 240].

A further property of R-hadrons about which little is known is their oscillatory behaviour. Neutral R-mesons will be able to convert into their anti-particles without violating any known conservation laws. Since the oscillation length depends on couplings and masses of particles which have yet to be discovered (if ever) then either minimal or maximal oscillations are conceivable [241, 242]. As discussed in Section 5.2 this may have implications for the ability of experiments to both discover and quantify a heavy squark which may be produced at a collider.

4.5 Sources of uncertainties

The understanding of the production of non-magnetically charged SMPs is not complete, but should be fully adequate for the purposes of a search-and-discovery mission. Further sophistication would be added once the first signals for new physics would point the way to a more specific scenario, rather than the generic ones considered here. In any search relying on QCD models, the following areas of uncertainty may be relevant:

- Production rates: are very much model-dependent, and contain some uncertainties from uncalculated higher-order contributions. These can be parameterised in the form of a K-factor.
- Event topologies: contributions from further parton emissions are treated by the parton-shower approximation, which should be sufficient for the bulk of the cross section, but not necessarily for topologies with well-separated further jets.
- Hadronisation, momenta: the fragmentation function is guaranteed to give most of the momentum to the R-hadron, so uncertainties are restricted to the minijet of

a few further normal hadrons produced in the same general direction. The typical minijet energy could easily be uncertain by a factor of two.
- Hadronisation, flavours: some uncertainty, especially in the glueball and baryon sectors. The rate of the former is a completely free parameter. It should not affect the bulk of the production, mesonic states with u and d quarks only, which also will guarantee a rather even mixture of charged and uncharged states.
- R-hadron properties: the general pattern of states and masses appears to be well understood, especially in the dominant meson sector. Should, against all expectations, decays like $C_8 u\bar{d} \rightarrow C_8 g + \pi^+$ be kinematically allowed, they would have consequences for the charged/neutral ratio.

4.6 Production mechanisms of for magnetic monopoles

The interactions of magnetic monopoles at high energies are difficult to treat theoretically since perturbation theory is inapplicable due to the size of the electromagnetic coupling constant for monopoles ($\alpha_m = g^2/\hbar c = 137/4n^2$ for a Dirac monopole). Nevertheless, the scattering cross sections for monopoles incident on charged particles have been computed using non-perturbative techniques (see ref. [5] for a review of monopole scattering calculations). This has allowed the calculation of the stopping power of monopoles in material [243–246]. In addition the binding energy of monopoles to nuclear magnetic dipoles has been calculated [247, 248]. Since these calculations concern the interactions of monopoles in a detector, they are discussed in 5.1.2 and 6.4.2, respectively.

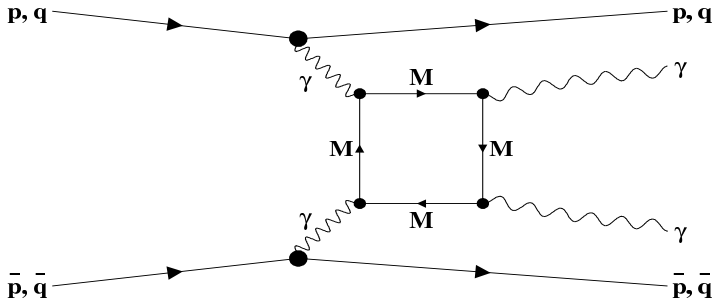

Fig. 9. A Feynman diagram of a multi-photon process mediated by an internal monopole line in $p\bar{p}$ collisions.

Even though a perturbative treatment of monopoles is impossible, experiments nevertheless must assume certain production processes in order to estimate the detector acceptance. The production mechanisms which have been assumed by experiments are typically those which would correspond to leading order pair production in a perturbative picture. A Drell–Yan-like mechanism to produce a monopole-antimonopole pair is a commonly considered scenario in hadron-hadron collisions

[249]. Searches at e^+e^- experiments have hypothesised monopole production through the annihilation reaction $e^+ + e^- \longrightarrow Z^0/\gamma \longrightarrow m\bar{m}$ [250]. In lepton-hadron collisions, pair production via photon-photon fusion has been envisaged [251]. To obtain calculations of cross-sections and of the kinematic distributions of produced monopoles, the formalism for the electroweak production of $\mu^+\mu^-$ is used, with appropriate phase space modifications to account for the larger monopole mass. However, it is important to emphasise that little is known about processes in which monopoles could be directly produced, and that the above reactions are 'best guesses'. Thus, some experiments also use random phase-space models to calculate acceptance. Examples of the methods used by experiments to model monopole pair production are discussed in Section 7.2.

It has also been proposed in Refs. [252] and [253], respectively, that virtual monopoles mediating e^+e^- and hadron-hadron collisions would be manifest via photonic radiation, as illustrated in Fig.9 for $p\bar{p}$ collisions. Calculations of cross sections of such process assume that perturbation theory can be used for monopoles. Limits [254, 255] obtained using these calculations, which are discussed later in Section 7.2.5 have been criticised [256].

5 Interactions of SMPs

This section describes the expected interactions of SMPs in particle detectors. The dominant types of interactions are electromagnetic and strong interactions. An outline is given of the theory of electromagnetic energy loss for electrically and magnetically charged particles. Compared to the electromagnetic case, nuclear interactions of SMPs containing heavy coloured objects are poorly understood. A review is given here of various models which have been proposed to describe these nuclear interactions and their uncertainties are also pointed out.

5.1 Ionisation energy loss

The most commonly used observable in SMP searches is the measurement of the continuous ionisation energy loss $\frac{dE}{dx}$. Both electrically and magnetically charged SMPs lose energy principally through ionisation energy loss as they propagate through matter and for both types of particle the theory of electromagnetic energy loss is well established.

5.1.1 Ionisation energy loss by electrically charged particles in material

As an electrically charged particle moves through a material it loses energy either by interactions with atomic electrons or by collisions with atomic nuclei in the material. The first of these results in the liberation of electrons from the atoms in the material (i.e. ionisation) while the second results in the displacement of atoms from the lattice. The energy loss due to the second process is called the Non-Ionising Energy Loss (NIEL). The differential energy loss (stopping power), (dE/dx), due to the ionisation energy is much larger than the NIEL [257] in practical particle detectors.

For fast particles of charge Z_1 in a medium of atomic number Z_2 the mean ionisation energy loss is given by the Bethe-Bloch formula [1].

$$\frac{dE}{dx} = \frac{4\pi e^4 Z_1^2}{m_e c^2 \beta^2} n \left(\frac{1}{2} \ln \left(\frac{2 m_e c^2 \beta^2 \gamma^2 T_{max}}{I_e^2} \right) - \beta^2 - \frac{\delta}{2} \right) \tag{18}$$

where e and m_e are the charge and mass of the electron, n is the number of electrons per unit volume in the material, β is the relativistic velocity of the incident particle, $\gamma = 1/\sqrt{1-\beta^2}$ and I_e is the mean ionisation potential of the material. The latter can be parameterised by [258];
$I_e(Z_2) = (12Z_2 + 7)$ for $Z_2 \leq 13$ or $(9.76Z_2 + 58.8Z_2^{-0.19})$ eV for $Z_2 > 13$.
The quantity T_{max} is the maximum kinetic energy which can be imparted to a free electron in a single collision and is given, for a particle of mass M, by

$$T_{max} = \frac{2 m_e c^2 \beta^2 \gamma^2}{1 + 2\gamma m_e/M + (m_e/M)^2}. \tag{19}$$

The term δ represents the density effect which limits the relativistic rise at high energy and it has been calculated by Sternheimer *et al.* [259]. This term is only relevant for particles with $\beta\gamma \gg 3$ and for massive particles $T_{max} \approx 2 m_e c^2 \beta^2 \gamma^2$. Slight differences occur for positive and negative particles moving with low velocity [260].

For low energies when the velocity of the incident particle is comparable or less than the velocity of the electrons in the atom, the so-called Lindhard region, this formula is no longer valid. The energy loss is then proportional to the particle velocity β [261]:

$$\frac{dE}{dx} = N \xi_e 8\pi e^2 a_o \frac{Z_1 Z_2}{Z} \frac{\beta}{\beta_o}, \tag{20}$$

where N is the number of atoms per unit volume, $\xi_e \approx Z_1^{1/6}$, a_o is the Bohr Radius of the hydrogen atom and $Z^{\frac{2}{3}} = Z_1^{\frac{2}{3}} + Z_2^{\frac{2}{3}}$. This formula holds for $\beta < Z_1^{\frac{2}{3}} \beta_o$ where $\beta_o = \frac{e^2}{2\epsilon_0 hc}$ ($\approx .0073$) is the electron velocity in the classical lowest Bohr orbit of the hydrogen atom.

The intermediate region, in which neither the Bethe–Bloch formula (Eq. 18) nor the

Lindhard formula (Eq. 20) are valid, is defined by the velocity range $\beta_1 \leq \beta \leq \beta_2$, where $\beta_1 = \max[\alpha Z_1^{1/3}/(1+\alpha Z_1^{1/3}), (2Z_2^{0.5}+1)/400]$, $\beta_2 = \alpha Z_1/(1+\alpha Z_1)$ and α is the fine structure constant. This region is described by Anderson and Barkas [262]. In this region a polynomial can also be used to join up the two regions [258] of the form;

$$\frac{dE}{dx} = A\beta^3 + B\beta^2 + C\beta + D \tag{21}$$

where A, B, C, D are derived from the four simultaneous equations obtained by equating $\left(\frac{dE}{dx}\right)_{el}$ and $\frac{d\left(\frac{dE}{dx}\right)_{el}}{d\beta}$ at β_1 and β_2 for the Eqs. 18, 20 and 21. This gives:

$A = \frac{1}{\triangle\beta^2}\left(\frac{y_1}{\beta_1} + k - \frac{2\triangle y}{\triangle\beta}\right)$
$B = \frac{1}{\triangle\beta^2}\left(3(\beta_1+\beta_2)\frac{\triangle y}{\triangle\beta} - (\beta_1+2\beta_2)\frac{y_1}{\beta_1} - \triangle y^2 k\right)$
$C = \frac{1}{\triangle\beta^2}\left(\beta_1(\beta_1+2\beta_2)k + \frac{\beta_2(2\beta_1+\beta_2)y_1}{\beta_1} - \frac{6\beta_1\beta_2\triangle y}{\triangle\beta}\right)$
$D = \frac{1}{\triangle\beta^2}\left[\frac{1}{\triangle\beta}\left(\beta_1^2 y_2(3\beta_2-\beta_1) + \beta_2^2 y_1(\beta_2-3\beta_1)\right) - \beta_1\beta_2\left(\beta_1 k + \beta_2\frac{y_1}{\beta_1}\right)\right]$
where $\Delta\beta = \beta_2 - \beta_1$, y_1,y_2 are the $\frac{dE}{dx}$ values computed from Eqs. 18 and 20 at velocities β_1 and β_2, respectively,$\Delta y = y_1 - y_2$, $k = \frac{1}{\beta_2^3}\left[2\frac{4\pi e^4 Z_1^2}{m_e c^2} n(\gamma_2^2 - \ln\left(\frac{2m_e c^2\beta_2^2\gamma_2^2}{I(1-\beta_2^2)}\right)\right)]$ and $\gamma_2 = 1/\sqrt{1-\beta_2^2}$.

The variation of $\frac{dE}{dx}$ with $\beta\gamma$ is illustrated in Fig. 10 by a calculation made for μ^+ in copper [1]. The rise with $\beta\gamma$ in the Lindhard region from Eq. 20 turns into a fall as $\beta\gamma$ increases, as expected from Eq. 18. The accuracy of the rather arbitrary polynomial procedure between the two regions can be assessed from extrapolating the rise at low $\beta\gamma$ and the fall at higher $\beta\gamma$ into the worst possible case of a discontinuous join. The variation of $\frac{dE}{dx}$ with material is shown in Fig. 11 [1].

5.1.2 Ionisation energy loss by magnetically charged particles in material

Since a Dirac monopole has a magnetic charge equivalent to an electric charge of $137e/2$, such a particle would be expected to suffer ionisation energy loss at a rate several thousand times greater than that of a particle with electric charge e [243, 244]. A Dirac monopole would thus be expected to leave a striking ionisation signature. Ionisation energy loss could also lead to a monopole becoming stopped in detector material before reaching a tracking chamber.

The energy loss in the form of ionisation of magnetic monopoles passing through material due to interactions with atomic electrons has been shown to follow a form similar to the Bethe-Bloch equation (Eq. 18) but without the multiplicative factor $1/\beta^2$ [243, 244]. The velocity-dependent Lorenz force is responsible for the interaction between a moving magnetic monopole and an atomic electron in the material. In contrast, for a moving electrically charged particle the velocity-independent Coulomb force is responsible for the interactions. The velocity dependence of the Lorenz force causes the cancellation of the $1/\beta^2$ factor in the formula for $\frac{dE}{dx}$ for

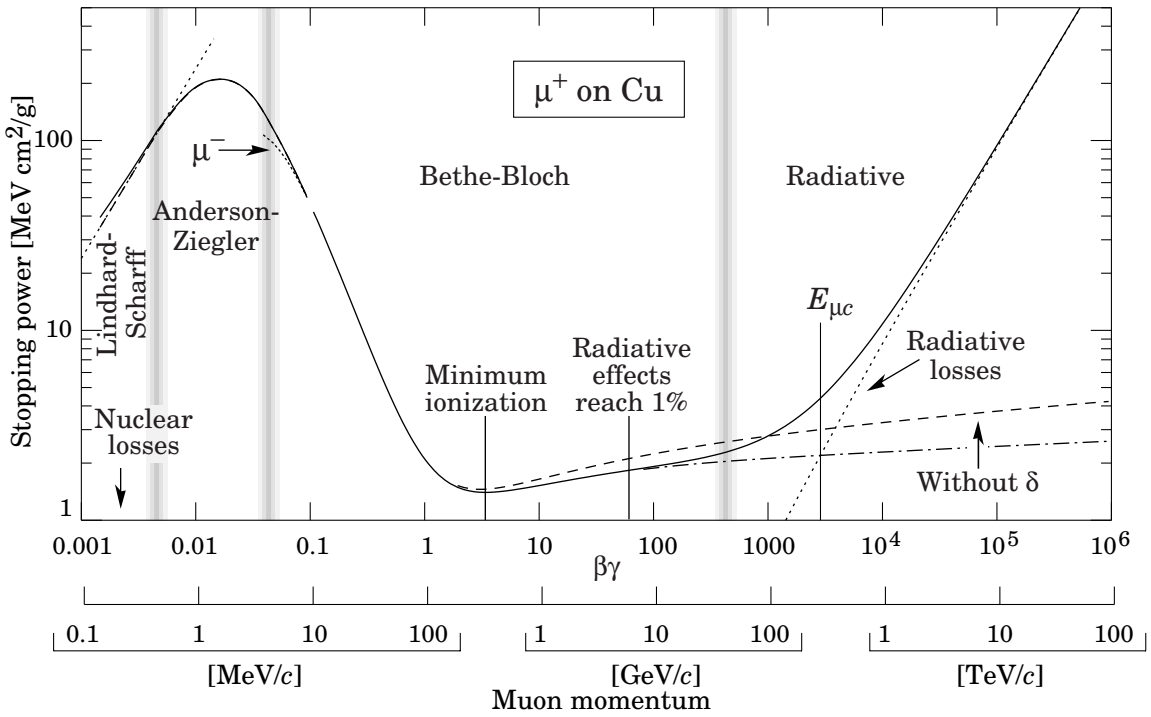

Fig. 10. Stopping power ($\frac{dE}{dx}$) for positively charged muons in copper as a function of $\beta\gamma = p/M$ taken from the Particle Data Group [1]. The solid curve indicates the total stopping power. The radiative effects apparent at very high energies are much less relevant for particles heavier than muons. The different regions indicated by the vertical bands are described in Ref. [1] as are the small difference between positive and negative charges at low values of $\beta\gamma$ (the Barkas effect [263]) shown by the short dotted lines labelled μ^-.

magnetic monopoles (compare Eqs. 18 and 22). The detailed formula for the stopping power of a magnetic monopole of strength g is given in [243] as

$$\frac{dE}{dx} = \frac{4\pi e^2 g^2}{m_e c^2} n \left(\frac{1}{2} \ln \left(\frac{2 m_e c^2 \beta^2 \gamma^2 T_{max}}{I_m^2} \right) - \frac{1}{2} - \frac{\delta}{2} + \frac{K(|g|)}{2} - B(|g|) \right) \quad (22)$$

and the modifications at very low velocity in [244]. Here I_m is the mean ionisation potential for magnetic monopoles which is close in value to I_e (Eq. 18). The relationship between I_m and I_e can be expressed as $I_m = I_e \exp -D/2$. Sternheimer [264] has shown, for several solids, that $D(\mathrm{Li}) = 0.34$, $D(\mathrm{C}) = 0.22$, $D(\mathrm{Al}) = 0.056$, $D(\mathrm{Fe}) = 0.14$, $D(\mathrm{Cu}) = 0.13$, and $D(\mathrm{W}) = 0.07$. The correction terms $K(|g|) = 0.406, 0.346$ and $B(|g|) = 0.248, 0.672$ for $g_D = 1, 2$ Dirac Monopole strengths, respectively [243]. Fig. 12 (left) shows the stopping power for a unit Dirac magnetic monopole in aluminium as a function of the velocity of the monopole. Inspection of Eqs. 18 and 22 shows that the ratio of the stopping power for a unit Dirac monopole and a unit electric charge moving with velocity β is $\sim 4700\beta^2$. It can be seen from Fig. 12 that, as a monopole slows down, the ionisation becomes less dense, in contrast to the case of electrically charged particles for which the opposite is true. This adds to the striking nature of a track left by a monopole.

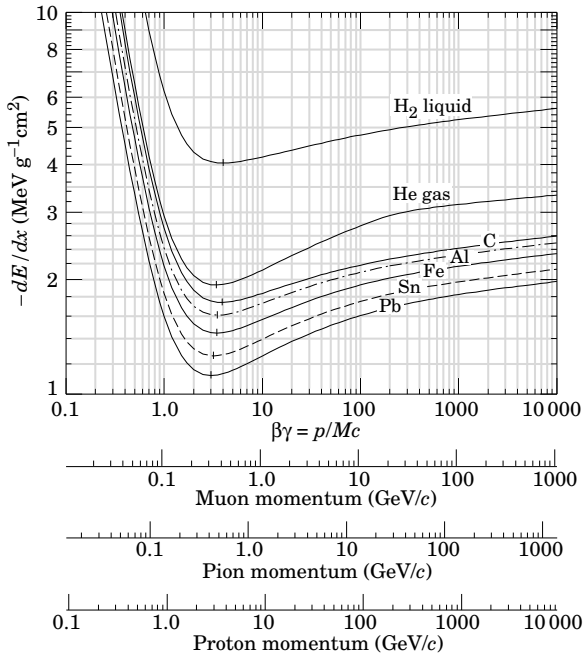

Fig. 11. The stopping power ($\frac{dE}{dx}$) for particles in different materials (omitting radiative effects) [1].

The large differential ionisation energy loss of monopoles makes it relevant to discuss the range. The range R, of monopoles in aluminium is computed [251] by integrating the stopping power shown in fig 12. So that

$$R = \int_0^E \frac{dE}{dE/dx} = M \int_0^\gamma \frac{d\gamma}{dE/dx(\beta\gamma)} \tag{23}$$

Fig. 12 (right) shows the computed range (normalised to mass), for a Dirac monopole versus $P/M = \beta\gamma$ where P and M are the momentum and mass of the monopole, respectively.

The theory of energy loss described above is implemented as part of a GEANT package to describe monopole interactions in a detector [265].

5.2 Nuclear interactions of SMPs

As heavy (charged or neutral) hadrons propagate through a medium, they may undergo scattering from the nuclei of the material of the apparatus. For R hadrons the interaction cross sections are expected to be of the order of those for pion scattering (see below). As is shown in this section it is expected that the energy loss of an R-hadron through such scattering can be sufficiently small as to allow it to penetrate through to an outer muon chamber and be reconstructed as a slow moving exotic particle. However, in extreme cases such interactions can have a large

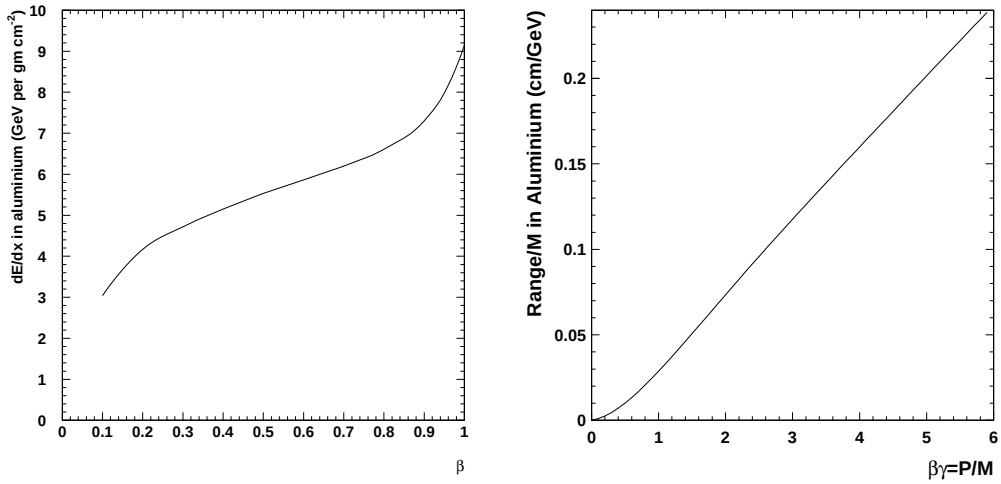

Fig. 12. Left: the $\frac{dE}{dx}$ for a Dirac monopole in aluminium as a function of the velocity of the monopole taken from [243] and adjusted for the electron density in aluminium. Right: the ratio of range to mass for a Dirac monopole in aluminium versus $\beta\gamma$, calculated from the stopping power, $\frac{dE}{dx}$.

impact on experimental searches. For example, these interactions can lead to R-hadrons being 'stopped' inside the detector material, because they come to the end of their ranges due to electromagnetic and hadronic energy losses. Also, R-hadrons could undergo charge exchange reactions in a hadron-absorbing material such as a calorimeter, in which case the initial charge at the production vertex is not necessarily the same after traversing the material. An understanding of such effects is crucial to quantify a discovery or assess a discovery potential. This section provides an overview of the theory of R-hadron scattering processes and a description of the phenomenological approaches which have been used to describe them. Before discussing these different approaches, we summarise which general observations can be made, independently of any specific model.

One important feature of R-hadron scattering common to all approaches is the passive nature of the exotic heavy coloured object. The probability that the parton C_i of colour state i will interact perturbatively with the quarks in the target nucleon is small, since such interactions are suppressed by the squared inverse mass of the parton. As a consequence, the heavy hadron can be seen as consisting of an essentially non-interacting heavy state C_i acting as spectator, accompanied by a coloured hadronic cloud of light constituents, responsible for the interaction. Hence the interaction cross section will be typical of that of a meson. In addition, the effective interaction energy of the heavy object is small. As an example, consider a $C_8 q\bar{q}$ state with a total energy E=450 GeV and a mass m of the C_8 parton of 300 GeV, the Lorentz factor will be γ=1.5. Although the kinetic energy of the R-hadron is 150 GeV, the kinetic energy of the interacting $q\bar{q}$ system is only $(\gamma - 1)m_{q\bar{q}} \approx 0.3$ GeV, (if the quark system consists of up and down quarks). For R-hadrons produced at the Tevatron or LHC with masses above 100 GeV, the centre-of-mass energy of

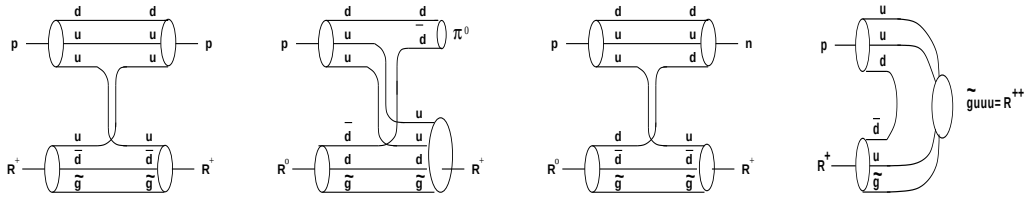

Fig. 13. R-hadron-proton scattering processes. (a) Elastic scattering, (b) Inelastic scattering leading to baryon and charge exchange, (c) Inelastic scattering leading to charge exchange, (d) Resonance formation.

the system of quarks and a stationary nucleon can thus be at most around a few GeV. Thus, the energy scales relevant for heavy hadron scattering processes from nucleons are low and comparable with low-energy hadron-hadron scattering for which Regge theory is often applied. The heavy state C_i serves only as a reservoir of kinetic energy.

Although R-hadrons may scatter elastically or inelastically the energy absorbed in an elastic scattering process, such as that illustrated in Fig. 13 (a), is expected to be small [266], since the high-mass R-hadron scatters on a lower mass target nucleus, and inelastic collisions are expected to be largely responsible for the energy loss of an R-hadron. These inelastic collisions may cause the conversion of one species of R-hadron to another in two ways: baryon exchange, which was overlooked until recently [232], and charge exchange, as shown in Fig. 13 (b) and (c), respectively. In the first process, an exothermic inelastic R-meson-nucleon interaction results in the release of a pion. The reverse reaction is suppressed by phase space and because of the relative absence of pions in the nuclear environment. Thus, most R-mesons will convert early in the scattering chain, in passing through hadron absorbing material, e.g. a calorimeter, to baryons and remain as baryons. This is important, since baryons have larger scattering cross sections. Baryon formation offers one opportunity for a charge exchange process to take place. Charge exchange may arise in any meson-to-meson, meson-to-baryon, or baryon-to-baryon process. Although exact predictions of individual processes are difficult to make, the low energies involved in R-hadron scattering imply that reggeon and not pomeron-exchange will dominate, and thus charge exchange reactions may well form a substantial contribution to all interactions. This may lead to striking topologies of segments of tracks of charged particles with opposite signs of charge on passage through hadron absorbers or calorimeter material. It is also interesting to note that such a configuration can also arise if a neutral R-meson, formed as an intermediate state during scattering, oscillates into its own anti-particle and then subsequently interacts to become a charged R-hadron [241, 242].

Several phenomenological approaches have been developed [26, 232, 267] to describe R-hadron nuclear scattering which are described later in Sections 5.2.1 and 5.2.2. Although these differ in the phenomenology used, they are largely based on

the generic picture of R-hadron scattering described above, much of which was first introduced in [266]. Low-energy hadron-hadron data are typically used to estimate scattering cross sections and several of these models are based on modified Regge paramaterisations of the data. Uncertainties in the models arise from several sources. Most models assume R-meson scattering processes to be dominant despite it being likely that a meson will convert into a baryon and then stay baryonic as it propagates through matter. A further theoretical uncertainty arises from resonance production. The formation of resonant R-hadron states, as shown in Fig. 13 (d), is expected to take place during hadronic interactions. To date, no explicit modelling of R-hadron resonances has yet been attempted. However, it has been argued that the the minimum centre-of-mass energy required for a scattering process is above the expected mass of the main resonances [232]. Nevertheless, since little is known about such resonances it is important to note that they may play an important role in accounting for R-hadron energy loss and conversions.

Below, we will discuss for each of the phenomenological approaches the interaction cross section or interaction length, scattering processes included, and energy losses.

5.2.1 Models based on Regge theory

Consider a gluino R-hadron scattering proces $RN \rightarrow R'X$, where R is the initial R-hadron before scattering, N is a single nucleon (proton or neutron), R' is the R-hadron after scattering, and X is the remaining system produced in the scattering, the latter is expected to be a nucleon and possibly a number of other light hadrons.

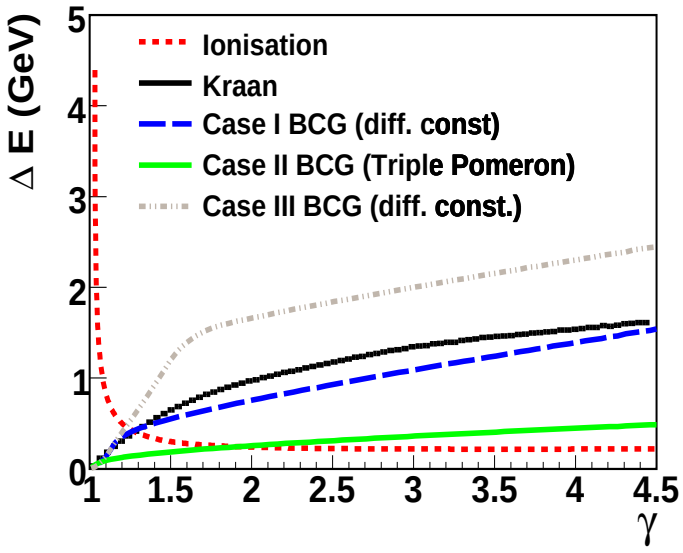

Fig. 14. Predictions from four phenomenological models of expected hadronic energy loss per interaction as a function of the Lorentz factor γ. Also shown is the ionisation energy loss corresponding to the passage of an R-hadron with charge $\pm e$ through 18 cm of iron.

Baur, Cheung and Gunion (BCG) [267] propose three different ansatzes for the functional form of the cross section for gluino R-hadron scattering processes:

(1) $\frac{d\sigma}{d|t|dm_X} \propto 1$ for $|t| \leq 1$ GeV^2 and 0 for $|t| > 1$ GeV^2
(2) $\frac{d\sigma}{d|t|dm_X^2}$ given by a triple-pomeron form used to describe single inclusive particle production in pion-nucleon scattering
$\frac{d\sigma}{d|t|dm_X^2} \propto \frac{1}{m_X^2}\beta^2(|t|)(\frac{s}{m_X^2})^{2(\alpha_P(|t|)-1)}(m_X^2)^{\alpha_P(0)-1}$ where $\alpha_P(|t|) = 1 - 0.3|t|$ and $\beta(|t|) = \frac{1}{(1+|t|/0.5)^2}$.
(3) $\frac{d\sigma}{d|t|dm_X} \propto 1$ for $|t| \leq 4$ GeV^2 and 0 for $|t| > 4$,

where t is the four-momentum transferred from R to R', and m_X is the mass of the remaining system of final state particles produced. The cross section $\sigma_T(RN)$ for gluino R-hadron scattering on a nucleon is derived from the cross section $\sigma_T(\pi N)$ for pion nucleon scattering. The normalisation of the cross section is determined by constraints on the collision length $\lambda_T(R)$ of an R-hadron. The evaluation of $\lambda_T(R)$ is made by correcting the pion collision length $\lambda_T(\pi)$.

$$\frac{\lambda_T(R)}{\lambda_T(\pi)} \equiv \frac{\sigma_T(\pi N)}{\sigma_T(RN)} = (\frac{C_F}{C_A})\frac{\langle r_\pi^2\rangle}{\langle r_R^2\rangle} \tag{24}$$

The colour factors $C_F = 4/3$ and $C_A = 3$ arise due to the low-mass colour-octet constituent of the R-hadron. The term $\langle r^2\rangle$ is the squared transverse size of the particle. In the case of a pion and an R-hadron r^2 is given by $\langle r_R^2\rangle \propto 1/m_g^2$, and $\langle r_\pi^2\rangle \propto 4/m_q^2$. Here, m_q and m_g are the constituent masses of light quarks and gluon constituent masses, respectively, which were assumed equal in this approach. This leads to a collision in length in iron of R-mesons of around 19 cm. However, the uncertainties in the constituent masses of the partons would affect the collision length, and a value of 38 cm has also been considered within the BCG approach.

As mentioned above, this model does not take into account R-baryons or conversion from mesons into baryons. Charge exchange reactions are possible since the R-hadron is considered to be stripped of its system of quarks following a nuclear scattering. A refragmentation process, governed by a probability to fragment into a charged or neutral state then allows the formation of a new type of R-hadron.

The energy loss of hadron R scattering on nucleon N in the process $RN \rightarrow R'X$ is given by

$$\Delta E = \frac{m_X^2 - m_N^2 + |t|}{2m_N}. \tag{25}$$

Here ΔE is then evaluated according to the parameterisation chosen for the differential cross section $\frac{d\sigma}{d|t|dm_X^2}$. The distribution of mean energy loss per collision as a function of γ for the three different scenarios of this approach is shown in Fig. 14. All three approaches show a rising energy loss with γ. However, there are large differences between the various scenarios. For comparison, the ionisation energy loss corresponding to the passage of an R-hadron with charge $\pm e$ through 18 cm of

iron (1 interaction length for R-mesons in the approach by Kraan discussed below in Section 5.2.2) is also shown.

This approach has been extended by Mafi and Raby [26](MR), where again a single particle inclusive scattering process $RN \rightarrow R'X$ involving only R-mesons was considered. However, MR consider two Regge trajectories: an isosinglet pomeron, and an isovector reggeon ρ trajectory. Using these, triple pomeron and reggeon-reggeon-pomeron cross-section forms were extracted. The presence of reggeon exchange incorporates charge exchange processes naturally without relying on the BCG assumption that an R-hadron is stripped of its soft partonic system in an interaction and then forced to fragment. Two values of the collision length $\lambda_T = 19$ cm and $\lambda_T = 38$ cm are used in their analysis to estimate R-hadron stopping in different scenarios and the scattering cross section functional form was rescaled to achieve these values. The relative proportion of reggeon and pomeron were also allowed to vary between the extreme cases of 100% reggeon and 100% pomeron exchange. As mentioned above, charge exchange processes are naturally included in this approach. Baryon exchange processes are however omitted. The typical energy loss per collision is of the order of several GeV and is comparable with the BCG approaches.

5.2.2 Model based on geometrical cross sections

Since the behaviour of the hadron-hadron scattering cross sections at values of the centre-of-mass energy below several GeV is specific to the type of hadrons interacting, it is not necessarily a reliable general guide to the scattering of R-hadrons. Therefore, in a complementary approach to the Regge-based models of MR and BCG the constant geometrical cross section is used by Kraan [232] over the full scattering energy regime.

The total nucleon interaction cross section is approximated by the asymptotic values for the cross sections for normal hadrons scattering off nucleons. The model assumes that only u and d quarks are present in R-hadrons and that each quark which can interact represents a contribution of 12 mb to the total scattering cross section. Thus, the scattering cross sections of a gluino R-meson and R-baryon are 24 mb and 36 mb, respectively. A gluino-gluon state can be assumed to have the same cross section as a gluino R-meson, since the geometrical cross section is approximated by the high-energy hadron cross section, where gluon exchange would dominate. The gluon-gluon coupling is a factor 9/4 larger than the quark-gluon coupling, but a meson has two quarks, resulting in a cross section of a gluino-gluon state which is (9/4)/(1+1)$\approx$1 times the cross section for a gluino R–meson. Translating this into interaction lengths, for R-baryons the average nuclear interaction length (i.e. amount of material where on average one interaction takes place) is 12 cm in iron, 31 cm in carbon, and 660 cm in hydrogen. For R-mesons these numbers are 3/2 larger.

This model includes predictions for all possible $2 \rightarrow 2$ and $2 \rightarrow 3$ processes. The relative rates of $2 \rightarrow 2$ and $2 \rightarrow 3$ processes are, in the asymptotic region, set to 15% and 85%, respectively, as suggested by hadron-hadron scattering data. A phase space factor is used to determine the proportion of $2 \rightarrow 2$ and $2 \rightarrow 3$ processes as the scattering centre-of-mass energy is reduced. Within the sets of $2 \rightarrow 2$ or $2 \rightarrow 3$ interactions each allowed process is assigned the same matrix element and the different rates of processes is determined by phase space. Included in these processes is charge exchange, and, for the first time, baryon exchange. Fig 15 shows the fraction of R-mesons which convert into R-baryons when travelling in iron. As was already mentioned in Section 5.2, conversion from baryons back to mesons is highly suppressed.

Energy losses are determined by implementation of the model into the GEANT framework (GEANT-3 [232] and GEANT-4 [268]), which allows a more sophisticated treatment of energy loss in a nuclear reaction than was possible in the analytical approaches of BCG and MR. Issues related to nucleus scattering like Fermi motion, binding energy of the nucleons inside the nucleus, evaporation energy and instability of a nucleus are thus included. Figure 14 displays the nuclear energy loss per interaction for an R-meson (the curve labelled Kraan). The energy losses from this model are found to lie between the different BCG approaches. Ionisation losses are also shown and they dominate energy losses only at low beta values ($\beta < 0.75$).

6 Search techniques

Following the previous section on the interactions of SMPs in materials, this section describes how these interactions can be used to search for SMPs in colliders. Search techniques include the use of ionisation energy loss, Cherenkov radiation and time of flight. Finally, we summarise search techniques which are only applicable to

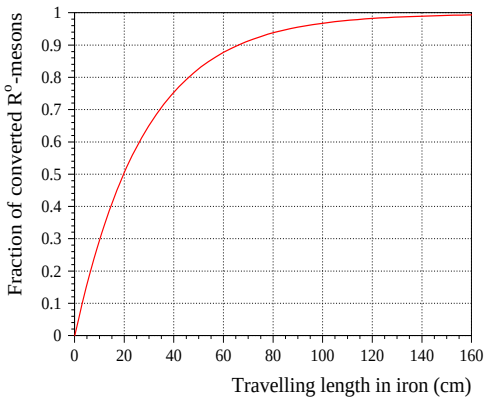

Fig. 15. Fraction of R-mesons converted into R-baryons as predicted in the model of Kraan [232].

magnetically charged SMPs.

6.1 Methods based on ionisation energy losses

The most commonly used observable in SMP searches is the measurement of the continuous ionisation energy loss $\frac{dE}{dx}$.

6.1.1 Measurements of ionisation energy losses in tracking systems

Ionisation energy loss can be used to identify heavy charged particles with tracking chambers. The measurement of $\frac{dE}{dx}$ is part of the routine program of calibrating charged particle tracking chambers. However, a number of systematic studies must be performed in order to optimise the detector calibration. Examples of the application of ionisation loss measurements in different collider environments can be found in Section 7.1, and the accompanying table 5.

It can be seen from Eq. 18 that the value of $\frac{dE}{dx}$ is dependent on the velocity factors β, γ. The particle's momentum ($p = M\beta\gamma$) is measured independently, usually from the curvature of the track in the magnetic field. Hence, comparing the measured value of $\frac{dE}{dx}$ with an independent measurement of track momentum, the particle mass can be determined. Fig. 16 shows an example of what mass separation was achieved in the OPAL experiment when simultaneously measuring $\frac{dE}{dx}$ and momentum. The regions in which SMPs possessing various values of charge and mass could be manifest are shaded.

Several issues must be taken into account in the identification of charged particles by $\frac{dE}{dx}$ measurements. First of all, considerable fluctuations occur in single measurements of $\frac{dE}{dx}$. These are not Gaussian but are asymmetric with a high-energy tail due to the emission of energetic secondary electrons (δ rays), giving rise to the Landau distribution [269]. Examples of methods adopted to avoid complications due to these high-energy tails include disregarding abnormally large single measurements of $\frac{dE}{dx}$ and taking the mean of the remaining measurements [270] or suppressing tail distributions [271]. Another method is to perform a maximum likelihood fit of a Landau distribution to the sample of measurements on a track [272] to determine the mean value of $\frac{dE}{dx}$ for the track. The particle masses determined from the $\frac{dE}{dx}$ at a fixed momentum had smaller high-mass tails using this method than with the others [272]. Hence this is likely to be the best technique to employ in searches for unknown particles, since there will be less background by smearing from the lower mass region. The large numbers of measurements needed for reliable $\frac{dE}{dx}$ determination means that silicon vertex detectors with small numbers of detector layers are likely to be of limited usefulness in searches for unknown SMPs.

Further problems in measuring $\frac{dE}{dx}$ for unknown massive particles could arise due

to saturation of the electronics used in the track detectors. For such searches the electronics must have a wide enough dynamic range otherwise large values of $\frac{dE}{dx}$ become unmeasurable due to saturation. This is particularly true for magnetic monopoles, for which $\frac{dE}{dx}$ is significantly larger than that for electrically charged particles, but may already play a role for slow electrically charged ones. Although saturated hits have a tracking resolution much worse than that of typical unsaturated data, the presence of many saturated channels is itself a distinctive feature of the presence of a high-mass charged particle. A characteristic pattern of a charged particle helix can generally easily be recognised from the spatial distribution of saturated hits. The technique of searching for saturated hits has been applied in Ref. [273]. Saturation of electronics as a consequence of highly ionising particles may in particular have a non-negligible effect in the future LHC collider experiments where the resulting dead time as a result of electronics saturation may be of the order of the bunch crossing time. The effect of highly ionising particles on the CMS silicon strip tracker has been studied in Refs. [274, 275].

There are several kinds of backgrounds producing highly ionising signals. An important background source to such studies is positively charged nuclei. These typically arise as spallation products from secondary interactions of particles produced in the primary interaction. Such interactions take place with nuclei in the material of the apparatus. This accounts for stronger limits for negatively charged SMPs using this approach, since spallation products are positively charged. Another background arises from the finite resolution of a tracking chamber, causing, for example, two overlapping tracks to be measured as one; this results in a highly ionizing signal. These backgrounds are mainly caused by photon conversions. Finally, interactions of the colliding beams with residual gas atoms in the beam pipe can also produce highly ionising spallation products. However, most background events can usually be effectively removed by the application of a lower cut on the momentum [276].

6.1.2 Methods using ionisation damage in plastic foils

Next to $\frac{dE}{dx}$ measurements to identify heavy particles in tracking chambers, heavily ionising single particles (magnetic or electrically charged) can be detected by the damage they cause to certain plastic foils eg. foils made from plastics such as lexan, CR39 and Makrofol [124]. Such damage is caused by both the NIEL and the ionisation energy loss. The effect of the damage is made visible by chemically soaking the foil in a concentrated alkali solution which etches the region around the damage centre into small holes (pits) which are visible under a microscope [278]. The value of $\frac{dE}{dx}$ of a heavily ionising track can be determined from the etch rate i.e. the ratio of the rate of increase in depth of the pit to the decrease in overall thickness of the foil due to the chemical action. Fig. 17 shows the pits produced by sulphur ions in a heavily etched CR39 foil (type EN3) as reported in [279]. The etching process only makes the tracks visible for ionisation levels above a threshold value so that the lightly ionising tracks remain invisible and only the heavily ionising tracks

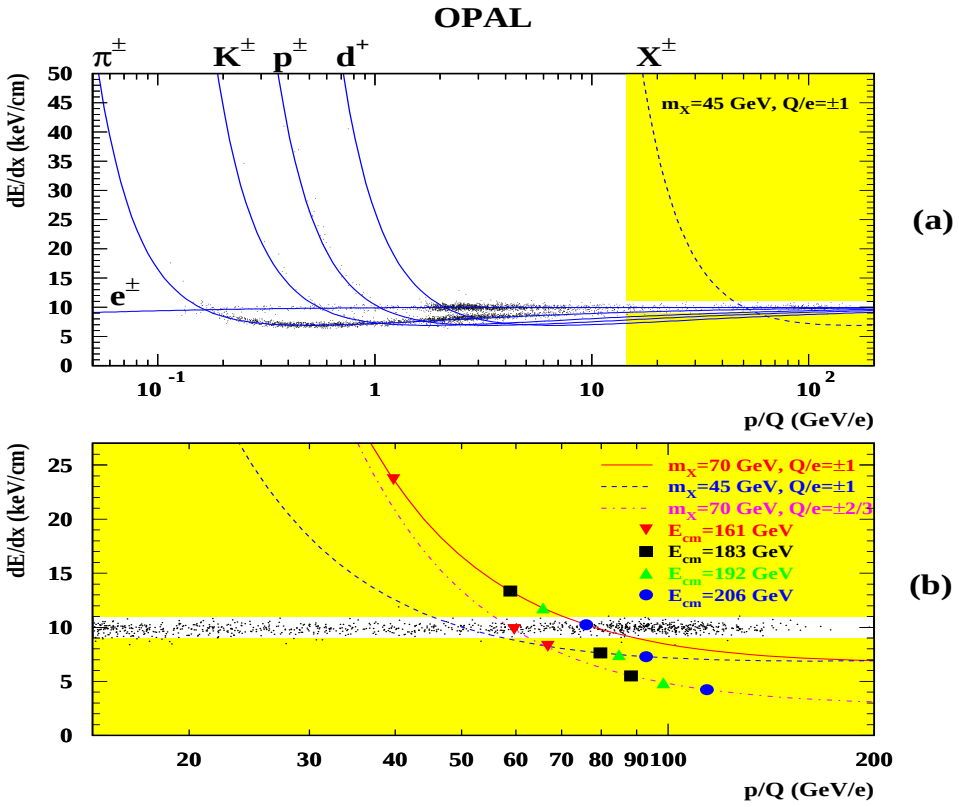

Fig. 16. Measurements of $\frac{dE}{dx}$ vs $\frac{p}{Q}$ as measured by the OPAL experiment [277], where Q is the charge of the particle. The smooth curves show the expected values of the mean values of $\frac{dE}{dx}$ for the known particles, while the dotted points are the measured values. The regions in which unknown massive particles are sought are shaded. Also shown are lines which illustrate the expected $\frac{dE}{dx}$ values of SMPs with specific masses and charges.

are seen. For heavy ions of velocity β and atomic number Z, the experiment of Ref. [279] found that the threshold corresponded to ions with $Z/\beta \sim 8$ for CR39 (type EN3). In collider experiments [250, 279–283], the layers of foils surround the beam pipe at an interaction point and are left to be exposed to the products of the beam interactions. After the exposure the foils are soaked in the appropriate chemical to etch out the damage centres. Usually, the inner layer foil is scanned under a microscope to search for etched pits. The outer layers are then scanned for pits which align with those found in the inner layer to search for heavily ionising continuous tracks.

6.2 Ring Imaging Cherenkov detection

Another way to exploit the electromagnetic interactions of SMPs to identify them is via the Cherenkov effect [1, 284]. A particle, travelling with velocity β which is

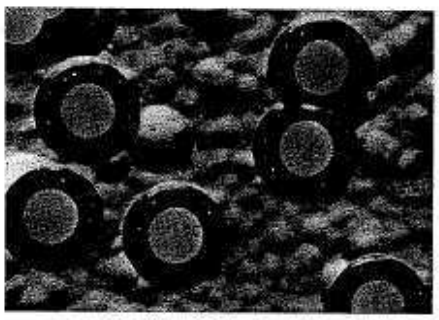

Fig. 17. Microphotograph of a heavily etched CR39 sheet (type EN3) exposed to sulphur ions of 200 GeV/nucleon [279]. The sheet thickness was reduced from 1.4 mm to 0.2 mm by the heavy etching. Note the holes produced by the sulphur nuclei.

faster than the speed of light in a medium of refractive index n, emits light waves by the Cherenkov effect in a cone at an angle of $\cos\theta = 1/n\beta$ relative to the track direction. The number of Cherenkov photons per unit path length is proportional to $\sin^2\theta$. Particles with velocity less than the speed of light in the medium do not emit Cherenkov light. Unlike the other LEP experiments, the DELPHI detector contained Ring Imaging Cherenkov (RICH) systems [285–288] comprising two Cherenkov radiators with different refractive indices: one in the liquid and one in the gaseous phase. To select low-velocity massive particles it was required that neither detector should give a detected Cherenkov light signal for high-momentum tracks. The DELPHI experiment was able to use this technique for a number of SMP searches [289–291], the results of which are described in Section 7.1.

6.3 Methods based on time of flight

Another technique which can be used for the detection of SMPs is the method of time of flight. Although less widely used than the $\frac{dE}{dx}$ method, this method has been applied in several collider environments, examples of which can be found in Section 7. Massive particles are produced with a smaller velocity than light particles, and thus would have a larger time of flight. For electrically charged particles the mass of the particle can be determined by correlating the flight time with the track momentum, p, measured from another source e.g. from the track curvature in a magnetic field. Timing can be obtained from the detection of the tracks in scintillation counters. Since $M = p/\beta\gamma$, particles are identified by plotting a graph of $1/\beta^2$ against $1/p^2$ which is linear with slope $1/M^2$ for particles of mass M. The accuracy of determination of the mass due to the momentum and time of flight uncertainties, which are assumed to be uncorrelated, is

$$\left(\frac{\Delta M}{M}\right)^2 = \left(\frac{\Delta p}{p}\right)^2 + \left(\gamma^2\frac{\Delta\beta}{\beta}\right)^2 \tag{26}$$

where the uncertainty in the velocity $\Delta\beta/\beta = \Delta t/t$ with t the time of flight. For a typical timing resolution of $\Delta t \sim 1$ ns and performing time of flight over a distance of ~ 3 m [292], the mass resolution $\Delta M/M$ varies between 2% to 23% for particles in the range of $0.2 < \beta < 0.8$, neglecting the momentum resolution. Hence the technique is comparable to the $\frac{dE}{dx}$ technique in the precision of the mass measurement [272].

Backgrounds in time of flight measurements can arise from instrumental effects such as mismeasured times or random hits in the scintillation counters. Cosmic rays may form a substantial background, as may K-decays in flight. In addition, at colliders with high-frequency bunch crossings and a large number of interactions per bunch, such as the LHC, the particles from one bunch may become confused with particles from another bunch. In this situation, it may not be possible to make a unique determination of the time of flight.

A slightly different technique which has not been used so far but could be used to detect heavy charged particles is to measure the track velocity with a tracking system based on wires and gas. The detection time of the signal of a traversing charged SMP is in simplified form given by

$$t = t_0 + t_{TOF} + t_{drift} + t_{electronics} \tag{27}$$

where t_0 is bunch crossing time, t_{TOF} is the time of flight from the beampipe to the wire, t_{drift} is the drift time of the signal inside the gas to the wire, and $t_{electronics}$ is the time for the transmission of the signal. For a slow particle, t_{TOF} is large. Since default track reconstruction programs are based on expectations for t_{TOF} for light particles, a misalignment occurs for slow moving particles. If the reconstruction of the track is successful, this pattern is very distinctive for heavy slow particles. It could in addition be used to support a heavily ionizing signal. This method has not yet been applied in data, but has been studied in Ref. [293] with the ATLAS muon reconstruction software [294].

6.4 Specific techniques for magnetic monopoles

In addition to the techniques described above, a number of approaches have been used purely to search for particles with magnetic charge. Examples of applications of the techniques discussed below are given in Section 7.2.

6.4.1 Parabolic tracks

Monopoles experience a force $g\mathbf{B}$ in a magnetic field $\mathbf{B}$ which causes them to accelerate. With the field aligned along the z axis they assume a parabolic trajectory

with

$$z(r) - z_v = \frac{g|\mathbf{B}|r^2}{2eP_T\beta_T\ 10^9} + \frac{r}{\tan\theta_0} = \frac{g_D 20.54|\mathbf{B}|r^2}{2P_T\beta_T} + \frac{r}{\tan\theta_0} \qquad (28)$$

where z_v is the z coordinate of the vertex and $z(r)$ is the coordinate of a point on the trajectory at distance r from the proton beam with lengths in metres and $|\mathbf{B}|$ in Tesla. The transverse momentum and transverse velocity of the monopole are P_T GeV/c and β_T, respectively, and g_D is the pole strength in units of the Dirac Monopole. The initial angle of the monopole to the magnetic field direction is θ_0 and e is the unit of electric charge. In this equation g is the magnetic pole strength which is negative (positive) for South (North) poles which decelerate (accelerate) in the $+z$ direction in the magnetic field.

A simulation of the passage of a monopole, anti-monopole $(m\bar{m})$ pair at the TASSO experiment [295] is shown in Fig.18. Fig.18 (top) shows the $r-\phi$ plane (transverse to the magnetic field direction) of the paths of the two particles which are produced at the primary interaction point (IP). However, as seen in the lower plots, the paths of the particles are clearly disturbed by the magnetic field in the $s-z$ view, where z is a distance parallel to the beam axis and s is the total distance travelled by the monopole along its path.

6.4.2 Searching for stopped magnetic monopoles

A further method to search for monopoles utilises the fact that the $\frac{dE}{dx}$ of magnetic monopoles is so large that they tend to stop in the beam pipe or apparatus surrounding the interaction region. When a monopole stops, i.e. reaches a speed comparable to that of an electron in a Bohr orbit of the atom ($\beta \sim 0.01$), it is expected to become bound to the nuclei of the atoms of the material. The binding energy is dependent on the magnetic dipole moment of the nucleus [296–298] which depends on the nuclear spin. Hence magnetic monopoles should remain bound in materials such as aluminium (nuclear spin 5/2). Since the binding energy of a magnetic monopole to a nucleus with zero magnetic moment is expected to be small, the monopoles may diffuse out of materials made of mainly even-A and even-Z nuclei with spin zero i.e. zero magnetic moment, e.g. carbon. The strong divergence of the monopole magnetic field, $B = \mu_o g/4\pi r^2$, causes a persistent current to flow if the monopole is passed through one or more superconducting (sense) coils . In contrast, divergenceless magnetic fields from ubiquitous magnetic dipoles and higher moments cause the current to return to zero after complete passage through the coil. If the material surrounding the beam is cut into small pieces which are then passed through the superconducting coil a residual persistent current signifies the presence of a monopole in the sample. The current is measured using a Superconducting Quantum Interference Device (SQUID) connected to the sense coils. This method was invented to search for monopoles in lunar rocks [299–302]. The response of the superconducting coils can be calibrated by the traversal of the coil by one end of a long, thin solenoid, the magnetic field at the end of which approximates to

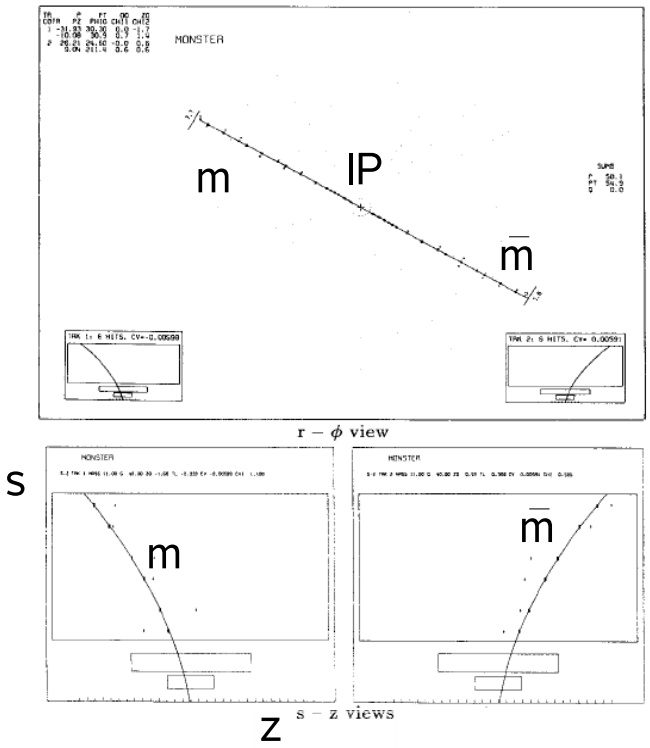

Fig. 18. Simulated monopole, anti-monopole production at the TASSO detector [295]. The top plot shows the paths of the particles (produced at the centre) in the r/ϕ view. The lower left (right) plot shows the path of the monopole (anti-monopole) as it is accelerated (decelerated) in the magnetic field, in the $s-z$ view, where s is the total distance travelled.

that of a magnetic monopole. Since the induced monopole current is persistent, it is also possible to increase the sensitivity of the apparatus by repeated traversals of the same sample of material. This technique of gradually building up a signal is especially useful when searching for particles with values of the magnetic charge substantially less than the Dirac charge g_D. Using this technique experiments have searched for magnetic charges as low as $\frac{1}{10}g_D$ [251, 299]. The apparatus used for the H1 search [251] is typical of such searches and is illustrated in Fig.19.

In addition to using a SQUID, it is also possible to use strong external magnetic fields to look for stopped monopoles. In Refs. [303–305] materials in which monopoles could be stopped were placed in front of a pulsed solenoid. A magnetic field of around 80 kG is expected to be large enough to liberate a monopole and accelerate it towards the detection systems comprising scintillators and plastic track detectors. Searches have been sensitive to charges in the range 0.03-0.24g_D.

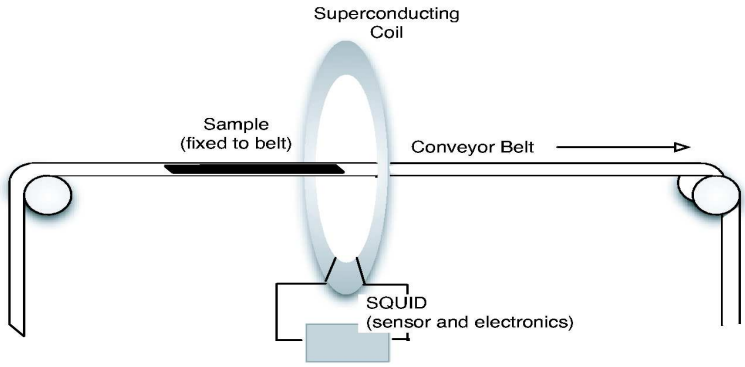

Fig. 19. A schematic diagram showing the SQUID apparatus used by the H1 experiment [251]. The conveyer belt travelled in small steps until the sample was passed completely through the coil. At each step the current in the superconducting coil was read.

7 Searches at colliders

This section gives an overview of the various *direct* searches which have been performed for SMPs at colliders, i.e. searches based on detecting SMPs by their passage through the detector. The results of direct SMP searches broadly fall into three different classifications.

- **The first class** concerns general searches for SMPs, which are made without assumptions on the properties of the SMP, other than the values of the electric or magnetic charge, spin and mass. Predicted cross sections are not available and model-independent upper limits on production cross sections are extracted within a specific mass acceptance region. Such searches are designed to be sensitive to SMPs with a wide range of values of mass and charge, and thus cover many of the SMPs predicted in Section 2, as well as unexpected particles.
- **The second class** of searches assumes the existence of certain types of SMPs with specific quantum numbers. These searches are based on minimal theoretical scenarios in which the production mechanisms and mass-dependent cross sections are assumed to be known. The influence on the SMP production cross sections of any other exotic particles which may be predicted within these scenarios, eg via loop diagrams, is small. This allows lower limits on SMP masses to be derived which depend dominantly on the properties of the SMP and not on other model parameters.
- **The third class** concerns searches made within theoretical scenarios for which the search results are quoted in terms of the complicated model parameter space.

Searches for electrically charged particles have been made in all three classes whereas, owing to the difficulties in calculating short-distance monopole interactions, monopole searches are typically made within the first class, with comparatively few searches also quoting a mass limit. It should be noted that a given study can present sets of results which fall into different classes.

This section is organised as follows. In Section 7.1 direct searches for electrically charged particles are reviewed. Searches at e^+e^-, hadron-hadron, and lepton-hadron facilities are described. Searches in each collision environment are described in the class order given above. We then make a short summary of all of the direct collider searches, pointing out the most stringent limits which have been obtained. Finally, some *indirect* searches, i.e. searches for physics signals in which SMPs play an indirect role (for example from their presence in loop diagrams) but may not manifest themselves as final-state particles, are briefly touched upon at the end of Section 7.1. The same structure is adopted for the description of monopole searches in Section 7.2, although in this case the vast majority of search results fall within the first classification.

The intention in this section is not to provide an exhaustive compendium of all results in this field, such as that which can be found in Ref. [1]. However, tables of selected results showing the most stringent limits extracted for electrically charged particle searches which belong to class 1 and to classes 2 and 3 are summarised in Tabs. 4, 5, respectively. Tab. 6 summarises magnetic monopole searches.

7.1 Searches for electrically charged SMPs

Searches for SMPs have been performed at e^+e^-, lepton-hadron, and hadron-hadron colliders. The majority of recent searches has been performed at LEP and comparatively few studies have been made at the Tevatron and HERA.

7.1.1 Searches at e^+e^- experiments

The early studies at low-energy e^+e^- facilities in the 1980s, such as PETRA ($\sqrt{s} = 27 - 35$ GeV), PEP ($\sqrt{s} = 29$ GeV) and Tristan ($\sqrt{s} = 50 - 61$ GeV), comprised generic searches for SMPs with unexpected mass and charge, and, in particular, searches for particles possessing fractional charges, as inspired by the possibility of the existence of free quarks [1]. Although the notion of the existence of free quarks had fallen out of favour in the 1990's, the experiments at LEP ($\sqrt{s} = 91.2, 130 - 209$ GeV) continued to search for fractionally charged objects, and, in addition, made a number of SMP searches within exotic scenarios, such as SUSY. Owing to the high collision energies and large luminosity samples at LEP-1 (LEP-2), typically ~ 100 (~ 700) pb^{-1}, the most stringent results were usually extracted at LEP. Unless stated to the contrary, the LEP results quoted here were based on luminosity samples of approximately these magnitudes.

The e^+e^- searches for generic SMPs used simple topological cuts to look for the exclusive or inclusive production of SMPs. The principal experimental observable used was the ionisation energy loss measured in a tracking system. This was the approach adopted by the low energy experiments [306–313] and by ALEPH [273,

276], OPAL [277, 314–316] and L3 [317–319]. For the DELPHI studies, a RICH detector was used, in combination with ionisation measurements from a TPC [289, 290, 320].

The most stringent e^+e^- limit, in terms of mass reach, for fractionally charged particles, was obtained recently at LEP-2 by OPAL [277]. For this study, the collision centre-of-mass energy spanned 130-209 GeV. An exclusive pair-production mechanism $e^+e^- \rightarrow X\bar{X}$ was assumed, and model-independent upper limits on the production cross section for weakly interacting scalar and spin $\frac{1}{2}$ particles with charge $\pm e$ of between 0.005 and 0.03 pb were extracted at 95% confidence level (CL), for a sensitive mass region between 45 and 103 GeV. This work also made a search for particles possessing fractional charges $\pm\frac{2}{3}e$, $\pm\frac{4}{3}e$, $\pm\frac{5}{3}e$, with the resultant cross-section limits lying between 0.005 and 0.02 pb at 95% CL. Using a substantially smaller luminosity sample ($\sim$ 90 pb^{-1}), and for centre-of-mass energies of 130-183 GeV, DELPHI was able to place limits on the production cross-section of SMPs with charges $\pm\frac{2}{3}e$ [290], for masses in the range 2-91 GeV. In this work a free squark model was assumed, and cross-section limits of between 0.04 and 0.6 pb were obtained at 95% CL. Using an exclusive slepton pair-production model, DELPHI also extracted upper cross-section limits in the range 0.05-0.3 pb for SMPs with charge $\pm e$ for masses up to 93 GeV [289, 290]. Less stringent cross section limits for SMPs with charge $\pm e$ were also extracted by ALEPH [273]. The L3 experiment [317–319] searched for signatures of charged heavy leptons at LEP2. However, the results of these studies did not include any upper cross-section limits which are relevant for generic SMPs.

Searches at LEP-1 for fractionally charged objects made by ALEPH [276, 315] and lower energy e^+e^- colliders typically expressed their results in terms of limits on R_X, the ratio of the cross section for the single or pair production of SMPs to that of exclusive $\mu^+\mu^-$ production. Fig. 20 shows limits on R_X (to 90% CL), which were obtained from e^+e^- experiments for fractionally charged SMPs with masses below 45 GeV [276, 306–313] for the putative charges $\pm\frac{1}{3}e$, $\pm\frac{2}{3}e$, and $\pm\frac{4}{3}e$. Also shown is the ratio of the upper limit on the single inclusive production cross section of an SMP with charge $\pm e$ to the exclusive dimuon cross section. The LEP-1 results from ALEPH [276] and OPAL [315] were based on luminosity samples of 8 and 74 pb^{-1}, respectively and extend down to 5-10 GeV in mass. The lower energy e^+e^- limits exclude SMPs with masses as low as $\sim$ 1 GeV. To obtain the results shown in Fig. 20 the experiments assumed that the SMPs follow a momentum distribution suggested for a heavy particle: $E\frac{d^3N}{dp^3}$ =constant [219] (see Section 4.3). The extracted limits are very sensitive to the form of the momentum distribution. ALEPH demonstrated that the limits can change by more than a factor of five if the momentum dependence is derived from a fit to the Feynman-x spectra of inclusively produced hadrons [276].

In addition to the results described above, OPAL also extracted mass-dependent cross-section limits on the single inclusive production of SMPs with charges $\pm e$,$\pm\frac{4}{3}e$,

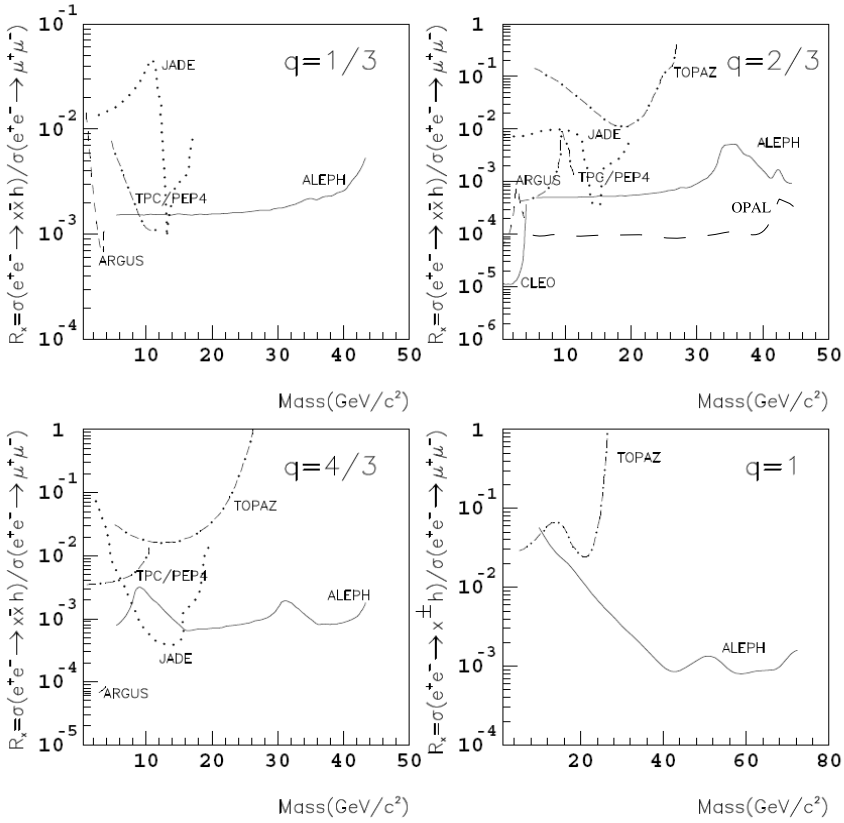

Fig. 20. The upper limits at 90% CL on the ratio R_X as extracted at LEP-1 (ALEPH [276] and OPAL [315]) and lower-energy experiments [306–313].

$\pm\frac{5}{3}e$, and $\pm 2e$. However, the experiment was not sensitive to particles with charge $\pm\frac{1}{3}e$. Furthermore, ALEPH and OPAL and some of the lower energy experiments [306, 307, 309, 311] also presented limits on the exclusive pair-production of SMPs with specific charges. The obtained limits on SMPs with charges $\pm\frac{2}{3}e, \pm e, \pm\frac{4}{3}e, 2e$ were of similar values to the limits they quoted for the inclusive cases.

The possibility of the production of SMPs with values of charge substantially in excess of e, such as Q-balls, has been investigated by experiments using plastic track detectors. While these were primarily monopole searches, the experiments were also sensitive to non-magnetically charged particles with unexpected values of electric charge. These works are often overlooked in studies which survey SMP searches although they are extremely important in extending the range in charge to which collider experiments are sensitive. Several such experiments took place at LEP-1 [250, 283]. In Ref. [283] the MODAL passive detector was deployed at the vacant I5 intersection point at LEP and was exposed to e^+e^- collisions corresponding to an integrated luminosity of 48 nb^{-1}. The experiment was sensitive to SMPs with electric charges of up to approximately $|240e|$ at low masses, with decreasing charge sensitivity as the mass increases. An upper limit on the production

cross-section of highly ionising particles of 70 pb was extracted, assuming that the efficiency was equal to the maximum value of acceptance for a pair of highly ionising particles. A second search [250], using passive detectors deployed at the OPAL intersection point, was exposed to a far higher luminosity (8.7 pb^{-1}). However, this experiment quoted its sensitivity only for particles possessing various values of magnetic charge (see Section 7.2.1).

In addition to the generic searches, model-dependent (class 2) searches for electromagnetically charged and weakly interacting SMPs have also been made. Using the $\frac{dE}{dx}$ technique heavy lepton limits have been extracted at LEP [277, 321] for a range of putative non-SUSY, heavy leptons, such as so-called sequential and mirror leptons (see Section 2.3.1). Using centre-of-mass energies up to 209 GeV, the L3 experiment [319] was able to exclude new leptons with masses below around 103 GeV to 95% CL. Varying the exotic scenario changes the limit by less than 1%.

A number of searches have been made by the LEP experiments for stable SMPs within SUSY scenarios. ALEPH [322] has obtained lower-mass limits for stable coloured sparticles through an analysis of LEP-1 and LEP-2 data. In Ref. [322] MSSM scenarios with a stable gluino or squark and R-parity conservation was assumed (see Sections 2.1.1- 2.1.4). For a stable gluino hypothesis, the process $e^+e^- \rightarrow q\bar{q}\tilde{g}\tilde{g}$ with LEP-1 data was considered. In this scenario a radiated gluon splits into two stable gluinos. The hypotheses that R-hadrons would be formed as either as neutral or charged states were both considered. In the former case, R-hadron jets were identified via a discrepancy between their measured hadronic energy loss and the measurement of the total momentum of charged particles within the jet. A range of topological event shape variables were also used to suppress background. In the latter case $\frac{dE}{dx}$ measurements, together with topological variables, were used to identify R-hadron events. A lower-mass limit for gluinos of 27 GeV was evaluated at 95% CL with this work. A similar analysis by DELPHI [323] gave a lower limit of 18 GeV. Differences in the limits arise due to several factors. ALEPH used around 4 million hadronic Z^0 events compared with 1.6 million events used by DELPHI. Furthermore, different topological variables were considered and different analysis techniques used to suppress background. In addition, ALEPH employed a model of R-hadron scattering in material which is based on the geometric cross-section, whilst DELPHI used the first BCG ansatz (see Section 5.2). The gluino mass limits of ALEPH and DELPHI were extracted assuming a direct production mechanism and are applicable to any MSSM scenario containing long-lived gluinos. Thus, these works can be considered to belong to the second class of searches.

The ALEPH work also sought evidence of stable stops and sbottoms via the reaction $e^+e^- \rightarrow \tilde{q}\bar{\tilde{q}}$, using $\frac{dE}{dx}$ measurements. Since the partners of the left and right handed states of the top (or bottom) mix to form mass eigenstates, the lower mass limits depend on the choice of mixing angle [9, 10]. In this study, a stop (sbottom) mixing angle of 56° (68°) was used. At these values the stop and sbottom cou-

plings to the Z vanish. This allowed the extraction of conservative mass limits: 95 GeV (stop) and 92 GeV (sbottom), at 95% CL. As for the stable gluino work, the squark mass limits are relevant for any MSSM scenario accommodating long-lived squarks.

Similarly, stable heavy slepton limits which are valid for all MSSM scenarios in which the slepton is stable have also been evaluated. Direct pair-production mechanisms $e^+e^- \to \tilde{l}_R^+\tilde{l}_R^-$ and $e^+e^- \to \tilde{l}_L^+\tilde{l}_L^-$ were assumed in a DELPHI search [291]. Within the MSSM, the cross section for each of these processes depends only on the relevant slepton mass. Lower-mass limits for the superpartners of the left (right) muon and tau of 98 (97) GeV were obtained at 95% CL. Mass limits of a similar value were also obtained by ALEPH [324] and OPAL [325]. Mass limits on selectrons are very model dependent owing to an additional t-channel neutralino exchange process.

Searches for sleptons are usually interpreted within a slepton NLSP or a sleptons co-NLSP GMSB scenario, as described in Section 2.1.2. Such class 3 results exclude regions in parameter space defined by quantities such as the slepton masses, the effective SUSY-breaking scale, and the gravitino mass [291, 324, 325]. Since stable slepton scenarios represent only a small part of the GMSB parameter space, we do not provide a detailed description of these results here.

Another type of class 3 SUSY search looks for NLSP charginos which are nearly mass degenerate with the LSP neutralino [318, 326–328] , as can occur in AMSB and gravity mediated SUSY-breaking scenarios (see Section 2.1.4). For mass differences of less than approximately the pion mass, the charginos are stable during their passage through the detector. A search by ALEPH [326] provided the most stringent lower-mass limit of 101 GeV for stable charginos at 95% CL. However, as for the GMSB searches, this result is dependent on the SUSY model parameters. Refs. [318, 326–328] provide a detailed description of the model parameter spaces excluded by collider studies.

7.1.2 Searches at lepton-hadron experiments

There have been few searches for electrically charged SMPs in lepton-hadron scattering experiments. Those which have taken place are generic (class 1) searches. A search for free quarks was performed by the EMC experiment [329] in low-energy deep-inelastic μ-Beryllium scattering (DIS). This experiment was sensitive to values of the photon virtuality, Q^2, and the invariant mass of the entire hadronic final state, W, which extended to around 100 GeV^2 and 20 GeV, respectively. Sets of scintillator counters were used to gain sensitivity to the anomalously low ionisation energy loss expected from free quarks. The ratio of the upper limit on the single inclusive production cross section for SMPs to the total inelastic muon cross section was determined to be around 10^{-6}. The experiment was sensitive to SMPs

with charges $\pm\frac{1}{3}e$ and $\pm\frac{2}{3}e$ for masses up to 15 GeV and 9 GeV, respectively. The limits on the production cross-section were smaller than those obtained in neutrino-nucleon scattering [330–332].

There has been one recent dedicated search for SMPs produced in high-energy lepton-hadron scattering, which was made by the H1 experiment [272]. This used a data sample corresponding to processes with an average W of 200 GeV, and in which the exchanged boson was quasi-real (photoproduction). In photoproduction processes, the exchanged photon can be ascribed a partonic structure, and, in this picture, the H1 study is therefore equivalent to the hadron-hadron searches described in 7.1.3. However, there are differences between final states produced by photoproduction and hadron-hadron interactions, for example, due to the contributions of so-called direct and anomalous photoproduction processes [333]. Thus, the two environments are not identical, and this search is therefore complementary to searches performed at a hadron-hadron facility.

The H1 experiment used measurements of $\frac{dE}{dx}$ in its drift chamber to search for SMPs depositing anomalously high amounts of ionisation energy. A minimum bias sample corresponding to 6 pb^{-1} of luminosity was used. At 95% CL an upper cross-section limit of 0.19 nb was extracted for the production of SMPs. No production model was assumed for this study and the mass range explored is determined by the capability of the H1 tracking chamber. Since the apparatus was fully sensitive to SMPs with charge $\pm e$ in the region of transverse momentum and mass $0.2 < p_T/M < 0.7$, this implies a sensitivity in mass of up to around 100 GeV, assuming an SMP pair-production mechanism.

7.1.3 Searches at hadron-hadron experiments

Early class 1 searches for fractionally charged particles produced in pp interactions at the ISR ($\sqrt{s} = 52$ GeV) were able to set upper cross-section limits for particles possessing fractional charges $\pm\frac{1}{3}e$,$\pm\frac{2}{3}e$, and $\pm\frac{4}{3}e$, and masses less than around 20 GeV [334]. A host of lower energy hadron-hadron experiments also performed such searches, usually for masses less than around 10 GeV [1].

Searches for SMPs in $p\bar{p}$ collisions at the Tevatron have been made by the CDF collaboration [335–337]. These were based on relatively low-luminosity samples of 26 nb^{-1} [335], 3.5 pb^{-1} [336] and 90 pb^{-1} [337]. By the end of the Tevatron Run-II data-taking period, the D0 and CDF experiments should each have collected several fb^{-1} of luminosity and we anticipate that the above mentioned studies be updated. Here we consider the works in Refs. [336,337] which supersede the early, very low-luminosity CDF study [335].

In Ref. [336] SMPs leaving a slow ($0.25 < \beta < 0.65$) muon-like track were sought. The analysis also relied on measurements of ionisation energy loss, muon-like tracks and time of flight information from the calorimeter. Model-independent

upper limits on the production cross section (calculated to 95% CL) of between 120 and 5 pb were derived for the pair production of fractionally charged fermions of masses between 50 and 500 GeV. The electric charges considered were $\pm\frac{2}{3}e$,$\pm e$, and $\pm\frac{5}{3}e$.

Using theoretical models, these data were also used to extract mass limits under the assumption that the SMP possessed a specific colour charge (singlet, octet or decuplet). These, and the remaining search results described here belong to the second classification of searches. The mass limits for an SMP with a given colour and electric charge vary between 140 and 255 GeV at 95% CL.

The third CDF work [337] did not employ time of flight information, and relied on searches for particles losing anomalous amounts of ionisation energy. This study considers the possibility of fourth-generation quarks (see Section 2.3.1), and was able to set lower-mass limits at 95% CL for exotic quarks with charges $\pm\frac{2}{3}e$ and $\pm\frac{1}{3}e$ at 220 GeV and 190 GeV, respectively. Furthermore, this work considered the production of fourth generation quarks without hadronisation and charge exchange effects. The limits obtained (0.3-2 pb over a mass range 100-270 GeV) broadly correspond to a generic search for the pair production of particles with charge $\pm e$, assuming a strong production mechanism.

Stable gluinos have not been explicitly considered in the Tevatron works. However, it has been argued [338] that existing Tevatron limits on stable charged particles [337] and anomalous mono-jet production [339] imply lower limits on the gluino mass to be roughly 170-310 GeV; the lower (upper) value corresponds to an extreme scenario in which gluino R-hadrons are produced solely as neutral (charged) states.

A heavy slepton hypothesis which assumed a Drell-Yan like production mechanism was also studied in [337] and production cross-section limits were extracted. However, the expected cross section in exotic scenarios such as GMSB is more than an order of magnitude below this level of sensitivity. Contrary to the situation for exotic quark searches, heavy lepton mass limits from SMP searches have, so far, only been extracted by the LEP experiments.

7.1.4 Summary and discussion of direct searches

A selection of class 1 searches is summarised in Tab. 4. Since these studies focus on generic SMPs, for which the production mechanisms are *a priori* unknown, it is important that searches were conducted in each of the different collision environments. Evidence for particles with fractional charges $\pm\frac{1}{3}e$, $\pm\frac{2}{3}e$, $\pm e$, $\pm\frac{4}{3}e$, and $\pm\frac{5}{3}e$ was sought. Plastic track detectors deployed at LEP extend the SMP charge sensitivity to around $|240e|$. The mass sensitivity at the various accelerators for the pair production of generic SMPs with charge $\pm e$ extended to 100 (HERA),101 (LEP), and 500 GeV (Tevatron). None of the above generic searches were sensitive

$\sqrt{s}$ (GeV)	Collision	Experiment	Mass range (GeV)	Charge (e)	Cross-section limit (pb)	CL (%)	Ref.
1800	$p\bar{p}$	CDF	100-270	± 1	0.3-2	95	[337]
1800	$p\bar{p}$	CDF	50-500	$\pm\frac{2}{3}$	10-100	95	[336]
				± 1	5-50		
				$\pm\frac{4}{3}$	5-70		
300	ep	H1	< 100	± 1	190	95	[272]
130-209	e^+e^-	OPAL	45-102	$\pm\frac{2}{3}$	0.005-0.02	95	[277, 316]
			45-102	± 1	0.005-0.03		
			45-100	$\pm\frac{4}{3}$	0.005-0.02		
			45-98	$\pm\frac{5}{3}$	0.005-0.02		
189	e^+e^-	DELPHI	68-93	± 1	0.02-0.04	95	[289]
130-183	e^+e^-	DELPHI	2-91	± 1	0.05-0.3	95	[290]
130-183	e^+e^-	DELPHI	2-91	$\pm\frac{2}{3}$	0.04-0.6	95	[290]
130-172	e^+e^-	ALEPH	45-86	± 1	0.2-0.5	95	[273]
91.2	e^+e^-	ALEPH	5-45	$\pm\frac{1}{3}$	$3-10$	90	[276]
				$\pm\frac{2}{3}$	$1-12$		
			10-72	$\pm 1^*$	1.6 - 140		
				$\pm\frac{4}{3}$	$1.4-4$		
91.2	e^+e^-	OPAL	3-45	$\pm\frac{2}{3}$	0.2-1.0	90	[315]
				$\pm\frac{2}{3}^*$	0.15-0.9	95	
				$\pm 1^*$	0.15-3.0		
				$\pm\frac{4}{3}^*$	0.18-0.21		
				$\pm 2^*$	0.27-0.3		
91.2	e^+e^-	Kinoshita *et al.*	1-45	$\lesssim\|240e\|$	70	95	[283]

Table 4
A summary of selected direct searches for electrically charged SMPs belonging to class 1. The searches are categorised according to centre-of-mass energy, colliding particles, and experiment. A range in cross-section limit is provided for an SMP with a given charge. The mass range corresponds to the region for which the upper cross-section limit is quoted. The limits were derived under the assumption of a pair-production mechanism, with the exception of those results marked with the symbol *. For these limits, a single SMP inclusive production mechanism was assumed. The confidence level to which the limits were extracted is also shown.

to particles with charge much below $\sim |\frac{1}{3}e|$. Dedicated searches for millicharged particles with charges as low as $\sim 10^{-5}e$ have been made at accelerators and elsewhere albeit typically for particles with masses less than ~ 1 GeV [3, 95]. These searches are thus beyond the scope of this report. It is relevant for the massive particles considered here to note that there exist no direct experimental searches which are sensitive to particles with charge $\lesssim|\frac{1}{3}e|$ and mass $1\lesssim M\lesssim 1000$ GeV, and that indirect astrophysical constraints tend only to exclude such SMPs with charges less than around $|10^{-6}e|$ [96].

For the class 2 searches, lower mass limits were obtained when considering a specific type of SMP and an assumed production cross section. A compilation of lower

$\sqrt{s}$ (GeV)	Collisions	Experiment	Particle	Mass limit (GeV)	Ref.
1.8 TeV	$p\bar{p}$	CDF	4^{th} generation quark	$m_{t'} > 220$, $M_{b'} > 190$	[337]
130-209	e^+e^-	OPAL	Heavy leptons	$m_{l'} > 102$	[277]
133-208	e^+e^-	L3	Heavy leptons	$m_{l'} > 103$	[321]
91.2-209	e^+e^-	ALEPH	Squark	$m_{\tilde{t}} > 95, m_{\tilde{b}} > 92$	[322]
130-183	e^+e^-	DELPHI	Squark	$m_{\tilde{t}} > 80, m_{\tilde{b}} > 40$	[290]
130-183	e^+e^-	DELPHI	Free squark	$m_{\tilde{t}} > 84$	[290]
91.2	e^+e^-	ALEPH	Gluino	$m_{\tilde{g}} > 27$	[322]
91.2	e^+e^-	DELPHI	Gluino	$m_{\tilde{g}} > 18$	[323]
189-209	e^+e^-	ALEPH	Slepton	$m_{\tilde{\tau}} > 97, m_{\tilde{\mu}} > 97$	[324]
130-208	e^+e^-	DELPHI	Slepton	$m_{\tilde{\tau}} > 98, m_{\tilde{\mu}} > 98$	[291]
189-209	e^+e^-	OPAL	Slepton	$m_{\tilde{\tau}} > 98, m_{\tilde{\mu}} > 98$	[325]
189-209	e^+e^-	ALEPH	Chargino	$m_{\chi^\pm} > 101$	[326]
130-189	e^+e^-	DELPHI	Chargino	$m_{\chi^\pm} > 93$	[327]
189	e^+e^-	L3	Chargino	$m_{\chi^\pm} > 94$	[318]

Table 5
A summary of selected classes 2 and 3 searches which have been made for electrically charged SMPs. The searches are described according to the collision centre-of-mass energy, colliding particles, experiment, the type of SMP, and the resultant mass limit. The squark, gluino, and slepton searches are valid for any MSSM scenario in which these particles are long-lived. The squark and slepton limits correspond to values of mixing angles which predict the lowest possible cross-sections. The chargino limits are model-dependent and were extracted in AMSB and AMSB-like scenarios. All limits were extracted at 95% CL.

limits for masses of specific types of particles is shown in Fig. 21. The stable quark limits are taken from Ref. [337] which assumed a fourth-generation quark model. The stable squark and gluino mass limits from LEP [322] are ~ 90 and 27 GeV, respectively. Stable heavy squark or gluino hypotheses have not yet been considered by Tevatron experiments although it could naively be expected that, in a minimal SUSY scenario with squark or gluino LSPs, mass limits with Tevatron data would be similar to those already obtained for stable quarks. Stable stau and smuon mass limits of around 98 GeV have been obtained at LEP [291, 324, 325]. Non-SUSY heavy lepton mass limits have also been extracted at LEP [289,319,340]. The mass limit is largely insensitive to the type of new lepton, and we quote here the L3 mass limit of 103 GeV [319] for mirror leptons. A summary of selected searches made within classes 2 and 3 is given in Tab. 5.

7.1.5 Indirect collider searches

Indirect mass limits of up to around $\frac{M_Z}{2}$ for fourth generation quarks and leptons, squarks (assuming a non-vanishing coupling to the Z^0), sleptons, charginos, and exotic particles with electric charges as low as $\sim 0.2e$ can be inferred from measurements of the Z^0 invisible width [1, 96]. Each limit is generally applicable for a scenario in which SMPs are pair produced through the decay of a Z^0, and not recorded in a detector. Whilst the majority of the aforementioned particles would

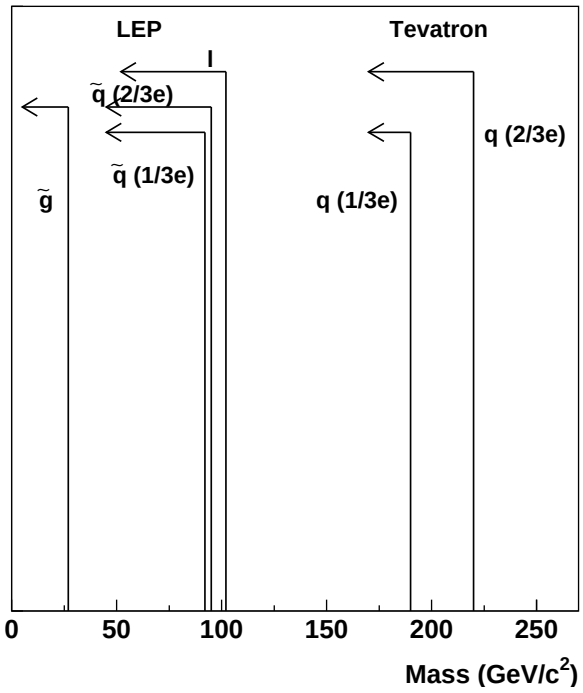

Fig. 21. Lower mass limits for stable gluinos [322], squarks [322], fourth-generation quarks [337], and heavy leptons [319]. The lengths of the vertical lines have no significance.

certainly be detected in the direct searches, it is, however, conceivable that fractionally charged particles may have been missed. LEP-1 limits for exclusive pair production processes were not made for SMPs with charges below $\pm\frac{2}{3}e$. Furthermore, in a free quark picture, these particles may possess a large interaction cross-section, and rapidly become stopped in detector material. In these scenarios, the indirect limits provide a valuable complement to the direct searches.

Similarly, indirect mass limits can be used to support the stable gluino limits from direct searches, which are dependent on the phenomenological models used to describe R-hadron energy loss. These models possess theoretical uncertainties which are not trivial to estimate. Indirect lower limits on the masses of colour octet particles of around 6 GeV can be set from the partial width of any purely hadronic exotic contribution (negative or positive) to Z-decays [341].

Mass constraints on gluinos have also been set by studying the QCD colour factors from 4-jet angular correlations and the differential 2-jet rate in Z-decays [342]. In addition, the modification in the running of α_s as a consequence of the existence of stable coloured particles has been used to set limits on the mass of these particles [343]. These lower mass limits also extend to around 6 GeV.

A body of searches has been performed for magnetic monopoles produced at accelerators, in cosmic rays, and bound in matter [1]. Although no reproducible evidence for the existence of monopoles has been found, several apparent observations have intermittently caused great excitement in the field. In 1973 a particle consistent with being a monopole with charge around $2g_D$ was recorded at a cosmic ray experiment [344]. While the event remains to be fully understood, the authors later established that a monopole could not be responsible for the observation [345]. In the 1980's isolated observations [346, 347] of cosmic ray monopole candidates were made using SQUID detectors. However, instrumental effects could not be ruled as being responsible for the signals and the observations are inconsistent with monopole flux limits set at other cosmic ray facilities [348].

During the 1990's monopole searches remained a routine part of the experimental programs of collider experiments. This section discusses searches for monopoles directly produced at electron-positron annihilation, hadron-hadron and lepton-hadron facilities. Direct searches include, for example, searches for monopoles leaving tracks in plastic track detectors, and searches for monopoles trapped in detector material. As will be shown, most searches are concerned with the possibility of monopoles possessing the Dirac charge. However, even in the absence of theoretical motivation, it is prudent to also consider scenarios with particles possessing as wide a charge-range as is experimentally possible. We therefore describe the regions in magnetic charge and mass which have been explored. The discussion will be followed by a brief discussion of indirect monopole searches.

7.2.1 Searches at e^+e^- experiments

A variety of methods have been used to search for monopoles at e^+e^- experiments. The most commonly used approach, the deployment of plastic track detectors around the beam interaction point, has been used in searches at the PETRA [349], PEP [350, 351], KEK [352, 353] and LEP-1 [250, 283] facilities. The most competitive exclusion limit for Dirac monopoles was extracted with passive detectors deployed at the OPAL intersection point at LEP-1 [250]. No monopoles were observed and an upper cross-section limit for the production of Dirac monopoles of 3 nb was computed at 95% CL. Since the acceptance depends on the monopole mass and charge, the maximum value of acceptance was used in this extraction. It was also assumed that monopoles would be exclusively produced in pairs and distributed isotropically in phase space. The experiment was sensitive to monopoles with magnetic charge between $0.9g_D$ and $3.6g_D$ and for masses up to 45 GeV.

An earlier experiment at LEP by the MODAL [354] group used CR-39 plastic sheet detectors at the I5 LEP interaction point [283], as mentioned in Section 7.1.1. As in

the case of [250] this experiment was sensitive to monopole masses up to around 45 GeV albeit with poorer sensitivity to the monopole production cross section ($\sigma < 0.7\mu$b at 95% CL for Dirac monopoles). However, the experiment was sensitive to lower values of magnetic charge ($0.1g_D$). Lower-energy plastic track experiments at e^+e^- facilities have also been made albeit with a lower mass sensitivity [349–353].

Searches for monopoles leaving parabolic tracks have been made [295, 355] (see Section 6.4.1). These assumed an exclusive pair-production mechanism. Together, these works gave sensitivity to values of the magnetic charge between $0.03 - 0.1g_D$ for monopole masses below 17 GeV.

7.2.2 Searches in lepton-hadron collisions

There has been only one search for monopole production in lepton-hadron scattering. A search was made for monopoles which could have been stopped in the aluminium beampipe of the H1 experiment at HERA [251]. The beampipe was exposed to an integrated luminosity of 62 pb^{-1}. The SQUID apparatus, which was used in this experiment is shown in Fig. 19. To calculate the acceptance in this study it was assumed that monopoles were produced in pairs via photon-photon fusion processes. Limits were extracted for two different assumed reactions: $ep \rightarrow eM\bar{M}p$ and $ep \rightarrow eM\bar{M}X$. In the former (latter) case the monopoles were treated as spin 0 ($\frac{1}{2}$) objects. No evidence was found for the presence of trapped magnetic monopoles. This work set mass-dependent upper limits on the production cross section of monopoles with charges $g_D, 2g_D, 3g_D$, and $6g_D$ for masses up to around 140 GeV. The cross-section limits (calculated at 95% CL) vary between around 0.2 and 100 pb depending on the charge, mass and assumed monopole spin.

7.2.3 Searches at hadron-hadron experiments

A recent study at CDF [249] obtained upper cross-section limits for monopoles possessing the Dirac charge for masses up to 900 GeV. This work used 35.7 pb^{-1} of integrated luminosity and employed a specially built highly ionising particle trigger requiring large light pulses at both ends of a TOF scintillator bar. In addition, track reconstruction software was optimised to search for characteristic parabolic trajectories. A Drell-Yan-like pair-production mechanism, as described in Section 4.6, was used to simulate the kinematic properties of monopoles. Using this model, cross sections of greater than 0.2 pb (at 95% CL) were ruled out for masses between 200 and 700 GeV. Using the same Drell-Yan formalism as a cross-section prediction, this can be interpreted as a lower mass limit of 360 GeV.

Another recent search at the Tevatron involved the use of the SQUID technique by the E882 experiment to detect monopoles bound in detector material at the D0 and CDF experiments [356, 357]. In these works three sets of samples were taken from the D0 and CDF detectors during their upgrades for Tevatron Run-2 data-

taking: the Be beampipe and Al extension cylinders from D0, Pb from the CDF Forward Electromagnetic Calorimeters, and one half of an Al cylinder supporting the CDF Central Tracking Chamber. These detector pieces were exposed to integrated luminosities of 172 ± 8 pb^{-1} (D0) and 180 ± 9 pb^{-1} (CDF). Three different assumptions were made concerning the angular distribution of monopoles in the monopole-antimonopole centre-of-mass system: $\frac{d\sigma}{d\theta} \propto$ constant, $\frac{d\sigma}{d\theta} \propto 1 + cos^2\theta$, and $\frac{d\sigma}{d\theta} \propto 1 - cos^2\theta$. Upper limits on the production cross section of monopoles with charge $g_d, 2g_d, 3g_D$ and $6g_D$ were found to be 0.6,0.2, 0.07, and 0.02 pb, respectively, at 90% CL, when taking the isotropic case. Using the modified Drell-Yan formalism as a cross-section prediction, these correspond to mass limits of 265, 355, 410, and 375 GeV, respectively. Varying the angular distributions according to the three assumed forms described above leads to a spread of around 10 GeV in these mass values.

Taken together, the works [356, 357] and [249] represent the most comprehensive limits for the production of monopoles in hadron-hadron collisions. The searches each employ complementary methods, and together are sensitive to the production of monopoles with charges between g_D and $6g_D$ and masses up to around 900 GeV. Nevertheless, since both CDF and D0 are expected to accumulate several fb^{-1} of luminosity at the completion of the Tevatron program, there remains sensitivity to search for monopoles with a cross section around an order-of-magnitude lower than that which has already been excluded. In addition, a further search could address the possibility of the production of monopoles with a charge less than g_D.

Other searches [279–281] at the Tevatron based on substantially smaller samples of luminosity have used plastic track detectors placed around the interaction point. Again, no evidence for monopole production was found and the exclusion limits on cross sections are typically several thousand times larger, and the mass limits around three times smaller than those obtained in [249, 356, 357].

Lower energy hadron-hadron experiments have employed a variety of search techniques including plastic track detectors [358,359] and searches for trapped monopoles [303–305]. The latter searches used external magnetic fields to accelerate stopped monopoles and were sensitive to a very wide charge range (0.03-24g_D) albeit for masses less than 30 GeV.

7.2.4 Summary and discussion of direct searches

In Tab. 6, the upper cross-section limits from monopole searches and their charge and mass sensitivities are given. It is difficult to compare the mass and cross-section exclusion limits extracted in the various searches because of the theoretical uncertainties on monopole production. What can be reliably calculated is the region of finite acceptance for a monopole with a specific charge and mass, and then, with some model dependence, the derived upper limit on the production cross section.

$\sqrt{s}$ (GeV)	Collision	Experiment	Charge sensitivity (g_D)	Mass sensitivity (GeV)	Charge (g_D)	Cross-section limit (pb)	Ref.
1960	$p\bar{p}$	CDF	-	100-900	1	0.2	[249]
1800	$p\bar{p}$	E882	-	-	1	0.6	[356, 357]
					2	0.2	
					3	0.07	
					6	0.2	
1800	$p\bar{p}$	M. Bertani *et al.*	0.4-5	< 850	> 0.5	200	[279]
56	pp	Hoffmann *et al.*	0.3-7	< 30	0.3-3	0.1	[358]
63	pp	Carrigan *et al.*	0.07-24	< 30	0.2-1.2	0.13	[305]
					1.2-24	0.4	
25-28	pN	Carrigan *et al.*	0.03-24	< 13	0.03-24	5×10^{-6}	[303, 304]
300	ep	H1	>0.1	< 140	1	2.2	[251]
					2	0.18	
					3	0.07	
					6	0.04	
88-94	e^+e^-	J.L. Pinfold *et al.*	0.9-3.6	< 45	1	0.3	[250]
				< 41.6	2	0.3	
89-93	e^+e^-	MODAL	0.1-3.6	< 44.9	1	70	[283]
34	e^+e^-	P. Musset *et al.*	0.98-5.9	< 16	0.98-5.9	0.04	[349]
29	e^+e^-	D. Fryberger *et al.*	0.29-2.9	< 14	0.29-2.9	0.03	[350, 351]
35	e^+e^-	TASSO	0.15-1	≤ 17	0.15	4	[295]
					.44	0.04	
					1	0.08	
10.6	e^+e^-	CLEO	0.03-0.12	< 5	0.03	0.8	[355]
					0.07	0.24	
					0.12	1.6	

Table 6
A summary of selected direct searches for monopoles. The searches are categorised according to the collision centre-of-mass energy, the colliding beams, the experiment, the quoted acceptance regions in charge and mass, and the cross-section limits for specific values of magnetic charges. The symbol "-" denotes that an experiment did not explicitly quote an acceptance region. The cross section limit from Ref. [249] is quoted for monopole masses between around 200 and 700 GeV, a region in which the limit is roughly constant. The cross section limits from Ref. [251] are quoted for a monopole mass of 100 GeV, which is approximately one half of the average photon-proton centre-of-mass energy at the experiment. The cross section limits for works [295] and [355] are quoted for mass values of 8 and 2.5 GeV, respectively. At these values cross-section limits are available for the different charge hypotheses considered.

Mass limits, extracted under the assumption of a known production cross section, are the least reliable information reported by experiments.

As motivated by Dirac's argument (see Section 2.4.1), a large number of experiments have searched for monopoles possessing the Dirac charge. Fig. 22 shows the upper cross-section limits, which have been obtained. The limits are shown versus

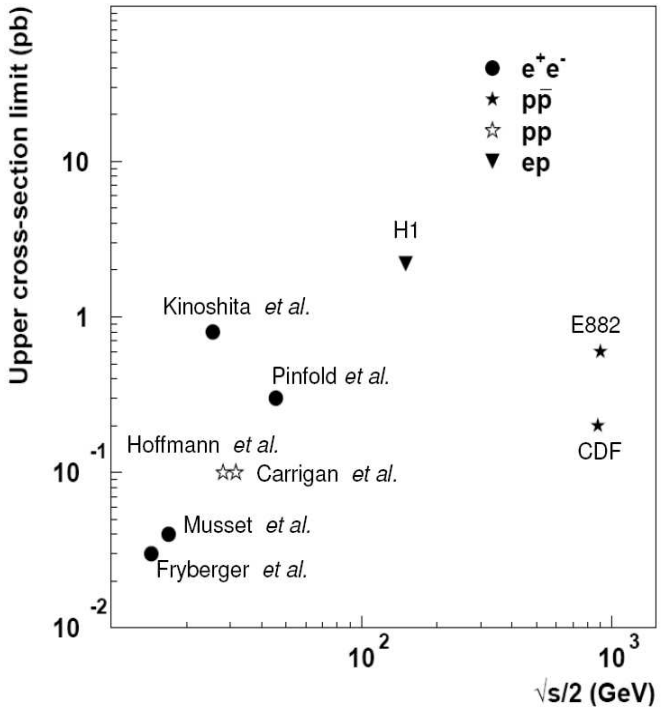

Fig. 22. Summary of upper limits on the monopole production cross section at a range of experiments at different centre-of-mass energies [249–251, 305, 349, 351, 353, 356–358].

one half of the centre-of-mass energy of the experiments, which is indicative of the largest mass value to which an experiment is sensitive, currently 900 GeV at the Tevatron [357] . There also exist theoretical arguments for considering particles with charges up to $6g_D$. To reach these values it is usually necessary to look for stopped monopoles owing to the vastly increased energy loss associated with high-charge monopoles. Searches for monopoles with magnetic charges up to $6g_D$ have so far only taken place at two high energy colliders: HERA [251] and the Tevatron [357].

Sensitivity to low magnetic charges ($\gtrsim \frac{1}{10} g_D$) was provided by the H1 [251] and MODAL [283] searches. Low-energy e^+e^- experiments searching for parabolic tracks [295, 355] and hadron-hadron searches in which external magnetic fields were used to accelerate trapped monopoles [303–305], provided sensitivity to charges as low as $0.03g_D$. However, these searches were only sensitive to monopoles of masses less than around 30 GeV.

There have been no dedicated searches for monopoles with charges less than $0.03g_D$. Searches for electrically charged particles with anomalous ionisation energy loss (Section 7.1) could be sensitive to monopoles in this low charge region. However, this depends on the dynamic range and calibration of the read-out electronics of the tracking devices, which were used in these searches. In addition, measurements of charged particles with high transverse momentum could also provide sensitivity

to low charge monopoles. Since a monopole with a large mass ($\gtrsim$ 100 GeV) and low charge would not leave an identifiable parabolic track, the signature would be a straight track consistent with a very high-momentum electrically charged particle.

7.2.5 Indirect searches

Mass sensitivity at colliders can be increased via indirect searches, which rely on processes mediated by virtual monopole loops, as shown in Fig. 9 in Section 4.6. Such processes can lead to multi-photon final-states arising from electromagnetic radiation from monopoles. The D0 experiment were able to exclude monopole masses between 610 and 1580 GeV [255], while L3 reports a lower mass limit of 510 GeV [254] using this approach. However, it should be stressed that these cross-section calculations employ perturbative techniques [252, 253] with uncertainties which are difficult to estimate and the derived cross-section limits have been criticised for this [256].

An indirect lower limit on the mass of Dirac monopoles of 120 GeV has also been inferred from measurements of the anomalous magnetic moment of the muon [360]. However, it should again be emphasised that this result relies on perturbative techniques and that the result is therefore questionable.

8 SMPs at the LHC

The LHC will allow searches for SMPs with masses up to several TeV, representing an order of magnitude increase in mass sensitivity compared with earlier colliders. As explained in Section 2, well motivated extensions of the SM predict the production of a range of SMPs at the LHC. However, it is important that the LHC experiments perform searches for SMPs which are motivated not only by what is currently theoretically favoured but also by what is experimentally feasible. Therefore, in this section we discuss the sensitivity of the two high-luminosity and multi-purpose experiments, ATLAS [361,362] and CMS [363,364], to SMPs with a variety of properties. In addition, we also briefly discuss the planned MOEDAL experiment [365, 366], which aims to deploy plastic track detectors around the LHCb vertex detector.

We use the findings of a number of studies which explore the feasibility of discovering SMPs at the LHC. These have been made both by interested phenomenologists and the experiments themselves (see for example [240, 338, 367–377]). The former works tend to apply simple ansatzes regarding detector performance whereas the latter use sophisticated detector simulation packages. While the latter studies provide a more realistic description of the detector response it is pertinent to note that the detector simulation programs are still being optimised and have yet to be

confronted and verified with collision data. Nevertheless, it is still possible to use the feasibility studies to draw a number of conclusions regarding the discovery potential for various SMPs and to highlight SMP-specific experimental challenges.

8.1 Detector sensitivity

8.1.1 Timing issues

One of the principal constraints on the design of a collider experiment and its ability to measure slow-moving SMPs is the bunch crossing time. The LHC crossing time of 25 ns, will be considerably shorter than that at LEP (25 μs), the Tevatron (396 ns) or HERA (96 ns). Therefore, for an SMP at the LHC to be detected or triggered in a certain detector system and be associated to the correct bunch crossing, it should arrive at most 25 ns after the default arrival time of a particle travelling at the speed of light [374, 378]. Later arrival would imply triggering or detection within the next crossing time window. The large size of the ATLAS and CMS detectors (the central ATLAS and CMS muon chambers extend to 10 and 7 m, respectively) ensures that this will be an important source of inefficiency in detecting SMPs. For example, it is only possible to reconstruct the track of a slowly moving SMP in the ATLAS central muon chambers within the correct bunch crossing window if $\beta \gtrsim 0.5$ [374]. Even if the SMP travels within the appropriate timing window, additional problems may arise from its slowness. The sampling time and reconstruction software of each sub-detector is optimised assuming particles travelling at luminal speed. Hence, the quality of the read-out signal or reconstructed track or cluster may be degraded for an SMP, especially for sub-systems far away from the interaction point. Detector simulations so far suggest that it will still be possible to trigger and measure slowly moving particles at ATLAS and CMS [369, 374]. However, this is an area which must continue to be studied as the simulation programs are further developed and the detectors better understood.

8.1.2 Important sub-detectors

The principal detector systems needed for SMP searches are the tracking systems. ATLAS and CMS both contain inner tracking systems capable of precision measurements of the momenta of tracks of charged SMPs [361, 363]. These devices can potentially be used to search for the 'classic' signature of SMPs losing anomalous amounts of ionisation energy in an inner detector, albeit probably with poorer precision than has been obtained in previous experiments. The ATLAS inner tracking system comprises a semiconductor tracker system and a transition radiation tracker (TRT). The precision with which $\frac{dE}{dx}$ can be exploited is limited since the TRT will only record hits satisfying high and low ionisation thresholds. The total number of high/low threshold hits and the time in which a channel is read out over a spe-

cific threshold can be used in SMP searches [374]. The CMS inner tracking system consists of silicon pixel and silicon strip detectors. As described in Section 5, the resolution in $\frac{dE}{dx}$ of such devices is poorer than with gaseous detectors. Work is ongoing to estimate the sensitivity of the CMS tracking system to SMPs [274].

Arguably the most important detector component in an SMP search at the LHC is the muon system since most proposed SMPs leave a signature of a slow-moving penetrating particle (see Sec. 6). The ATLAS [361] and CMS [363] experiments employ muon chambers which will be able to trigger on SMPs efficiently. They also offer considerably greater precision in track reconstruction than has been previously available at current colliders experiments [379–382]. The excellent momentum resolution implies that charge misidentification will be typically less than 1% [361], and that R-hadrons undergoing the charge exchange reactions described in Section 5.2 can therefore be identified [375]. In addition to providing the reconstruction of the track of an SMP, the muon systems will be able to provide time of flight measurements with an accuracy of around 1ns. The time of flight is likely to be one of the most powerful discriminants between SMPs and muons [369, 374]. Furthermore, in the event of a discovery, it will allow the reconstruction of the mass of an SMP. It has been shown that a mass resolution of around 20 GeV is possible for an R-hadron of mass 500 GeV at ATLAS [376] using this method. An understanding of the SMP mass resolution is important in both probing the mass hierarchy of particles in any exotic scenario and also in establishing the existence of different types of SMPs with similar masses. In addition to the time of flight information, the muon systems employ gaseous detectors which can provide $\frac{dE}{dx}$ measurements. These may also be used as discriminants in an SMP search and in measurements of SMP properties.

Since direct searches for most species of SMPs are based on charged particle signatures, calorimeters are less crucial, though still important, detector components. The ATLAS and CMS calorimeters can be employed in a number of ways in SMP searches. Measurements of electromagnetic and hadronic energy loss can distinguish between hadronic and leptonic SMP species. Furthermore, the electromagnetic calorimeters can also provide supplementary $\frac{dE}{dx}$ information. Calorimeter triggers based on jet multiplicity or global event properties, such as visible energy, can also be used to select events containing SMPs [374]. These same observables could be used in offline analyses for SMPs predicted to occur in specific event topologies.

A complementary way to detect SMPs at the LHC is via passive detectors. The MOEDAL collaboration [365, 366] proposes to deploy a plastic track-etch detector comprising three layers of CR39/lexan plastic around the LHCb vertex detector. The major systematic uncertainty in any search with MOEDAL will be background tracks from the radiation environment of the LHC, and this is presently under study.

8.2.1 Expected rates

Using PYTHIA we have calculated the expected yields for different types of SMPs at the LHC, following the accumulation of 10fb^{-1}. This corresponds to one year of low-luminosity operation at the LHC. Table 7 shows the expected yield of pair-production processes giving rise to different types of SMPs: gluinos, stops, fourth-generation quarks with charge $\pm\frac{2}{3}e$, heavy leptons and superpartners of left and right-handed leptons. Since predictions of this type are necessarily scenario-dependent, we have made conservative calculations assuming that the exotic particle is produced via SM couplings and that the influence of other exotic particles is minimal. The predictions do not include contributions from the cascade decays of other exotic particles.

Studies indicate that the acceptance of the ATLAS and CMS detectors following SMP selection cuts typically vary between 5% and 80% depending on the mass and type of SMP [367–372, 374, 375]. A detailed simulation for each type of SMP of detector inefficiencies and systematic uncertainties, such as the effects of nuclear scattering and delayed reconstruction, is ongoing and therefore beyond the scope of this paper. Furthermore, many systematic uncertainties, particularly for searches for hadronic SMPs, remain difficult to quantify even with detector simulations. This is discussed below, where we describe experimental issues related to specific types of SMPs which could be sought at the LHC.

8.2.2 Generic SMPs

Generic SMP's which possess electric charge and penetrate through the whole detector will leave a clear signature of a high-p_T, slow, muon-like track. Since no assumption, other than non-zero electric charge, is made regarding the properties

Particle	$M = 200$ GeV	$M = 500$ GeV	$M = 1.0$ TeV	$M = 1.5$ TeV	$M = 2.0$ TeV
$\tilde{g}$	2.3×10^7	1.8×10^5	2.3×10^3	100	8
$\tilde{t}$	4.3×10^5	3.7×10^3	47	2.1	0.1
t'	2.5×10^6	2.5×10^4	440	22	2
$\tilde{l}_L$	190	4.9	0.14	0.009	7×10^{-4}
$\tilde{l}_R$	82	2.1	0.06	0.004	3×10^{-4}
l'	1220	34	1.1	0.08	0.008

Table 7
PYTHIA predictions of the total number of SMP pairs expected at the LHC following the accumulation of 10fb^{-1} of integrated luminosity.

of a generic SMP it is not possible to calculate its expected production cross section. However, background is expected to be highly suppressed when making use of the time of flight technique [374]. Thus, penetrating SMPs with appropriate production cross sections would be easily observed. A null observation would also allow stringent upper limits on these cross sections. For SMPs which stop in the calorimeter and do not traverse the muon system, searches could rely on observing an excess of high-p_T tracks in the inner detectors. In conjunction with this, observables such as a charged particle leaving a signature of anomalous ionisation in the tracking chambers together with a characteristic energy deposition profile in the calorimeters could also be used. However, as described earlier in this section, the precision with which ionisation energy loss can be measured is likely to be poorer than obtained in earlier searches. This could make it difficult in particular to identify fractionally charged objects such as for example free quarks.

The planned MOEDAL experiment would be able to complement the above search strategies by allowing searches for electrically charged SMPs with $\frac{Z}{\beta} > 5$, which implies a maximum electric charge sensitivity of up to around $220e$ [383]. The present upper limit on the SMP electric charge to which ATLAS and CMS will be sensitive is still unclear. However, it is likely to be substantially below the reach of MOEDAL.

While it can be expected that the ATLAS and CMS tracking systems will be able to reconstruct particles with charges down to at least $\sim 0.5e$, studies have not been performed to establish this and to estimate the reconstruction efficiency. Measurements of SMPs with extremely low charge (millicharged-charged particles) would not be directly recorded in the LHC tracking chambers.

8.2.3 Heavy leptons and sleptons

The possibility of stable heavy leptons and sleptons at the LHC hs been considered in Refs. [368–373, 373, 377]. As these studies illustrated, the detection of these particles presents the fewest detector difficulties of all of the SMPs considered, although their direct cross section would be suppressed in relation to coloured SMPs. Heavy leptons and sleptons would manifest themselves as delayed, muon-like particles leaving little energy deposition in the hadronic calorimeters. Since these particles would not necessarily be associated with a jet, isolation criteria could also be used to identify them. In an extremely minimal scenario in which only the properties of the slepton or lepton would play a role in the production cross section, modelling these process is relatively straightforward. However, the presence of other exotic particles complicates the picture. In SUSY scenarios accommodating stable sleptons, e.g. GMSB, stable sleptons would be expected to be dominantly produced via the cascade decays of copiously produced squarks and gluinos at the LHC. Studies of stable sleptons have focused on their detection and the exploration of the parameter space of GMSB and GMSB-like models [368–373, 377]. For conservative

estimates of rates, Tab. 7 presents the expected yields of the stable superpartners of left and right handed leptons, which are produced directly and not via cascade decays. The latter quantities depend on masses and couplings of many SUSY sparticles so are extremely model-dependent. Making use of the time of flight technique (see Section 6.3), the discovery of leptons or sleptons possessing masses up to several hundred GeV should be possible in early LHC running with the ATLAS detector [368, 369, 371, 372]. In the optimistic situation of an SMP-discovery, the angular distribution of the pair-produced SMPs could allow discrimination between a lepton or slepton hypothesis, as outlined in Ref. [373].

8.2.4 Gluinos

Gluinos are produced through strong interactions and would thus be copiously produced at the LHC, as is shown in Tab. 7. A number of studies exploring the possibility of gluinos at the LHC have taken place [240, 338, 374, 375], which were mainly inspired by the recent split SUSY model. These studies indicate that stable gluinos possessing masses up to 1 TeV could be discovered in early LHC running. However, there are special issues associated with hadronic SMPs which must be addressed in a stable gluino search. For example, poorly understood nuclear interactions could potentially inhibit a discovery. It is possible, though extremely unlikely, that charged gluino R-hadrons could dominantly be stopped or convert into neutral states in the calorimeter and thus escape detection in the muon chambers. Furthermore, even if the R-hadrons remain charged then events could be produced containing tracks with different signs of charge in the inner and muon systems (so-called 'flippers'), possibly challenging the track reconstruction software. Current simulations suggest that the ATLAS reconstruction programs can deal with this situation, and it may in fact be used as a means of searching for R-hadrons [375]. However, in the absence of collision data to confirm this, a conservative approach would be to consider the most straightforward signature in which the R-hadron maintains the same non-zero charge in the inner and muon chambers. The string fragmentation model with default parameters (Section 4.3) and the geometric scattering model (Section 5.2.2) predict that the proportion of gluino R-hadrons produced at the LHC which possess the same non-zero electric charge at the production vertex and after their passage through a typical calorimeter is around 10%. In this situation, gluino R-hadrons could be found with masses up to at least 1 TeV in early LHC running when using measurements of muon-like tracks and topological variables, and significantly beyond when also making use of the time of flight technique [374]. However, it should be noted that calculations of nuclear scattering processes for R-hadrons are extremely uncertain and any search must take this into account.

Another pessimistic scenario can be envisaged if the fraction of gluino-gluon states formed in the hadronisation process is around unity, leading to no track in the inner detector. In this unlikely, but not inconceivable scenario, neutral R-hadrons which

convert into charged states via nuclear interactions may be visible as tracks in the muon systems. However, as for the charge 'flippers' this signature may again challenge reconstruction software and the event filtered away with background removal algorithms.

The most experimentally difficult scenario occurs in the case of gluino R-hadrons being produced as neutral particles and remaining neutral during their passage through the detector. Here, a signature of R-hadron production could be manifest through an anomalously high jet rate [338].

8.2.5 Stable squarks and quarks

Stable squarks and quarks at the LHC have been postulated, as described in Section 2 although no detector simulations of these have been published. Searches for stable heavy colour-triplet states would benefit from the strong production cross section and exploit the same techniques as for the stable gluino searches described above. Similarly, they would also be sensitive to uncertain nuclear interactions which could potentially reduce their discovery potential. The nuclear interactions of stable colour triplets have received far less attention than gluinos and searches would benefit from more phenomenology in this area. One model which treats both colour-octet and triplet states [232] predicts comparable energy loss and charge exchange rates for both types of particles. Should this model reproduce the data, it can therefore be expected that a similar sensitivity is obtainable as for stable gluinos, i.e. stable squark and quarks with masses up to at least 1 TeV could be discovered at early stages of the running of the LHC. Again, the angular distribution of the pair-produced SMPs could allow discrimination between a quark or squark hypothesis in case of a discovery.

8.2.6 Monopoles

Magnetic monopoles at the LHC will leave a number of striking signatures. However, little work has been done estimating the sensitivity of ATLAS and CMS to these particles. Those studies which do exist concern indirect searches in which magnetic monopoles are produced as internal loops [362]. Furthermore, as discussed in Section 4.6, calculations of these processes suffer from unquantifiable uncertainties [252, 253]. Even in the absence of detailed studies of direct magnetic monopole production it is possible to make several remarks concerning their detection. As described in Section 5.1.2, a Dirac monopole will typically lose several thousand times as much ionisation energy as a MIP. A detailed $\frac{dE}{dx}$ calibration is therefore not necessary to observe them. However, electronic saturation effects due to the enormous ionisation energy must be carefully studied in any search. Furthermore, customised track-finding algorithms may have to be written to account for the parabolic track trajectory followed by a magnetic monopole in a magnetic

field. It is also important to employ GEANT simulations to calculate the stopping of magnetic monopoles in detector material and the energy deposition of profiles of magnetic monopoles which progress to the calorimeters. A comprehensive search must consider the full mass and magnetic charge range which is experimentally available.

The MOEDAL experiment bypasses the problems described above of detecting magnetic monopoles with active detectors by using the plastic track technique. Current acceptance calculations indicate that MOEDAL will be sensitive to monopoles with masses up to around 6 TeV and charges up to around $3g_D$ [383]. MOEDAL may offer the most promising method of hunting magnetic monopoles at the LHC. However, this depends on the magnetic monopole production cross section since MOEDAL would be exposed to integrated luminosity around 100 times lower than that collected by ATLAS and CMS.

9 Summary

Searches for Stable Massive Particles have been made at colliders for several decades. So far, no particles beyond those accommodated within the Standard Model have been observed. The searches are motivated by a number of theories which address key issues in modern physics. A review has been given of theoretical scenarios predicting SMPs, the phenomenology needed to model their production at colliders, the experimental techniques used to find SMPs and the searches which have been made to date. The interplay between collider searches and open cosmological questions has also been addressed.

We look forward to the extension of these searches in the coming years at the LHC and at cosmic ray facilities. The discovery of an SMP would change our view of particle physics.

Acknowledgements

We gratefully acknowledge the following people who have helped us in the preparation of this paper by providing useful comments and suggestions to various sections: Lars Bergström, Wilfried Buchmüller, Bogdan Dobrescu, Beate Heinemann, Barry King, Maxim Perelstein, Jim Pinfold, Christoph Rembser, Peter Richardson, Pietro Slavich, and Tim Tait.

David Milstead is Royal Swedish Academy Research Fellow supported by a grant from the Knut and Alice Wallenberg Foundation.

References

[1] Particle Data Group, W.M. Yao et al., J. Phys. G33 (2006) 1.

[2] J. Preskill, Ann. Rev. Nucl. Part. Sci. 34 (1984) 461.

[3] M.L. Perl et al., Int. J. Mod. Phys. A16 (2001) 2137, hep-ex/0102033.

[4] M.L. Perl, E.R. Lee and D. Loomba, Mod. Phys. Lett. A19 (2004) 2595.

[5] K.A. Milton, Rept. Prog. Phys. 69 (2006) 1637, hep-ex/0602040.

[6] G. Gilbert, Nucl. Phys. B328 (1989) 159.

[7] L.E. Ibanez and G.G. Ross, Nucl. Phys. B368 (1992) 3.

[8] L.M. Krauss and F. Wilczek, Phys. Rev. Lett. 62 (1989) 1221.

[9] S.P. Martin, (1997), hep-ph/9709356.

[10] X. Tata, (1997), hep-ph/9706307.

[11] A. Djouadi, (2002), hep-ph/0211357.

[12] P.Z. Skands, (2006), Minireview to appear in 'TeV4LHC Workshop': Summary report,hep-ph/0601103.

[13] P. Skands et al., (2005), FERMILAB-CONF-05-521-T. In Les Houches 'Physics at TeV Colliders 2005' BSM Working Group: Summary report, hep-ph/0602198. See `http://www.ippp.dur.ac.uk/montecarlo/BSM`.

[14] P. Skands et al., JHEP 07 (2004) 036, hep-ph/0311123.

[15] B.C. Allanach et al., (2006), FERMILAB-CONF-05-517-T. In Les Houches 'Physics at TeV Colliders 2005' BSM Working Group: Summary report, hep-ph/0602198.

[16] S. Weinberg, Phys. Rev. D26 (1982) 287.

[17] Super-Kamiokande, M. Shiozawa et al., Phys. Rev. Lett. 81 (1998) 3319, hep-ex/9806014.

[18] H.K. Dreiner, (1997), hep-ph/9707435, In "Kane, G.L. (ed.): Perspectives on supersymmetry", 462.

[19] G.R. Farrar and P. Fayet, Phys. Lett. B76 (1978) 575.

[20] W. Buchmuller, K. Hamaguchi and J. Kersten, Phys. Lett. B632 (2006) 366, hep-ph/0506105.

[21] J.L. Feng, S. Su and F. Takayama, Phys. Rev. D70 (2004) 075019, hep-ph/0404231.

[22] S. Raby, Phys. Rev. D56 (1997) 2852, hep-ph/9702299.

[23] H. Baer, K.m. Cheung and J.F. Gunion, Phys. Rev. D59 (1999) 075002, hep-ph/9806361.

[24] A. Mafi and S. Raby, Phys. Rev. D63 (2001) 055010, hep-ph/0009202.

[25] S. Raby, Phys. Lett. B422 (1998) 158, hep-ph/9712254.

[26] A. Mafi and S. Raby, Phys. Rev. D62 (2000) 035003, hep-ph/9912436.

[27] M. Carena et al., Phys. Rev. D66 (2002) 115010, hep-ph/0206167.

[28] C. Balazs, M. Carena and C.E.M. Wagner, Phys. Rev. D70 (2004) 015007, hep-ph/0403224.

[29] S. Kraml and A.R. Raklev, Phys. Rev. D73 (2006) 075002, hep-ph/0512284.

[30] C. Balázs et al., Light scalar top quarks, In Les Houches 'Physics at TeV Colliders 2005' BSM Working Group: Summary report, hep-ph/0602198, 2006.

[31] H.C. Cheng, B.A. Dobrescu and K.T. Matchev, Nucl. Phys. B543 (1999) 47, hep-ph/9811316.

[32] C.H. Chen, M. Drees and J.F. Gunion, (1999), hep-ph/9902309.

[33] J.L. Feng et al., Phys. Rev. Lett. 83 (1999) 1731, hep-ph/9904250.

[34] M. Dine et al., Phys. Rev. D53 (1996) 2658, hep-ph/9507378.

[35] M. Dine, A.E. Nelson and Y. Shirman, Phys. Rev. D51 (1995) 1362, hep-ph/9408384.

[36] L. Alvarez-Gaume, M. Claudson and M.B. Wise, Nucl. Phys. B207 (1982) 96.

[37] S. Dimopoulos, S.D. Thomas and J.D. Wells, Nucl. Phys. B488 (1997) 39, hep-ph/9609434.

[38] J.A. Bagger et al., Phys. Rev. Lett. 78 (1997) 1002, hep-ph/9611229.

[39] G.F. Giudice and R. Rattazzi, Phys. Rept. 322 (1999) 419, hep-ph/9801271.

[40] B.C. Allanach et al., Eur. Phys. J. C25 (2002) 113, hep-ph/0202233.

[41] F.E. Paige et al., (2003), hep-ph/0312045.

[42] S. Ambrosanio, G.D. Kribs and S.P. Martin, Phys. Rev. D56 (1997) 1761, hep-ph/9703211.

[43] N. Arkani-Hamed and S. Dimopoulos, JHEP 06 (2005) 073, hep-th/0405159.

[44] G.F. Giudice and A. Romanino, Nucl. Phys. B699 (2004) 65, hep-ph/0406088.

[45] P. Gambino, G.F. Giudice and P. Slavich, Nucl. Phys. B726 (2005) 35, hep-ph/0506214.

[46] M. Toharia and J.D. Wells, JHEP 02 (2006) 015, hep-ph/0503175.

[47] N. Arkani-Hamed et al., Nucl. Phys. B709 (2005) 3, hep-ph/0409232.

[48] K.S. Babu, T. Enkhbat and B. Mukhopadhyaya, Nucl. Phys. B720 (2005) 47, hep-ph/0501079.

[49] L. Randall and R. Sundrum, Nucl. Phys. B557 (1999) 79, hep-th/9810155.

[50] G.F. Giudice et al., JHEP 12 (1998) 027, hep-ph/9810442.

[51] J.L. Feng and T. Moroi, Phys. Rev. D61 (2000) 095004, hep-ph/9907319.

[52] A.J. Barr et al., JHEP 03 (2003) 045, hep-ph/0208214.

[53] A. Brignole, L.E. Ibanez and C. Munoz, Nucl. Phys. B422 (1994) 125, hep-ph/9308271.

[54] C.H. Chen, M. Drees and J.F. Gunion, Phys. Rev. D55 (1997) 330, hep-ph/9607421.

[55] D.E. Kaplan, G.D. Kribs and M. Schmaltz, Phys. Rev. D62 (2000) 035010, hep-ph/9911293.

[56] Z. Chacko et al., JHEP 01 (2000) 003, hep-ph/9911323.

[57] M. Schmaltz and W. Skiba, Phys. Rev. D62 (2000) 095005, hep-ph/0001172.

[58] M. Schmaltz and W. Skiba, Phys. Rev. D62 (2000) 095004, hep-ph/0004210.

[59] H. Baer et al., JHEP 04 (2000) 016, hep-ph/0002245.

[60] H. Baer et al., JHEP 05 (2002) 061, hep-ph/0204108.

[61] H. Baer et al., Phys. Rev. D65 (2002) 075024, hep-ph/0110270.

[62] T. Appelquist, H.C. Cheng and B.A. Dobrescu, Phys. Rev. D64 (2001) 035002, hep-ph/0012100.

[63] C. Macesanu, C.D. McMullen and S. Nandi, Phys. Rev. D66 (2002) 015009, hep-ph/0201300.

[64] H.C. Cheng, K.T. Matchev and M. Schmaltz, Phys. Rev. D66 (2002) 036005, hep-ph/0204342.

[65] T. Appelquist and H.U. Yee, Phys. Rev. D67 (2003) 055002, hep-ph/0211023.

[66] G. Servant and T.M.P. Tait, Nucl. Phys. B650 (2003) 391, hep-ph/0206071.

[67] G. Servant, (2005), In Les Houches 'Physics at TeV Colliders 2005' BSM Working Group: Summary report, hep-ph/0602198.

[68] N.R. Shah and C.E.M. Wagner, (2006), hep-ph/0608140.

[69] M. Carena, T.M.P. Tait and C.E.M. Wagner, Acta Phys. Polon. B33 (2002) 2355, hep-ph/0207056.

[70] F. del Aguila, M. Perez-Victoria and J. Santiago, (2006), hep-ph/0601222.

[71] G. Burdman, B.A. Dobrescu and E. Ponton, (2006), hep-ph/0601186.

[72] D.G. M El Kacimi and H. Przysiezniak, (2006), In Les Houches 'Physics at TeV Colliders 2005' BSM Working Group: Summary report, hep-ph/0602198.

[73] J.L. Feng, A. Rajaraman and F. Takayama, Phys. Rev. D68 (2003) 085018, hep-ph/0307375.

[74] M. Perelstein, (2005), In Les Houches 'Physics at TeV Colliders 2005' BSM Working Group: Summary report, hep-ph/0602198.

[75] M. Perelstein, (2005), hep-ph/0512128.

[76] J. Hubisz et al., JHEP 01 (2006) 135, hep-ph/0506042.

[77] A. Birkedal et al., (2006), hep-ph/0603077.

[78] R. Harnik et al., Phys. Rev. D70 (2004) 015002, hep-ph/0311349.

[79] A. Delgado and T.M.P. Tait, JHEP 07 (2005) 023, hep-ph/0504224.

[80] W.D. Goldberger, Y. Nomura and D.R. Smith, Phys. Rev. D67 (2003) 075021, hep-ph/0209158.

[81] Y. Nomura and D.R. Smith, Phys. Rev. D68 (2003) 075003, hep-ph/0305214.

[82] Y. Nomura, D. Tucker-Smith and B. Tweedie, Phys. Rev. D71 (2005) 075004, hep-ph/0403170.

[83] Y. Nomura and D. Tucker-Smith, Nucl. Phys. B698 (2004) 92, hep-ph/0403171.

[84] Y. Nomura and B. Tweedie, Phys. Rev. D72 (2005) 015006, hep-ph/0504246.

[85] C. Friberg, E. Norrbin and T. Sjostrand, Phys. Lett. B403 (1997) 329, hep-ph/9704214.

[86] P. Fishbane, S. Meshkov and P. Ramond, Phys. Lett. B134 (1984) 81.

[87] P.M. Fishbane et al., Phys. Rev. D31 (1985) 1119.

[88] P.H. Frampton and P.Q. Hung, Phys. Rev. D58 (1998) 057704, hep-ph/9711218.

[89] H.J. He, N. Polonsky and S. Su, Phys. Rev. D64 (2001) 053004, hep-ph/0102144.

[90] R. Barbieri, T. Gregoire and L.J. Hall, (2005), hep-ph/0509242.

[91] N. Polonsky and S. Su, Phys. Rev. D63 (2001) 035007, hep-ph/0006174.

[92] B. Holdom, Phys. Lett. B166 (1986) 196.

[93] T. Appelquist, B.A. Dobrescu and A.R. Hopper, Phys. Rev. D68 (2003) 035012, hep-ph/0212073.

[94] B.A. Dobrescu, Phys. Rev. Lett. 94 (2005) 151802, hep-ph/0411004.

[95] S. Davidson, S. Hannestad and G. Raffelt, JHEP 05 (2000) 003, hep-ph/0001179.

[96] S.L. Dubovsky, D.S. Gorbunov and G.I. Rubtsov, JETP Lett. 79 (2004) 1, hep-ph/0311189.

[97] B. Batell and T. Gherghetta, Phys. Rev. D73 (2006) 045016, hep-ph/0512356.

[98] L.B. Okun, M.B. Voloshin and V.I. Zakharov, Phys. Lett. B138 (1984) 115.

[99] R. Foot et al., Mod. Phys. Lett. A5 (1990) 95.

[100] T. Muta, World Sci. Lect. Notes Phys. 57 (1998) 1.

[101] S.B. Gudnason, C. Kouvaris and F. Sannino, Phys. Rev. D73 (2006) 115003, hep-ph/0603014.

[102] S.B. Gudnason, C. Kouvaris and F. Sannino, (2006), hep-ph/0608055.

[103] M.J. Strassler and K.M. Zurek, (2006), hep-ph/0604261.

[104] L.L. Vant-Hull, Phys. Rev. 173 (1968) 1412.

[105] P.A.M. Dirac, Proc. Roy. Soc. Lond. A133 (1931) 60.

[106] P.A.M. Dirac, Phys. Rev. 74 (1948) 817.

[107] D. Griffiths, *Introduction to Electrodynamics* (Prentice Hall, 1999).

[108] G. 't Hooft, Nucl. Phys. B105 (1976) 538.

[109] E. Corrigan and D.I. Olive, Nucl. Phys. B110 (1976) 237.

[110] J.S. Schwinger, Phys. Rev. 144 (1966) 1087.

[111] J.S. Schwinger, Phys. Rev. 173 (1968) 1536.

[112] J.S. Schwinger, Science 165 (1969) 757.

[113] P.C.M. Yock, Int. J. Theor. Phys. 2 (1969) 247.

[114] A. De Rujula, R.C. Giles and R.L. Jaffe, Phys. Rev. D17 (1978) 285.

[115] D. Fryberger, Hadronic J. 4 (1981) 1844.

[116] H.V. Klapdor-Kleingrothaus and A. Staudt, *Non-accelerator particle physics* (Bristol, UK: IOP, 1995).

[117] G. 't Hooft, Nucl. Phys. B79 (1974) 276.

[118] A.M. Polyakov, JETP Lett. 20 (1974) 194.

[119] E. Huguet and P. Peter, Astropart. Phys. 12 (2000) 277, hep-ph/9901370.

[120] S.D. Wick et al., Astropart. Phys. 18 (2003) 663, astro-ph/0001233.

[121] AMANDA, W. Rhode, Prepared for *DARK 2002: 4th International Heidelberg Conference on dark matter in Astro and Particle Physics*, Cape Town, South Africa, 4-9 Feb 2002.

[122] MACRO, M. Ambrosio et al., (2004), hep-ex/0402006.

[123] G. Giacomelli and L. Patrizii, (2005), hep-ex/0506014.

[124] S. Cecchini et al., Radiat. Meas. 40 (2005) 405, hep-ex/0503003.

[125] T. Vachaspati and M. Barriola, Phys. Rev. Lett. 69 (1992) 1867.

[126] M. Barriola, T. Vachaspati and M. Bucher, Phys. Rev. D50 (1994) 2819, hep-th/9306120.

[127] Y.M. Cho and D. Maison, Phys. Lett. B391 (1997) 360, hep-th/9601028.

[128] Y.S. Yang, Proc. Roy. Soc. Lond. A454 (1998) 155.

[129] Y. Yang, *Solitons in field theory and nonlinear analysis* (New York, USA: Springer).

[130] W.S. Bae and Y.M. Cho, J. Korean Phys. Soc. 46 (2005) 791, hep-th/0210299.

[131] J.P. Gauntlett, J.A. Harvey and J.T. Liu, Nucl. Phys. B409 (1993) 363, hep-th/9211056.

[132] A.K. Drukier and S. Nussinov, Phys. Rev. Lett. 49 (1982) 102.

[133] T.D. Lee and G.C. Wick, Phys. Rev. D9 (1974) 2291.

[134] R. Friedberg, T.D. Lee and A. Sirlin, Phys. Rev. D13 (1976) 2739.

[135] R. Friedberg, T.D. Lee and A. Sirlin, Nucl. Phys. B115 (1976) 32.

[136] R. Friedberg and T.D. Lee, Phys. Rev. D15 (1977) 1694.

[137] S.R. Coleman, Nucl. Phys. B262 (1985) 263.

[138] S. Kasuya and M. Kawasaki, Phys. Rev. D62 (2000) 023512, hep-ph/0002285.

[139] S. Kasuya and M. Kawasaki, Phys. Rev. Lett. 85 (2000) 2677, hep-ph/0006128.

[140] A. Kusenko and M.E. Shaposhnikov, Phys. Lett. B418 (1998) 46, hep-ph/9709492.

[141] A. Kusenko et al., Phys. Rev. Lett. 80 (1998) 3185, hep-ph/9712212.

[142] A.G. Cohen et al., Nucl. Phys. B272 (1986) 301.

[143] L. Bergstrom and A. Goobar, *Cosmology and particle astrophysics* (Berlin, Germany: Springer, 2004).

[144] G. Steigman, Int. J. Mod. Phys. E15 (2006) 1, astro-ph/0511534.

[145] D.N. Spergel et al., (2006), astro-ph/0603449.

[146] W.L. Freedman et al., Astrophys. J. 553 (2001) 47, astro-ph/0012376.

[147] F. Zwicky, Helvetica Physica Acta 6 (1933) 110.

[148] V.C. Rubin and W.K.J. Ford, Astrophys J. 159 (1970) 379.

[149] The 2dFGRS, S. Cole et al., Mon. Not. Roy. Astron. Soc. 362 (2005) 505, astro-ph/0501174.

[150] SDSS, U. Seljak et al., Phys. Rev. D71 (2005) 103515, astro-ph/0407372.

[151] P. Astier et al., Astron. Astrophys. 447 (2006) 31, astro-ph/0510447.

[152] Supernova Search Team, A.G. Riess et al., Astrophys. J. 607 (2004) 665, astro-ph/0402512.

[153] M. Fairbairn and L.M. Griffiths, JHEP 02 (2002) 024, hep-ph/0111435.

[154] U. Seljak, A. Slosar and P. McDonald, (2006), astro-ph/0604335.

[155] C. Boehm, P. Fayet and J. Silk, Phys. Rev. D69 (2004) 101302, hep-ph/0311143.

[156] M. Drees et al., Phys. Rev. D63 (2001) 035008, hep-ph/0007202.

[157] P. Sikivie, AIP Conf. Proc. 805 (2006) 23, hep-ph/0509198.

[158] J.F. Navarro, C.S. Frenk and S.D.M. White, Astrophys. J. 490 (1997) 493, astro-ph/9611107.

[159] S. Ghigna et al., Astrophys. J. 544 (2000) 616, astro-ph/9910166.

[160] W.J.G. de Blok et al., Astrophys. J. 552 (2001) L23, astro-ph/0103102.

[161] A.A. Klypin et al., Astrophys. J. 522 (1999) 82, astro-ph/9901240.

[162] H. Pagels and J.R. Primack, Phys. Rev. Lett. 48 (1982) 223.

[163] W.B. Lin et al., Phys. Rev. Lett. 86 (2001) 954, astro-ph/0009003.

[164] A.V. Kravtsov, O.Y. Gnedin and A.A. Klypin, Astrophys. J. 609 (2004) 482, astro-ph/0401088.

[165] M. Markevitch et al., Astrophys. J. 606 (2004) 819, astro-ph/0309303.

[166] B.D. Wandelt et al., (2000), astro-ph/0006344.

[167] CDMS, D.S. Akerib et al., Phys. Rev. Lett. 93 (2004) 211301, astro-ph/0405033.

[168] G. Angloher et al., Astropart. Phys. 23 (2005) 325, astro-ph/0408006.

[169] DAMA, R. Bernabei et al., Phys. Lett. B480 (2000) 23.

[170] UK Dark Matter, G.J. Alner et al., Astropart. Phys. 23 (2005) 444.

[171] R. Gaitskell and V. Mandic, See `http://dendera.berkeley.edu/plotter/entryform.html`.

[172] E.A. Baltz and P. Gondolo, Phys. Rev. Lett. 86 (2001) 5004, hep-ph/0102147.

[173] G. Jungman, M. Kamionkowski and K. Griest, Phys. Rept. 267 (1996) 195, hep-ph/9506380.

[174] L. Bergstrom, Rept. Prog. Phys. 63 (2000) 793, hep-ph/0002126.

[175] P. Gondolo et al., JCAP 0407 (2004) 008, astro-ph/0406204.

[176] G. Servant and T.M.P. Tait, Nucl. Phys. B650 (2003) 391, hep-ph/0206071.

[177] G. Bertone, D. Hooper and J. Silk, Phys. Rept. 405 (2005) 279, hep-ph/0404175.

[178] W. Buchmuller et al., Phys. Lett. B588 (2004) 90, hep-ph/0402179.

[179] K. Jedamzik, (2006), hep-ph/0604251.

[180] A. Arvanitaki et al., Phys. Rev. D72 (2005) 075011, hep-ph/0504210.

[181] W. Buchmuller et al., (2006), hep-ph/0605164.

[182] P.F. Smith et al., Nucl. Phys. B206 (1982) 333.

[183] N. Arkani-Hamed and S. Dimopoulos, JHEP 06 (2005) 073, hep-th/0405159.

[184] G.D. Kribs and I.Z. Rothstein, Phys. Rev. D55 (1997) 4435, hep-ph/9610468.

[185] EGRET, P. Sreekumar et al., Astrophys. J. 494 (1998) 523, astro-ph/9709257.

[186] W. Hu and J. Silk, Phys. Rev. Lett. 70 (1993) 2661.

[187] G. German, G.G. Ross and S. Sarkar, Nucl. Phys. B608 (2001) 423, hep-ph/0103243.

[188] D.H. Lyth and E.D. Stewart, Phys. Rev. D53 (1996) 1784, hep-ph/9510204.

[189] D.H. Lyth and E.D. Stewart, Phys. Rev. Lett. 75 (1995) 201, hep-ph/9502417.

[190] T.W.B. Kibble, J. Phys. A9 (1976) 1387.

[191] A. Vilenkin, Phys. Rept. 121 (1985) 263.

[192] A.H. Guth, Phys. Rev. D23 (1981) 347.

[193] E.N. Parker, Ann. Rev. Astron. Astrophys. 8 (1970) 1.

[194] W. Beenakker et al., Nucl. Phys. B492 (1997) 51, hep-ph/9610490.

[195] W. Beenakker et al., Phys. Rev. Lett. 83 (1999) 3780, hep-ph/9906298.

[196] A. Freitas, A. von Manteuffel and P.M. Zerwas, Eur. Phys. J. C34 (2004) 487, hep-ph/0310182 + references therein. See `http://theory.fnal.gov/people/freitas/`.

[197] M. Spira, (1998), hep-ph/9812407.

[198] T. Plehn, D. Rainwater and P. Skands, (2005), hep-ph/0510144.

[199] S. Catani et al., JHEP 11 (2001) 063, hep-ph/0109231.

[200] L. Lonnblad, JHEP 05 (2002) 046, hep-ph/0112284.

[201] F. Krauss, JHEP 08 (2002) 015, hep-ph/0205283.

[202] S. Mrenna and P. Richardson, JHEP 05 (2004) 040, hep-ph/0312274.

[203] S. Hoche et al., (2006), hep-ph/0602031.

[204] Y.L. Dokshitzer, V.A. Khoze and S.I. Troian, J. Phys. G17 (1991) 1602.

[205] T. Sjostrand, S. Mrenna and P. Skands, JHEP 05 (2006) 026, hep-ph/0603175.

[206] G. Corcella et al., JHEP 01 (2001) 010, hep-ph/0011363.

[207] S. Moretti et al., JHEP 04 (2002) 028, hep-ph/0204123.

[208] T. Gleisberg et al., JHEP 02 (2004) 056, hep-ph/0311263.

[209] M.A. Dobbs et al., (2004), hep-ph/0403045, See `http://www.cedar.ac.uk/hepcode`.

[210] T. Stelzer and W.F. Long, Comput. Phys. Commun. 81 (1994) 357, hep-ph/9401258.

[211] F. Maltoni and T. Stelzer, JHEP 02 (2003) 027, hep-ph/0208156.

[212] G.C. Cho et al., Phys. Rev. D73 (2006) 054002, hep-ph/0601063.

[213] CompHEP, E. Boos et al., Nucl. Instrum. Meth. A534 (2004) 250, hep-ph/0403113.

[214] A. Pukhov, (2004), hep-ph/0412191.

[215] W. Beenakker, R. Hopker and M. Spira, (1996), hep-ph/9611232 + references therein. See `http://pheno.physics.wisc.edu/~plehn/`.

[216] M. Mühlleitner, A. Djouadi and Y. Mambrini, (2003), hep-ph/0311167 + references therein.

[217] E. Boos et al., (2001), hep-ph/0109068.

[218] J. Alwall et al., (2006), hep-ph/0609017.

[219] J.D. Bjorken, Phys. Rev. D17 (1978) 171.

[220] CDF, F. Abe et al., Phys. Rev. D45 (1992) 1448.

[221] B. Andersson et al., Phys. Rept. 97 (1983) 31.

[222] DELPHI, P. Abreu et al., Z. Phys. C73 (1996) 11.

[223] OPAL, G. Alexander et al., Z. Phys. C69 (1996) 543.

[224] ALEPH, A. Heister et al., Phys. Lett. B512 (2001) 30, hep-ex/0106051.

[225] SLD, K. Abe et al., Phys. Rev. D65 (2002) 092006, hep-ex/0202031.

[226] G. 't Hooft, Nucl. Phys. B72 (1974) 461.

[227] P. Minkowski and W. Ochs, Phys. Lett. B485 (2000) 139, hep-ph/0003125.

[228] C.K. Chua, W.S. Hou and S.Y. Tsai, Phys. Lett. B544 (2002) 139, hep-ph/0204186.

[229] E. Klempt, AIP Conf. Proc. 814 (2006) 723.

[230] W. Kilian et al., (2005), hep-ph/0507137.

[231] A. De Rujula, H. Georgi and S.L. Glashow, Phys. Rev. D12 (1975) 147.

[232] A.C. Kraan, Eur. Phys. J. C37 (2004) 91, hep-ex/0404001.

[233] N. Isgur and M.B. Wise, Phys. Lett. B232 (1989) 113.

[234] M.S. Chanowitz and S.R. Sharpe, Phys. Lett. B126 (1983) 225.

[235] F. Buccella, G.R. Farrar and A. Pugliese, Phys. Lett. B153 (1985) 311.

[236] UKQCD, M. Foster and C. Michael, Phys. Rev. D59 (1999) 094509, hep-lat/9811010.

[237] J.M. Cornwall and A. Soni, Phys. Lett. B120 (1983) 431.

[238] W.S. Hou, C.S. Luo and G.G. Wong, Phys. Rev. D64 (2001) 014028, hep-ph/0101146.

[239] T. Sjostrand and P.Z. Skands, Nucl. Phys. B659 (2003) 243, hep-ph/0212264.

[240] W. Kilian et al., Eur. Phys. J. C39 (2005) 229, hep-ph/0408088.

[241] U. Sarid and S.D. Thomas, Phys. Rev. Lett. 85 (2000) 1178, hep-ph/9909349.

[242] SUSY Working Group, R. Culbertson et al., (2000), hep-ph/0008070.

[243] S.P. Ahlen, Phys. Rev. D17 (1978) 229.

[244] S.P. Ahlen and K. Kinoshita, Phys. Rev. D26 (1982) 2347.

[245] S.D. Drell et al., Phys. Rev. Lett. 50 (1983) 644.

[246] J. Derkaoui et al., Astropart. Phys. 10 (1999) 339.

[247] L. Bracci and G. Fiorentini, Nucl. Phys. B232 (1984) 236.

[248] L.P. Gamberg, G.R. Kalbfleisch and K.A. Milton, Found. Phys. 30 (2000) 543, hep-ph/9906526.

[249] CDF, A. Abulencia et al., (2005), hep-ex/0509015.

[250] J.L. Pinfold et al., Phys. Lett. B316 (1993) 407.

[251] H1, A. Aktas et al., Eur. Phys. J. C41 (2005) 133, hep-ex/0501039.

[252] A. De Rujula, Nucl. Phys. B435 (1995) 257, hep-th/9405191.

[253] I.F. Ginzburg and A. Schiller, Phys. Rev. D60 (1999) 075016, hep-ph/9903314.

[254] L3, M. Acciarri et al., Phys. Lett. B345 (1995) 609.

[255] D0, B. Abbott et al., Phys. Rev. Lett. 81 (1998) 524, hep-ex/9803023.

[256] L.P. Gamberg, G.R. Kalbfleisch and K.A. Milton, (1998), hep-ph/9805365.

[257] A. Chilingarov et al., Nucl. Instrum. Meth. A449 (2000) 277.

[258] J. Lewin, Rutherford Laboratory Internal Note - RL-77 126/A (1977).

[259] R.M. Sternheimer, M.J. Berger and S.M. Seltzer, At. Data Nucl. Data Tabl. 30 (1984) 261.

[260] W.H. Barkas et al., Phys. Rev. 101 (1956) 778.

[261] J. Lindhard, V. Nielsen and P. Thomsen, Mat. Fys. Medd. Dan. Vid. Selks. 33 10 (1963) 1.

[262] H. Anderson and J. Ziegler, *The Stopping and Ranges of Ions in Matter* (Pergamon Press, 1977).

[263] W.H. Barkas et al., Phys. Rev. 101 (1956) 778.

[264] R.M. Sternheimer, Phys. Rev. 93 (1953) 351.

[265] G. Bauer et al., Nucl. Instrum. Meth. A545 (2005) 503.

[266] M. Drees and X. Tata, Phys. Lett. B252 (1990) 695.

[267] H. Baer, K. Cheung and J.F. Gunion, Phys. Rev. D59 (1999) 075002, hep-ph/9806361.

[268] R. Mackeprang, to be submitted to Nucl. Instr. Meth. A .

[269] B. Rossi, *High Energy Particles* (Prentice Hall, 1952).

[270] W.B. Atwood et al., Nucl. Instrum. Meth. A306 (1991) 446.

[271] H1, I. Abt et al., Nucl. Instrum. Meth. A386 (1997) 348.

[272] H1, A. Aktas et al., Eur. Phys. J. C36 (2004) 413, hep-ex/0403056.

[273] ALEPH, R. Barate et al., Phys. Lett. B405 (1997) 379, hep-ex/9706013.

[274] W. Adam et al., Nucl. Instrum. Meth. A543 (2005) 463.

[275] R. Bainbridge, Prepared for 8th Workshop on Electronics for LHC Experiments, Colmar, France, 9-13 Sep 2002.

[276] ALEPH, D. Buskulic et al., Phys. Lett. B303 (1993) 198.

[277] OPAL, G. Abbiendi et al., Phys. Lett. B572 (2003) 8, hep-ex/0305031.

[278] R.L. Fleischer, P.B. Price and R.M. Walker, *Nuclear tracks in solids: principles and applications* (Berkeley, University of California Press, 1975).

[279] M. Bertani et al., Europhys. Lett. 12 (1990) 613.

[280] P.B. Price, G.X. Ren and K. Kinoshita, Phys. Rev. Lett. 59 (1987) 2523.

[281] P.B. Price, G.R. Jing and K. Kinoshita, Phys. Rev. Lett. 65 (1990) 149.

[282] J.L. Pinfold et al., Nucl. Instrum. Meth. A302 (1991) 434.

[283] K. Kinoshita et al., Phys. Rev. D46 (1992) 881.

[284] P.A. Cerenkov, Phys. Rev. 52 (1937) 378.

[285] E.G. Anassontzis et al., Nucl. Instrum. Meth. A323 (1992) 351.

[286] W. Adam et al., Nucl. Instrum. Meth. A343 (1994) 68.

[287] W. Adam et al., Nucl. Instrum. Meth. A371 (1996) 12.

[288] E. Albrecht et al., Nucl. Instrum. Meth. A433 (1999) 47.

[289] DELPHI, P. Abreu et al., Phys. Lett. B478 (2000) 65, hep-ex/0103038.

[290] DELPHI, P. Abreu et al., Phys. Lett. B444 (1998) 491, hep-ex/9811007.

[291] DELPHI, J. Abdallah et al., Eur. Phys. J. C27 (2003) 153, hep-ex/0303025.

[292] DELPHI, P.A. Aarnio et al., Nucl. Instrum. Meth. A303 (1991) 233.

[293] A.C. Kraan, Interactions and detection of heavy stable hadronizing particles, PhD thesis, Niels Bohr Institute, 2004.

[294] J. Shank et al., Prepared for 8th International Conference on Advanced Technology and Particle Physics (ICATPP 2003): Astroparticle, Particle, Space Physics, Detectors and Medical Physics Applications, Como, Italy, 6-10 Oct 2003.

[295] TASSO, W. Braunschweig et al., Z. Phys. C38 (1988) 543.

[296] L. Bracci, G. Fiorentini and G. Mezzorani, Nucl. Phys. B258 (1985) 726.

[297] K. Olaussen and R. Sollie, Nucl. Phys. B255 (1985) 465.

[298] K.A. Milton et al., Int. J. Mod. Phys. A17 (2002) 732, hep-ph/0111062.

[299] L. Alvarez, Design of an electromagnetic detector for Dirac monopoles, Lawrence Radiation Laboratory Physics Note UCRL-AGM-470 (unpublished), 1963.

[300] L.W. Alvarez et al., Science 167 (1970) 701.

[301] L.W. Alvarez et al., Rev. Sci. Instrum. 42 (1971) 326.

[302] R.R. Ross et al., Phys. Rev. D8 (1973) 698.

[303] R.A. Carrigan, F.A. Nezrick and B.P. Strauss, Phys. Rev. D8 (1973) 3717.

[304] J. Carrigan, Richard A., F.A. Nezrick and B.P. Strauss, Phys. Rev. D10 (1974) 3867.

[305] J. Carrigan, Richard A., B.P. Strauss and G. Giacomelli, Phys. Rev. D17 (1978) 1754.

[306] JADE, W. Bartel et al., Zeit. Phys. C6 (1980) 295.

[307] J. Weiss et al., Phys. Lett. B101 (1981) 439.

[308] D. Besset et al., Phys. Lett. B118 (1982) 199.

[309] W. Guryn et al., Phys. Lett. B139 (1984) 313.

[310] TPC/Two Gamma, H. Aihara et al., Phys. Rev. Lett. 52 (1984) 2332.

[311] ARGUS, H. Albrecht et al., Phys. Lett. B156 (1985) 134.

[312] T.J.V. Bowcock et al., Phys. Rev. D40 (1989) 263.

[313] TOPAZ, I. Adachi et al., Phys. Lett. B244 (1990) 352.

[314] OPAL, M.Z. Akrawy et al., Phys. Lett. B252 (1990) 290.

[315] OPAL, R. Akers et al., Z. Phys. C67 (1995) 203.

[316] OPAL, K. Ackerstaff et al., Phys. Lett. B433 (1998) 195, hep-ex/9803026.

[317] L3, M. Acciarri et al., Phys. Lett. B462 (1999) 354, hep-ex/9909007.

[318] L3, M. Acciarri et al., Phys. Lett. B482 (2000) 31, hep-ex/0002043.

[319] L3, P. Achard et al., Phys. Lett. B517 (2001) 75, hep-ex/0107015.

[320] DELPHI, P. Abreu et al., Phys. Lett. B396 (1997) 315.

[321] L3, P. Achard et al., Phys. Lett. B517 (2001) 75, hep-ex/0107015.

[322] ALEPH, A. Heister et al., Eur. Phys. J. C31 (2003) 327, hep-ex/0305071.

[323] DELPHI, J. Abdallah et al., Eur. Phys. J. C26 (2003) 505, hep-ex/0303024.

[324] ALEPH, A. Heister et al., Eur. Phys. J. C25 (2002) 339, hep-ex/0203024.

[325] OPAL, G. Abbiendi et al., Eur. Phys. J. C46 (2006) 307, hep-ex/0507048.

[326] ALEPH, A. Heister et al., Phys. Lett. B533 (2002) 223, hep-ex/0203020.

[327] DELPHI, P. Abreu et al., Eur. Phys. J. C11 (1999) 1, hep-ex/9903071.

[328] OPAL, G. Abbiendi et al., Eur. Phys. J. C29 (2003) 479, hep-ex/0210043.

[329] European Muon Collaboration, J.J. Aubert et al., Phys. Lett. B133 (1983) 461.

[330] M. Basile et al., Nuovo Cim. Lett. 29 (1980) 251.

[331] CHARM, F. Bergsma et al., Z. Phys. C24 (1984) 217.

[332] WA25, D. Allasia et al., Phys. Rev. D37 (1988) 219.

[333] H1, I. Abt et al., Phys. Lett. B328 (1994) 176.

[334] G. Giacomelli and M. Jacob, Phys. Rept. 55 (1979) 1.

[335] CDF, F. Abe et al., Phys. Rev. Lett. 63 (1989) 1447.

[336] CDF, F. Abe et al., Phys. Rev. D46 (1992) 1889.

[337] CDF, D. Acosta et al., Phys. Rev. Lett. 90 (2003) 131801, hep-ex/0211064.

[338] J.L. Hewett et al., JHEP 09 (2004) 070, hep-ph/0408248.

[339] CDF, D. Acosta, Phys. Rev. Lett. 92 (2004) 121802, hep-ex/0309051.

[340] OPAL, G. Abbiendi et al., Eur. Phys. J. C14 (2000) 73, hep-ex/0001056.

[341] P. Janot, Phys. Lett. B564 (2003) 183, hep-ph/0302076.

[342] ALEPH, R. Barate et al., Z. Phys. C76 (1997) 1.

[343] F. Csikor and Z. Fodor, Phys. Rev. Lett. 78 (1997) 4335, hep-ph/9611320.

[344] P.B. Price et al., Phys. Rev. Lett. 35 (1975) 487.

[345] P.B. Price et al., Phys. Rev. D18 (1978) 1382.

[346] B. Cabrera, Phys. Rev. Lett. 48 (1982) 1378.

[347] A.D. Caplin et al., Nature 321 (1986) 402.

[348] MACRO, M. Ambrosio et al., Eur. Phys. J. C25 (2002) 511, hep-ex/0207020.

[349] P. Musset, M. Price and E. Lohrmann, Phys. Lett. B128 (1983) 333.

[350] K. Kinoshita, P.B. Price and D. Fryberger, Phys. Rev. Lett. 48 (1982) 77.

[351] D. Fryberger et al., Phys. Rev. D29 (1984) 1524.

[352] K. Kinoshita et al., Phys. Lett. B228 (1989) 543.

[353] K. Kinoshita et al., Phys. Rev. Lett. 60 (1988) 1610.

[354] J. Pinfold et al., CERN-LEPC-89-14,LEPC-P-5-Add-1,CM-P00043687.

[355] Cleo, T. Gentile et al., Phys. Rev. D35 (1987) 1081.

[356] G.R. Kalbfleisch et al., Phys. Rev. Lett. 85 (2000) 5292, hep-ex/0005005.

[357] G.R. Kalbfleisch et al., Phys. Rev. D69 (2004) 052002, hep-ex/0306045.

[358] H. Hoffmann et al., Lett. Nuovo Cim. 23 (1978) 357.

[359] B. Aubert et al., Phys. Lett. B120 (1983) 465.

[360] S. Graf, A. Schaefer and W. Greiner, Phys. Lett. B262 (1991) 463.

[361] ATLAS, ATLAS: Detector and Physics Performance Technical Design Report, CERN-LHCC-99-14.

[362] ATLAS, ATLAS: Detector and Physics Performance Technical Design Report, CERN-LHCC-99-15.

[363] CMS, CMS Physics: Technical Design Report v1:Detector Performance and Software, CERN-LHCC-2006-001.

[364] CMS, CMS Physics: Technical Design Report v1:Physics Performance, CERN-LHCC-2006-021.

[365] MOEDAL, A Search for Highly Ionizing Particles and Slow Exotic Decays at the LHC using the MOEDAL detectors: Letter of Intent, CERN/LHCC/98-15.

[366] MOEDAL, J.L. Pinfold, Nucl. Phys. Proc. Suppl. 78 (1999) 52.

[367] A. Nisati, S. Petrarca and G. Salvini, Mod. Phys. Lett. A12 (1997) 2213, hep-ph/9707376.

[368] G. Polesello and A. Rimoldi, (1999), ATLAS Muon Note, ATL-MUON-99-006.

[369] P. Zalewski, CMS Conference Note, CMS-CR-1999-019.

[370] S. Tarem et al., (2005), ATLAS Public Note, ATL-PHYS-PUB-2005-022.

[371] S. Ambrosanio et al., JHEP 01 (2001) 014, hep-ph/0010081.

[372] S. Ambrosanio et al., (2000), hep-ph/0012192.

[373] B.C. Allanach et al., JHEP 08 (2001) 051, hep-ph/0108097.

[374] A.C. Kraan, J.B. Hansen and P. Nevski, (2005), hep-ex/0511014.

[375] S. Hellman, D. Milstead and M. Ramstedt, (2006), ATLAS Public Note, ATL-PHYS-PUB-2006-005.

[376] S. Hellman, M. Johansen and D. Milstead, (2006), ATLAS Public Note, ATL-PHYS-PUB-2006-015.

[377] J.R. Ellis, A.R. Raklev and O.K. Oye, (2006), hep-ph/0607261.

[378] R. Hauser, Eur. Phys. J. C34 (2004) s173.

[379] D0 Muon Group, (1997), Technical Design of the Central Muon System, D0 Note 3365/1997.

[380] V.M. Abazov et al., Nucl. Instrum. Meth. A552 (2005) 372, physics/0503151.

[381] CDF, (1996), The CDF-II Technical Design Report, Fermilab-Pub-96-390-E.

[382] CDF, C.M. Ginsburg, Eur. Phys. J. C33 (2004) s1002.

[383] J.L. Pinfold, private communication.